AD A072481

Report No. PCRL-FR-79-004

July 1979

COMPRESSION-IGNITION SENSITIVITY STUDIES OF LIQUID PROPELLANTS FOR GUNS

Contract No. DAAK10-78-C-0315

Performance Period

24 August 1978 - 14 July 1979

DDC
RECEIVED
AUG 6 1979
C

Submitted to

U.S. Army Armament Research & Development Command
Dover, New Jersey

by

Neale A. Messina, Larry S. Ingram, Preston E. Camp,
Moshe BenReuven and Martin Summerfield

Princeton Combustion Research Laboratories, Inc.
1041 U.S. Highway One North
Princeton, New Jersey 08540

UNCLASSIFIED
SECURITY CLASSIFICATION OF THIS PAGE (When Data Entered)

REPORT DOCUMENTATION PAGE

READ INSTRUCTIONS BEFORE COMPLETING FORM

1. REPORT NUMBER
2. GOVT ACCESSION NO.
3. RECIPIENT'S CATALOG NUMBER

4. TITLE (and Subtitle)

6 Compression-Ignition Sensitivity Studies of Liquid Propellants for Guns

5. TYPE OF REPORT & PERIOD COVERED

9 Final Report, 24 August 1978 - 14 July 1979

6. PERFORMING ORG. REPORT NUMBER

14 PCRL-FR-79-004

7. AUTHOR(s)

10 Neale A. Messina, Larry S. Ingram, Preston E. Camp, Moshe BenReuven and Martin Summerfield

8. CONTRACT OR GRANT NUMBER(s)

DAAK10-78-C-0315

15

9. PERFORMING ORGANIZATION NAME AND ADDRESS

Princeton Combustion Research Laboratories, Inc.
1041 U.S. Highway One North
Princeton, New Jersey 08540

392 961

10. PROGRAM ELEMENT, PROJECT, TASK AREA & WORK UNIT NUMBERS

11. CONTROLLING OFFICE NAME AND ADDRESS

U.S. Army Armament Research & Development Command
Dover, New Jersey 07801

12. REPORT DATE

11 July 1979

13. NUMBER OF PAGES

152

14. MONITORING AGENCY NAME & ADDRESS (if different from Controlling Office)

12 153 p

15. SECURITY CLASS. (of this report)

UNCLASSIFIED

15a. DECLASSIFICATION/DOWNGRADING SCHEDULE

16. DISTRIBUTION STATEMENT (of this Report)

Approved for public release; distribution unlimited.

17. DISTRIBUTION STATEMENT (of the abstract entered in Block 20, if different from Report)

18. SUPPLEMENTARY NOTES

19. KEY WORDS (Continue on reverse side if necessary and identify by block number)

Compression-Ignition; Sensitivity; Secondary Ignition; Liquid Monopropellant Sensitivity; Explosion Sensitivity

20. ABSTRACT (Continue on reverse side if necessary and identify by block number)

The objective of the study reported herein was to provide a means of establishing the sensitivity of candidate liquid monopropellants to compression ignition at pressure levels and pressurization rates comparable to those of liquid propellant gun (LPG) systems, particularly during the start-up phase of the ballistic cycle. Experimental testing with a specially designed compression-ignition sensitivity apparatus was performed to delineate the safe operational domain for NOS-365 liquid monopropellant with respect to the →

DD FORM 1 JAN 73 1473 EDITION OF 1 NOV 65 IS OBSOLETE

UNCLASSIFIED
SECURITY CLASSIFICATION OF THIS PAGE (When Data Entered)

392 962

hazard associated with compression-ignition of collapsing bubbles in the liquid charge and ensuing runaway reaction. It is the purpose of this study to define the threshold conditions required to initiate runaway reaction, in the presence of finely distributed ullage. Furthermore the theory for the mechanism of ignition of liquid monopropellants by rapid compression is advanced by examining the assumptions and limitations of previous works.

Accession For
NTIS GRA&I
DDC TAB
Unannounced
Justification
By
Distribution/
Availability Codes
Dist | Avail and/or special
A

Foreword

This Final Report represents work performed by Princeton Combustion Research Laboratories, Inc. in support of the Statement of Work on Contract No. DAAK10-78-C-0315 during the period 24 August 1978 thru 14 July 1979.

Technical cognizance for this contract was provided at the U.S. Army Armament Research & Development Command, Dover, NJ by Dr. Anthony Beardell The authors wish to express special acknowledgement to Mr. Joseph Hershkowitz of ARRADCOM, Dover for many enlightening technical exchanges.

Table of Contents

	Page
Title Page	i
DD FORM 1423	ii
Foreword	iv
Table of Contents	v
1.0 Sensitivity of Liquid Monopropellants to Explosion by Rapid Compression	1
1.1 Origin of the Problem in Practical Liquid Propellant Gun (LPG) Systems	1
1.2 Sensitization of LP by Ullage or Dispersed Bubbles	2
2.0 Flow Visualization Studies of Dynamic Loading Characteristics of NOS-365 Liquid Monopropellant	3
2.1 Description of Test Equipment	3
2.2 System Operation	8
2.3 Results of Flow Visualization Studies	10
2.3.1 Inert Simulant (Water) Tests	10
2.3.2 NOS-365 Liquid Monopropellant Tests	17
2.4 Summary of Flow Visualization Test Results on Dynamic Loading Characteristics of a Liquid Charge	34
3.0 Starter Charge Pressurization Rate Tests	35
3.1 Description of Test Equipment	35
3.2 System Operation	39
3.3 Results of Starter Charge Tests	41
4.0 Compression-Ignition Sensitivity Studies of a Dynamically Loaded Liquid Propellant Charge	44
4.1 Description of Test Equipment	44
4.2 Phototransistor Light Sensor Assemblies	47
4.3 System Operation	49
4.4 The Data Acquisition System	52
4.5 Functional Testing: Inert Simulant (Water) Tests	53
4.6 NOS-365 Liquid Monopropellant Tests	60
4.7 Interpretation and Discussion of Compression-Ignition Sensitivity Studies	72
5.0 Theoretical Approach to Initiation of Explosion by Dynamic Compression of Liquid Explosive with Bubbles	74
5.1 Four Hypothetical Situations to Be Considered Theoretically	74
5.2 Scope of the Present Work: Fundamental Processes and Theoretical Considerations	75

6.0 Literature Analysis 78

6.1 Collapse of Bubbles in Inert Liquids 78
6.2 Hot Spot Initiation Theory 82
6.3 Detonation in Liquid Monopropellant: The Work by Stanford Research Institute (SRI) 87

6.3.1 Low Velocity Detonation (LVD) 87
6.3.2 Collapse of a Vapor Bubble 88

7.0 Physical Considerations in Theory of Liquid Propellant Compression with Isolated Bubbles 91

7.1 Chemical Reactions and Vaporization 91
7.2 Characteristic Length and Time Scales 92
7.3 The Effects of Liquid Compressibility 95
7.4 Summary 98

8.0 Analytical Model 99

8.1 The Liquid Phase 99
8.2 The Gas Phase 102
8.3 The Phase Interface Conservation Conditions 104

9.0 Method of Solution 106

9.1 The Two Time Scale Problem 106
9.2 Outline of Solution Procedure 107

9.2.1 Short Time Scale Analysis 107
9.2.2 Two Time Scale Analysis 107

10.0 References 109

Appendix A: Pressure Distributions During Bubble Collapse for Incompressible Liquid 113

Appendix B: Approximate Analysis of Liquid Compressibility 119

Appendix C: Flow Visualization Tester Assembly Procedure 132

Appendix D: Starter Charge Tester Assembly Procedure 138

Appendix E: L.P. Compression-Ignition Sensitivity Tester Assembly Procedure. 141

1.0 Sensitivity of Liquid Monopropellants to Explosion by Rapid Compression

1.1 Origin of the Problem in Practical Liquid Propellant Gun (LPG) Systems

Monopropellant liquid-propellant gun systems have been developed generally along two lines, the pre-loaded type (so-called bulk-loaded LPG) and the direct-injection type (so-called regenerative type). In each of these types, the liquid charge is brought rather rapidly up to gun operating pressure, ca. 30 to 60 kpsi, in a rise time on the order of 0.1 to 1 msec. Although hundreds of successful firings have been made with both types of gun, with several different types of liquid monopropellant, in sizes up to 4-inch barrels, a few destructive explosions have taken place, all of them on start-up during the rapid pressure rise associated with ignition of the gun. This almost-successful test-record suggests that the particular monopropellants selected are not themselves at fault, or explosions would have occurred with far greater frequency. The most plausible explanation that has emerged from all of the evidence available is that air bubbles due to excessive ullage in the firing chamber, brought in during the pre-firing fill process, become sudden hot spots of unusual severity during the start-up as a result of rapid compression. In at least one case, the evidence suggested that the bubbles might not have been air-filled but simply vapor-filled, formed by cavitation during the filling process. It is this recent LPG development record that forms the background and the rationale for the present investigation.

On the experimental side, Princeton Combustion Research Laboratories, Inc. has produced on a systematic basis rapid pressurizations of liquid propellant (LP) columns with various rates of pressure rise, with various amounts of ullage, both finely distributed and undistributed, and with various LP monopropellants, and has found operating domains of safe start-up for NOS-type and Otto Fuel II[5,12] propellants. Generally speaking, safe start-up without any sign of explosion or runaway exothermic reaction is obtainable by (a) elimination of all air in the system, a probably impractical requirement, (b) avoidance of sharp entry ports or other channel locations where cavitation may occur in the gun filling system, probably also an impractical requirement, (c) keeping the rate of pressure rise in start-up to less than ca. 20 kpsi/msec, a requirement that can be met by rational design of the ignition system, and (d) pre-pressurizing the charge of LP before the onset of the rapid pressure rise of the start-up, a fairly practical remedy that can be incorporated in an LPG control system. These four prescriptions define the domain of explosion-free start-up, on the basis of the LP compression experiments performed by PCRL.

It should be noted, as a matter of practical interest, that in defining this domain of safe start-up, it was necessary to provoke explosions in the test apparatus. The domain of safe start-up is defined by the "dividing surface" between the conditions that always produce explosion and those that never produce explosion. The apparatus was fitted in each case with a pressure-relief shear disc assembly, which always functioned properly. The most significant point of interest is that there was never any evidence of a destructive detonation, and that the apparatus was always re-usable after replacement of the pressure-relief shear disc plug. This experience supports the conclusions drawn from the evidence after the few destructive explosions that have occurred in recent practical LP gun development programs, that no detonations have occurred.

With this background, attention in the present research has been focused on the manner of initiation of runaway exothermic reaction in an LP field by a suddenly compressed hot gas bubble imbedded in the LP. In passing, we note that the problem of ullage in an explosive medium is not limited to the field of LP monopropellant gun systems. It can arise in LP monopropellant (e.g., hydrazine) power generating systems designed for aircraft and spacecraft use, and it can arise in the problem of premature warhead explosions due to setback acceleration of plastic-type warhead explosives in high velocity projectiles. Defining theoretically and experimentally the safe domain of operation for explosive media containing bubbles is a task of general significance.

1.2 Sensitization of LP by Ullage or Dispersed Bubbles

When a liquid monopropellant is rapidly compressed to about 50 kpsi, an estimate of the temperature rise shows that, if the liquid is free of bubbles and if the process is taken to be isentropic, it can increase by about 10 to 20 deg C, with some uncertainty in the calculation due to lack of precise data on compressibility and thermal expansion coefficient, among other properties. A bubble-free monopropellant is therefore unlikely to explode upon sudden pressurization.

However, with one or more small bubbles in the liquid, a "hot spot" can be generated by the adiabatic compression of the bubble, either air or vapor, and if the bubble is initially large enough, the sharp local rise in temperature can cause the bubble to retain its heat long enough to initiate exothermic chemical reaction, i.e., combustion. The resulting rapid gas generation can lead to rupture of the chamber or to a gun breech blow, if it is fast enough or if the volume expansion does not accommodate the generated gas. There is some evidence from firing test pressure records of regenerative-type direct-injection LP guns[53] and from explosion tests conducted at Princeton Combustion Research Laboratories, Inc. with nearly bubble-free LP fillings that, with only a few bubbles sparsely distributed in the liquid field, the rate of gas generation is slow enough to be accommodated by an LPG system as the volume expands at the start of a firing. In the present tests the severity of the explosions in a confined liquid propellant column was proportional to the space density of bubbles -- few bubbles led to only mild explosions. On the other hand, when in the PCRL compression tests the number of injected air bubbles was deliberately large, the resulting explosions were much more severe. As pointed out above, these were never so severe as to destroy the apparatus (except for the pressure-relief shear disc device). The conclusion is that it takes only a single bubble, if large enough, to start a run-away reaction, but it requires a large number of such bubbles acting simultaneously as hot spots to cause the hardware damage associated with such explosions.

2.0 Flow Visualization Studies of Dynamic Loading Characteristics of NOS-365 Liquid Monopropellant

In order to conduct compression-ignition sensitivity studies of a pre-compressed, multiple bubble liquid monopropellant medium representing conditions found in gun simulation studies performed as part of a hazards analysis by Pulsepower Systems, Inc., Princeton Combustion Research Laboratories, Inc., efforts have been directed toward the design, fabrication, and development of an apparatus which incorporates features to control the rate of dynamic loading of the liquid monopropellant, the volume percent of injected air ullage, and the resulting break-up phenomena of the ullage into some mean bubble distribution in the liquid propellant charge. The objective of the Flow Visualization phase of this study was to define the physical state of the liquid propellant charge after dynamic loading, at the system "fire"condition.

2.1 Description of Test Equipment

Figure 1 shows an assembly drawing of the Transparent Visualization Chamber and the Pneumatic Load L.P. Cylinder utilized in the Flow Visualization studies. The schematic drawing presented in Figure 2 identifies functional components such as valves, gas lines, liquid fill and discharge lines, and electrical connections. The Transparent Visualization Chamber was machined from a cast acrylic block with a 0.4375-inch diameter bore. The chamber is provided with an End Plug which carries the contact wire for actuation of the electronic strobe light. In the actual Liquid Propellant Compression Chamber, the End Plug carries the contact wire completing the circuit for ignition of an M52 electric primer which ignites the smokeless powder starter charge which, in turn, produces the desired pressurization rate to which the liquid propellant column in the Compression Chamber is to be subjected. The Transparent Visualization Chamber also contains a Bleed Valve for flushing residual ullage from the system prior to dynamic injection of the liquid propellant charge. A Kristal Type 601A pressure transducer is fitted into the chamber to monitor the pressure-time history of the dynamic loading process and is located 0.70-inch downstream of the centerline of the injection port. The injection port is designed so as to accept various flow guides to alter the cavitation dynamics of the injected liquid. The chamber bore is fitted with a Separator Piston which seals the bore and simulates the function of the Separator Piston in the Liquid Propellant Compression Chamber, i.e., to isolate the liquid propellant charge in the Compression Chamber bore from the hot combustion gases in the Starter Charge Chamber (see Assembly Drawing, Figure 3). A Projectile Piston is utilized to facilitate chamber filling under dynamic loading and provides the trigger to actuate the electronic strobe light upon chamber filling completion. The maximum stroke of the Projectile Piston is 2.7-inch, providing a maximum volumetric loading of liquid propellant of 0.41 cu.in. (6.65 cc).

The Pneumatic Load L.P. Cylinder is machined from 416 S.S. The 0.5-inch diameter bore contains a Pneumatic Piston which transfers the liquid

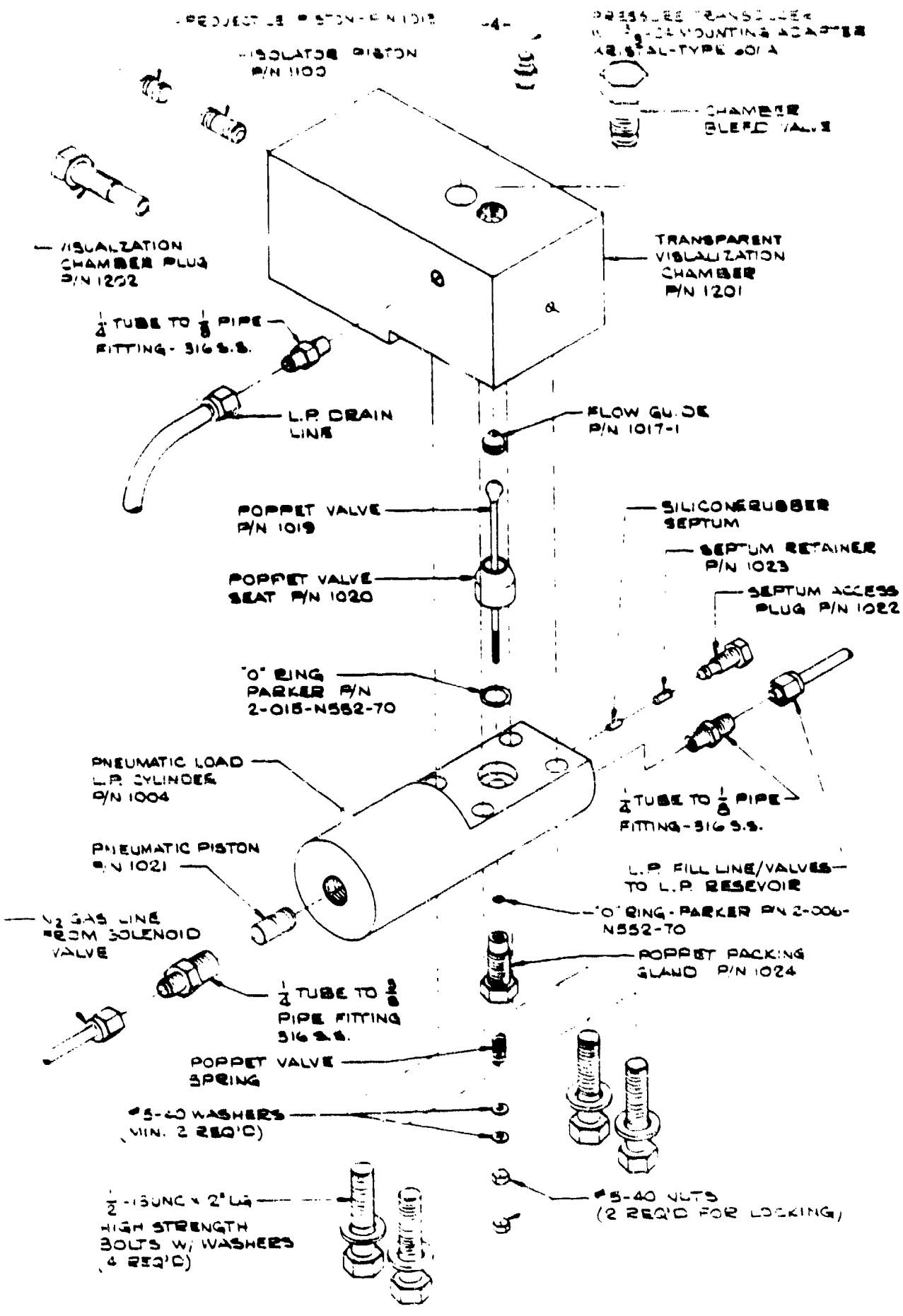

FIGURE 1. BUBBLE FLOW VISUALIZATION TESTER ASSEMBLY

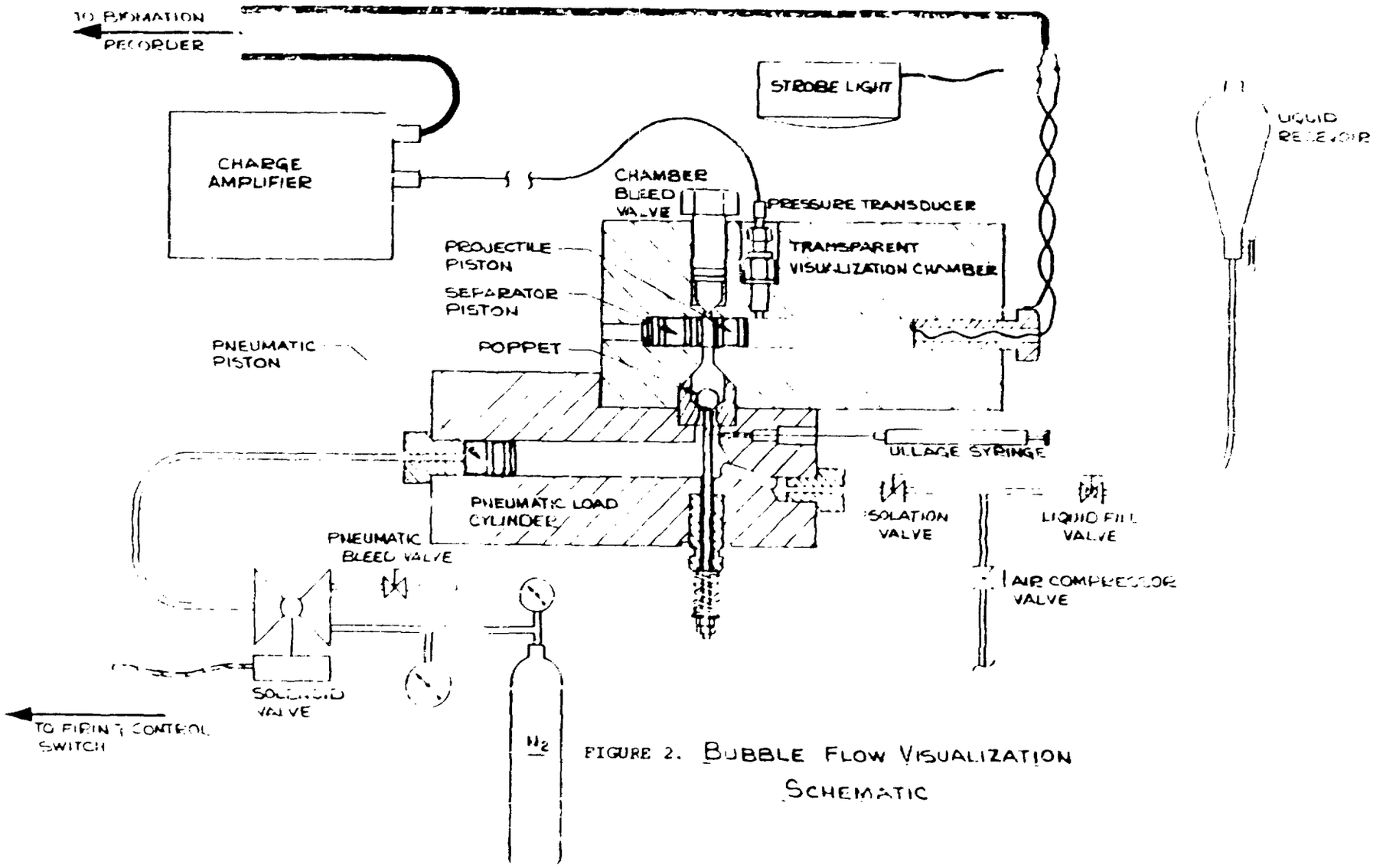

FIGURE 2. BUBBLE FLOW VISUALIZATION SCHEMATIC

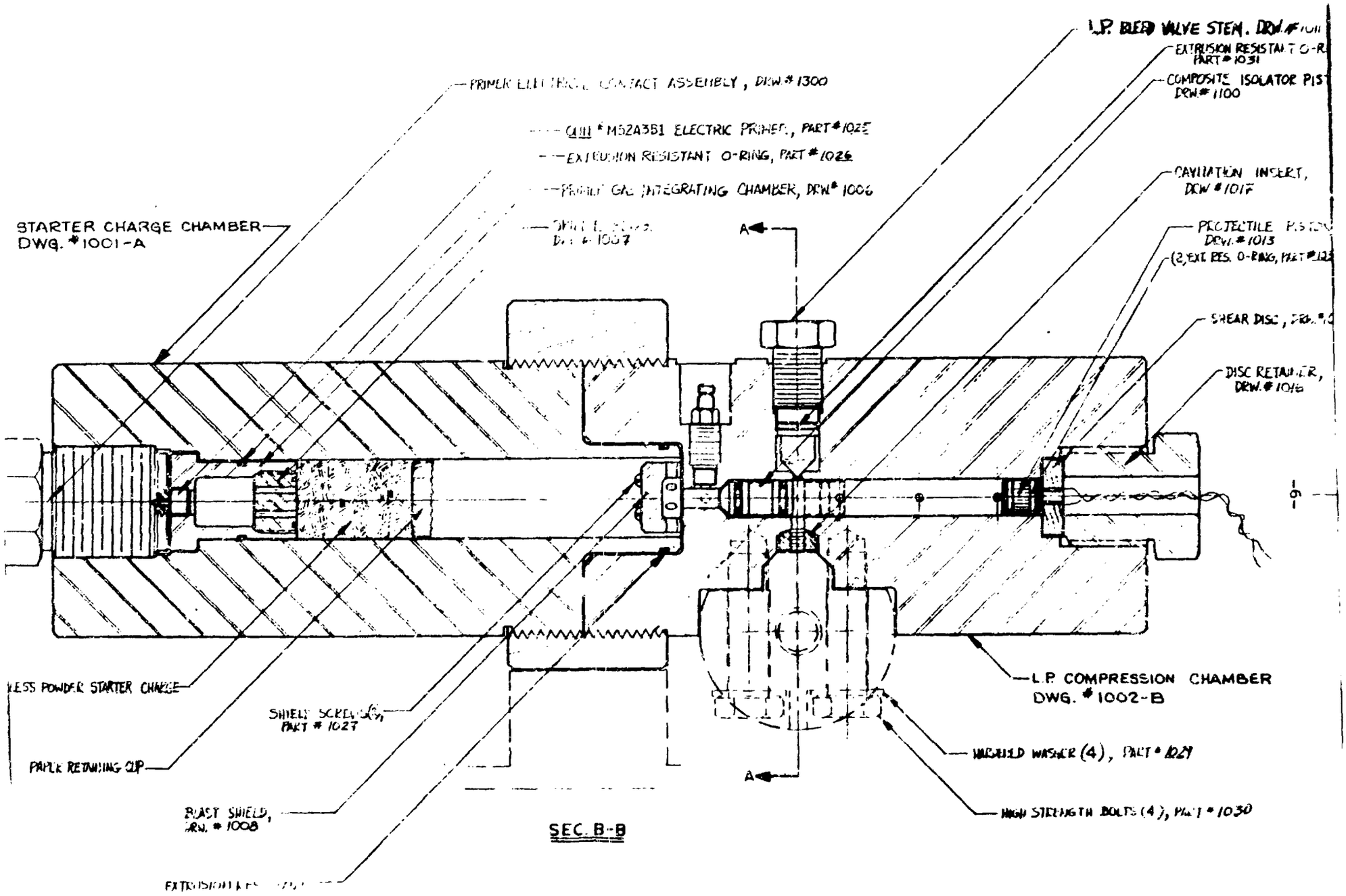

FIGURE 3. ASSEMBLY DRAWING: COMPRESSION-IGNITION SENSITIVITY TESTER OF DYNAMICALLY LOADED LIQUID PROPELLANT CHARGE.

PRINCETON COMBUSTION RESEARCH LABORATORIES, INC.

1041 U.S. HIGHWAY ONE NORTH / PRINCETON, NEW JERSEY 08540

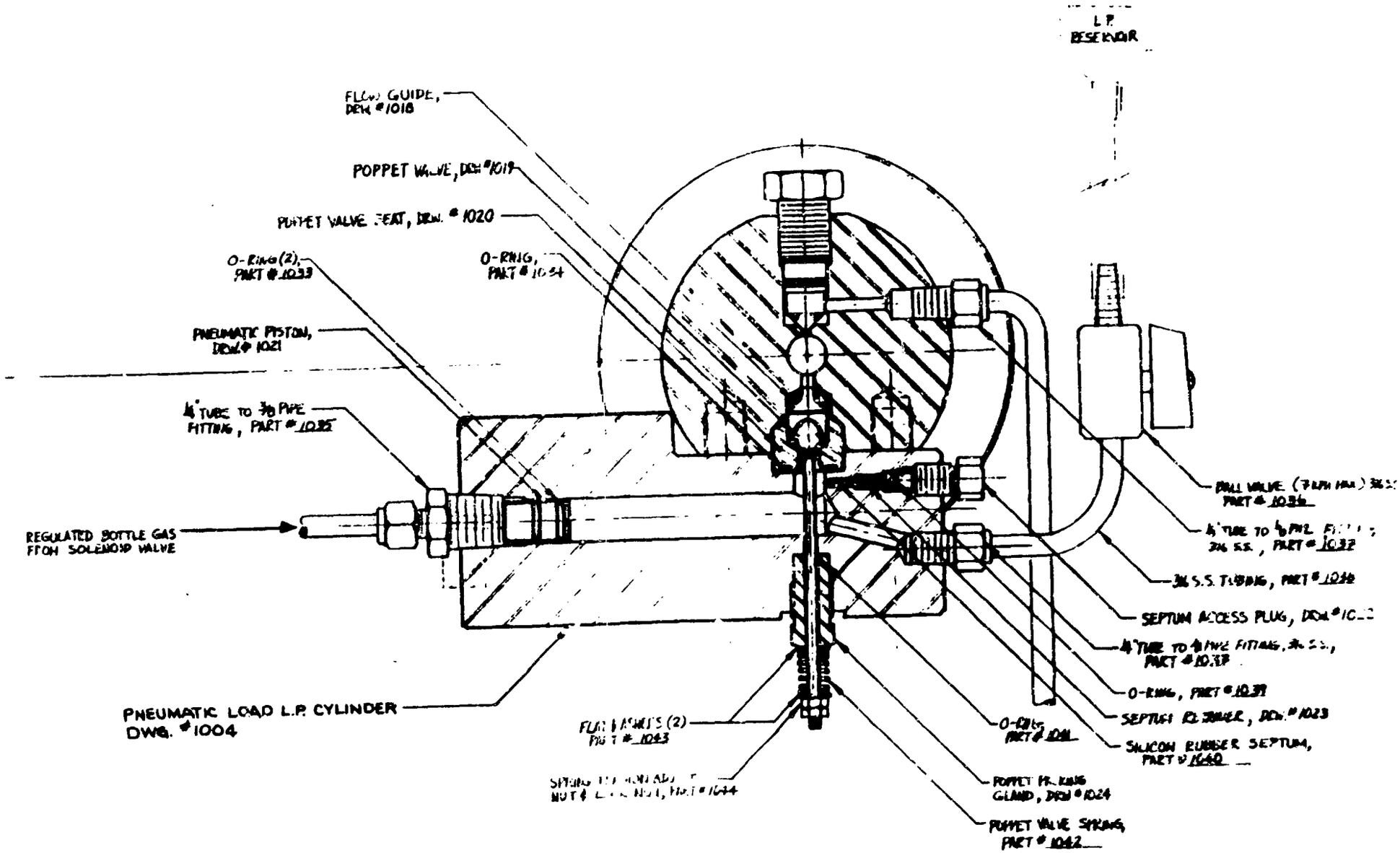

PRINCETON COMBUSTION RESEARCH LABORATORIES, INC.

1041 U.S. HIGHWAY ONE NORTH / PRINCETON, NEW JERSEY 08540

FIGURE 3. CONTINUED.

propellant charge through a Poppet Valve into the injection port of the Transparent Visualization Chamber. The Pneumatic Load L.P. Cylinder acts as a liquid syringe to control the dynamic loading process. A regulated supply of N_2 gas fed through a Solenoid Valve provides the driving pressure for acceleration of the Pneumatic Piston. The injection time is controlled by this driving pressure, for a fixed volumetric loading of liquid propellant. The Poppet Valve controls the steady state (equilibrium) pressure in the Transparent Visualization Chamber by adjustment of the Poppet Valve Spring compression. The Pneumatic Load L.P. Cylinder contains a Silicon Rubber Septum through which a Gas Ullage Syringe, i.e., hypodermic needle passes to introduce a precise loading of air ullage (volume percent, STP). Liquid propellant is introduced into the Pneumatic Loading L.P. Cylinder through a fill port. A photograph of the Transparent Visualization Chamber assembled to the Pneumatic Load L.P. Cylinder, with associated fill lines and valves is shown in Figure 4.

2.2 System Operation

The Transparent Visualization Chamber is first flushed clean of air. This is accomplished by first positioning the Separator Piston and the Projectile Piston with ends on either side of the Visualization Chamber fill port, thereby forming a 5/32-inch wide passageway for flow of liquid from fill port to Bleed Valve. The Poppet Valve is then manually held in the open position as a gravity-fed supply of liquid propellant flows into the Pneumatic Load L.P. Cylinder, through the Poppet Valve, Flow Guide, fill port, the 5/32-inch slice of Visualization Chamber bore, and out the Bleed Valve. In this manner the entire system including the initial bore volume between the two Visualization Chamber pistons can be flushed. With the Poppet Valve released, free to return to its normally closed position, a prescribed volumetric loading of gas ullage is introduced into the Pneumatic Load L.P. Cylinder with the gas syringe. The displaced liquid propellant volume is permitted to flow out through the Isolation Valve. All valves are then closed.

The dynamic loading sequence is now initiated by activating the circuit that opens the Solenoid Valve which releases the driving N_2 pressure into the Pneumatic Load L.P. Cylinder to accelerate the Pneumatic Piston. The motion of the Pneumatic Piston forces the liquid propellant and its gas ullage past the Poppet Valve once the force balance establishes Poppet Valve opening. The liquid propellant and its gas ullage flow through the Flow Guide, possibly resulting in cavitation depending on the nature of the orifice, into the bore of the Transparent Visualization Chamber. The Projectile Piston is then driven to the right allowing the charge to fill the bore until maximum stroke is achieved. The contact of the Projectile Piston with the contact wire in the End Plug completes a circuit that fires the electronic strobe light. Since the camera shutter is open and the entire device is placed in a darkened enclosure, a photograph of the resulting bubble distribution in the liquid propellant charge is obtained. The complete Flow Visualization Tester Assembly Procedure, Filling Procedure, Checklist, and Electronics and Photographic Equipment Set-Up is presented in Appendix C.

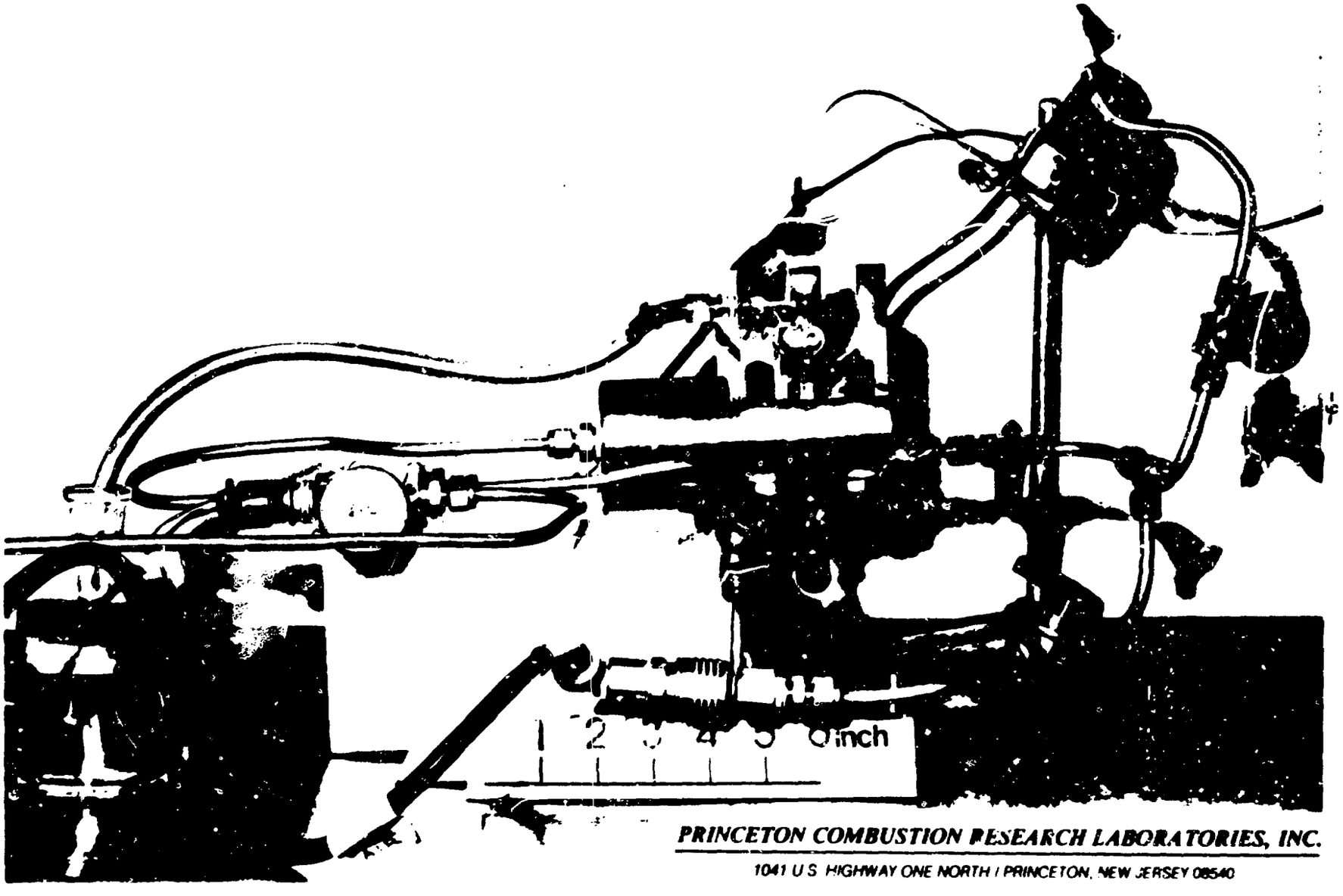

FIGURE 4. PHOTOGRAPH OF TRANSPARENT VISUALIZATION CHAMBER MOUNTED TO THE PNEUMATIC LOAD L.P. CYLINDER WITH ASSOCIATED FILL LINES AND VALVES.

2.3 Results of Flow Visualization Studies

2.3.1 Inert Simulant (Water) Tests

Functional tests of the system were performed with water to determine that all aspects of system operation checked-out. These functional tests with water also provided a baseline for comparison of dynamic loading tests performed with NUS-365 liquid monopropellant.

Flow visualization tests were conducted with water and air ullage volumes of 0%, 0.9% (0.060 cc), and 3.1% (0.206 cc). The driving pressure in all these tests was fixed at 300 psig. Figures 5a and 5b display oscillograph records of these water tests. A dual timebase mode of data recording and display was utilized. The time-scale is as follows. The first centimeter of the oscillograph record represents 40 ms. All subsequent recording is displayed at 4 ms/cm. The lower trace represents pressure in the Transparent Visualization Chamber bore. The vertical scaling is 200 psi/cm. The upper trace represents electronic strobe voltage, showing discharge characteristics once the contact wire in the End Plug completes the circuit. The traces in Figure 5b represent a time expansion of the traces in Figure 5a in the neighborhood of the "water hammer" spike. Table 1 contains information extracted from the oscillograph records on Visualization Chamber fill time, t_{fill} (msec), peak pressure associated with the "water hammer", p_{spike} (psig), and equilibrium pressure in the liquid column in the Visualization Chamber, p_{equil} (psig). Depending on the ullage loading, the fill time varies from 28.0 to 32.0 msec. The fill time is defined as that time from opening of the the Solenoid Valve to time of attainment of maximum stroke of the Projectile Piston (commensurate with discharge of the strobe). The spike pressure varies from 420 to 460 psig and the equilibrium pressure in the Visualization Chamber bore, a function of the Poppet Valve Spring compression, is approximately 240-260 psig. The Poppet Valve Spring compression is responsible for an observed equilibrium pressure in the liquid column less than that of the applied driving pressure by approximately 50 psi. The more the initial spring compression, the higher the restoring force exerted on the Poppet and the lower the resulting equilibrium pressure after injection. This is of no concern. We deliberately use a stiff spring on the Poppet Valve in order to assure prompt and complete closing of the Poppet Valve. Thus, if compression-ignition were to take place in the Sensitivity tests to be parfomed with live propellant, subsequent runaway reaction in the liquid would be confined to the Liquid Compression Chamber and would not propagate into the Pneumatic Load L.P. Cylinder.

Figures 6, 7, and 8 are photographs of the dynamically-loaded water column illustrating the physical condition of the charge at the instant of complete fill of the Visualization Chamber bore. These correspond to 0%, 0.9%, and 3.1% volumetric air loading, respectively. It is interesting to note that zero percent ullage, Figure 6, shows a considerable amount of bubbles distributed through the liquid charge and intense injection activity at the injector port. It should be realized that at the instant the

(a) 0% ullage

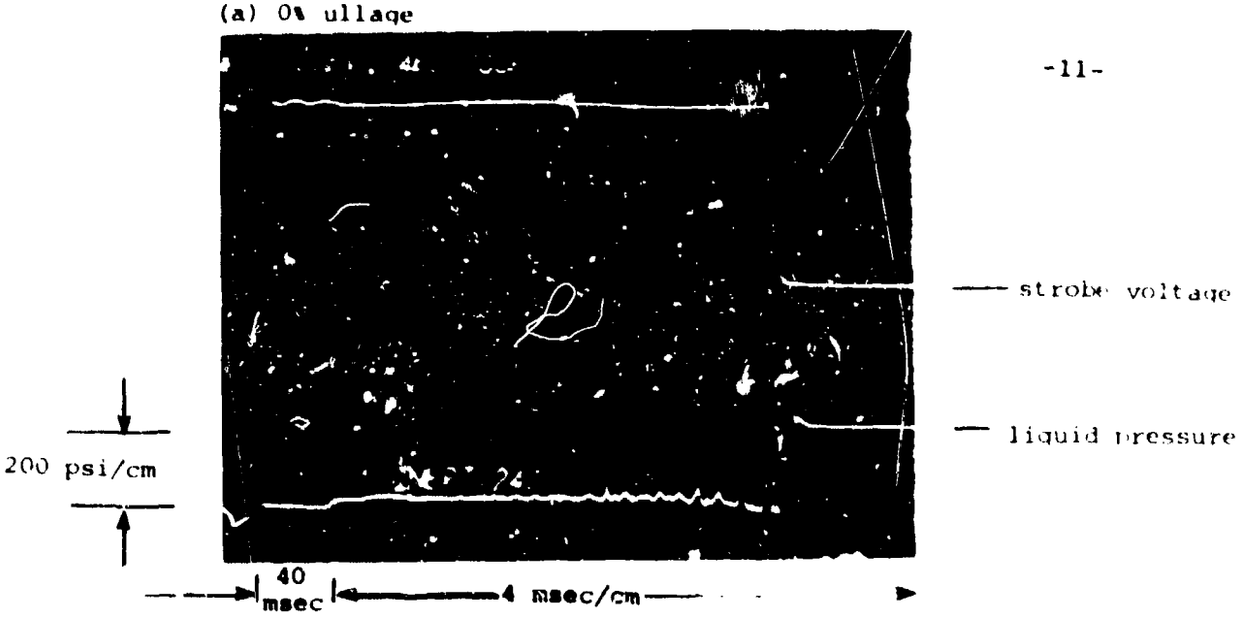

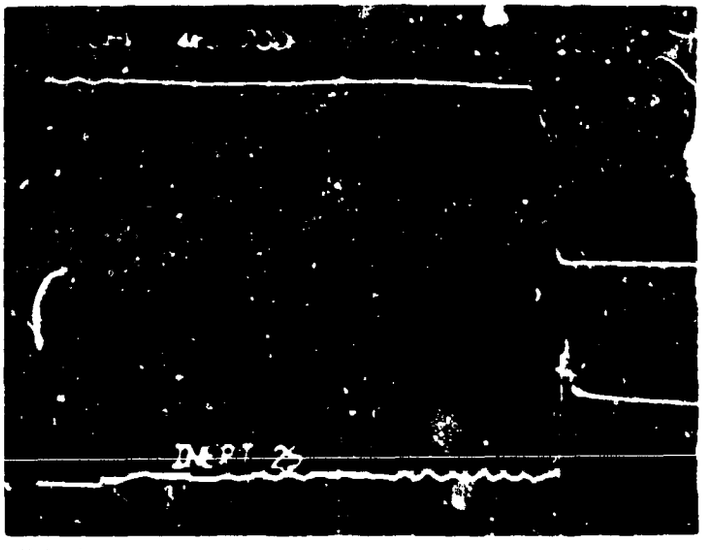

(b) 0.9% ullage

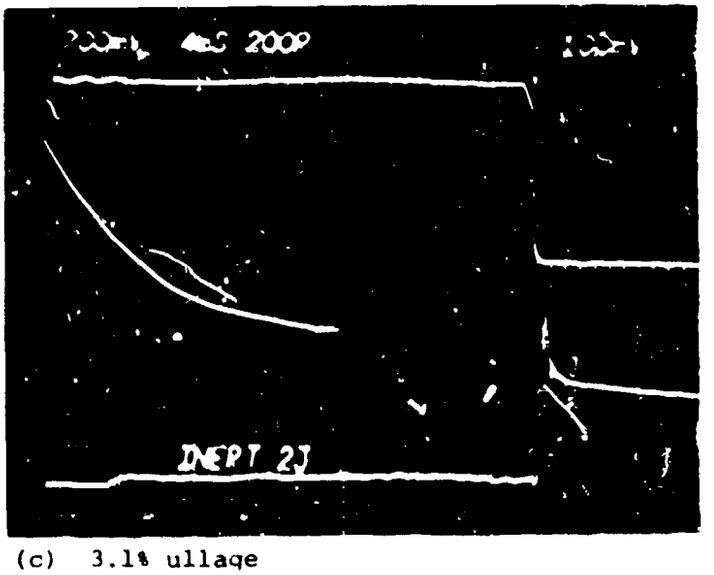

(c) 3.1% ullage

FIGURE 5a. OSCILLOGRAPH RECORDS OF WATER TESTS: 300 psig DRIVER PRESSURE.

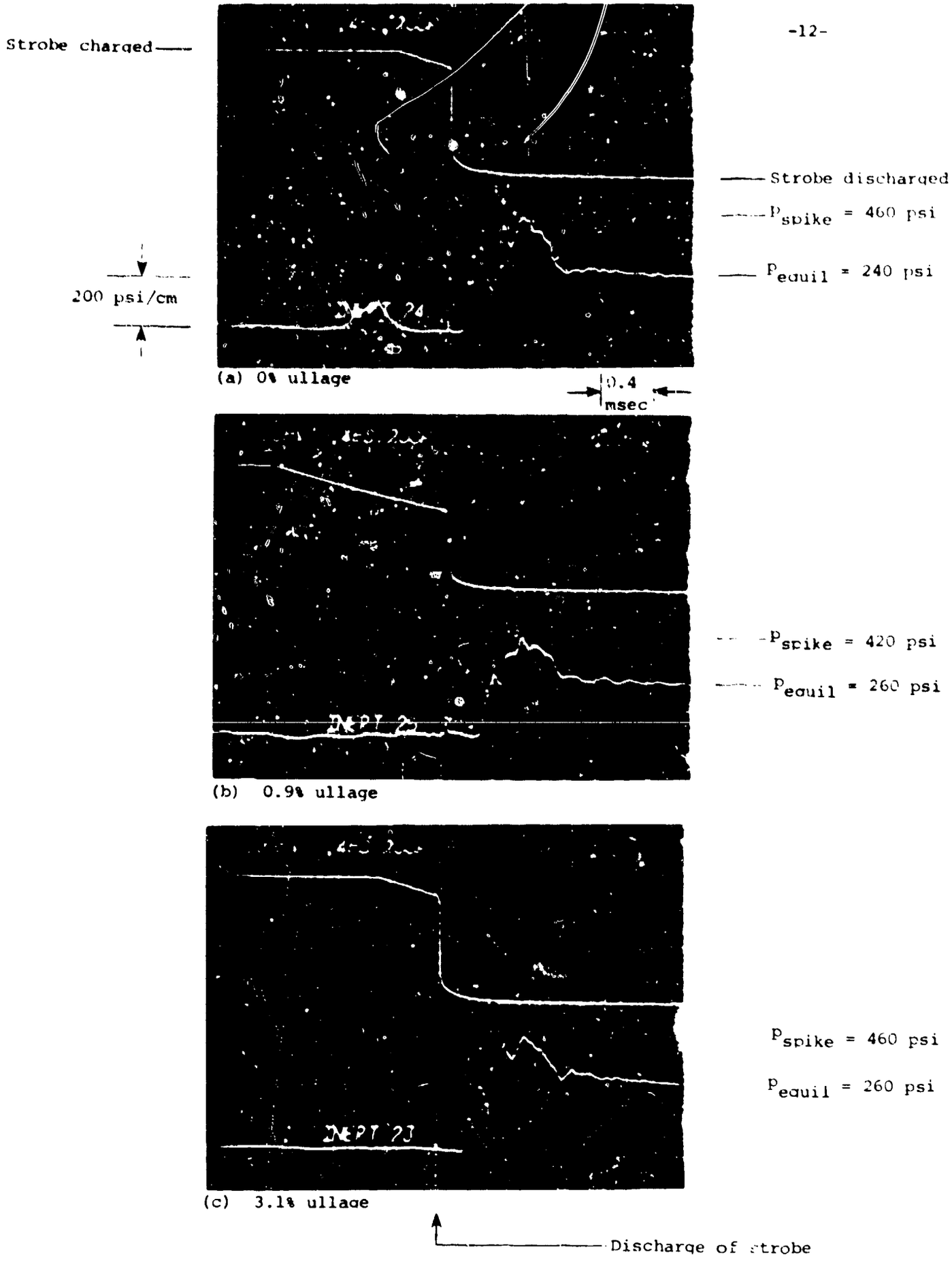

FIGURE 5b. EXPANSION OF OSCILLOGRAPH RECORDS

DRIVING PRESSURE: 300 psig

RUN NO.	LIQUID TYPE	ULLAGE (volume%, STP)	t_{fill} (msec)	p_{spike} (psig)	p_{equil} (psig)	d_{mean} (inch)
24	WATER	0.0	28.0	460	240	0.007
25	WATER	0.9	32.0	420	260	0.009
23	WATER	3.1	30.4	460	260	0.009
11	NOS-365	0.0	21.0	540	210	0.008
12	NOS-365	0.9	22.0	480	200	< 0.001
14	NOS-365	3.1	20.0	540	200	< 0.001

Note: The scale factor enployed in the Flow Visualization photographs is obtained by noting that the Kristal Type 601A Pressure Transducer port threads are machined 3/8-24 , i.e., a thread spacing of 0.0417 inch.

TABLE 1 TABULATION OF RESULTS OF VISUALIZATION STUDIES CONDUCTED WITH WATER AND NOS-365 LIQUID MONOPROPELLANT AT A DRIVING PRESSURE OF 300 psig.

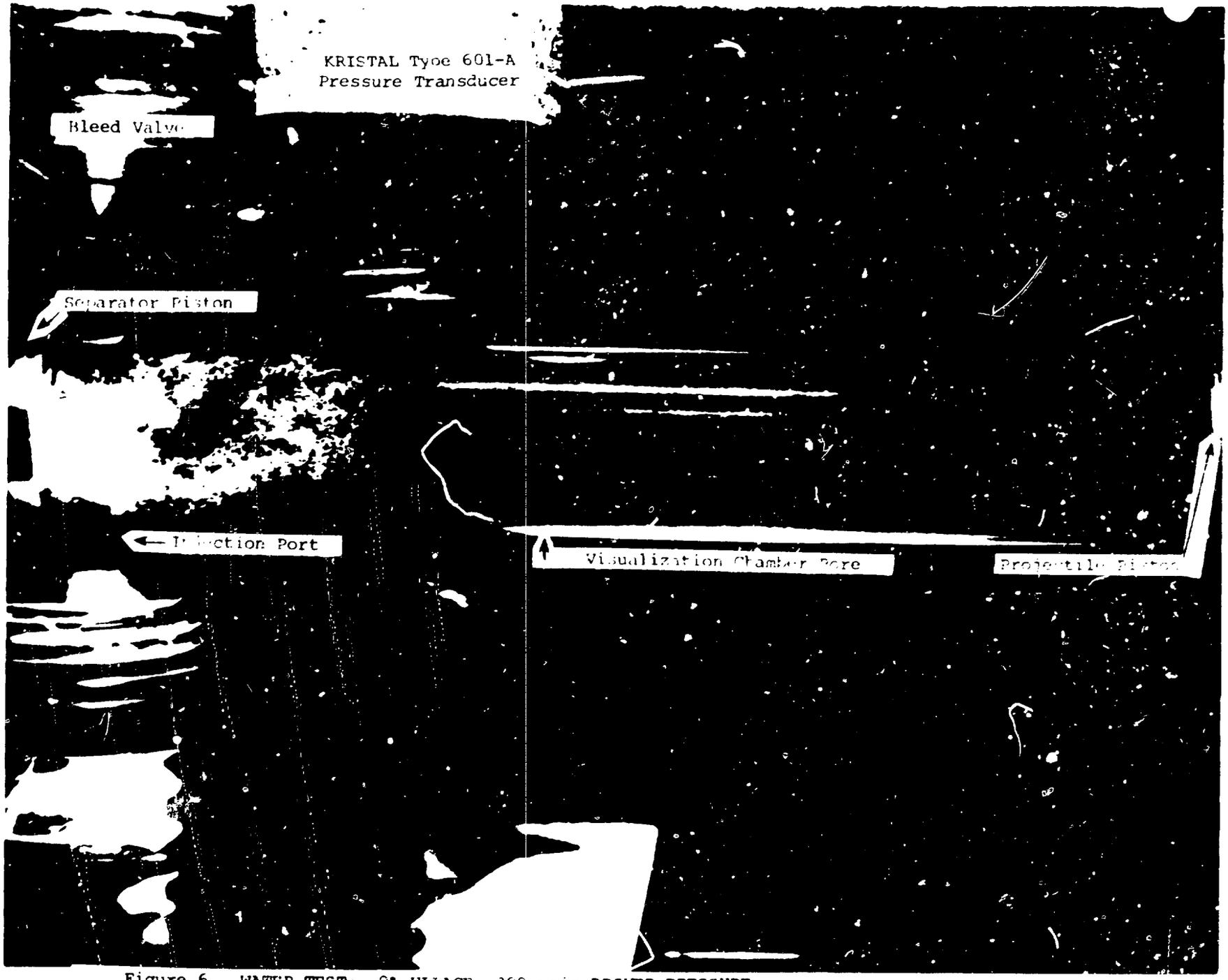

Figure 6. WATER TEST: 0% ULLAGE, 300 psig DRIVER PRESSURE

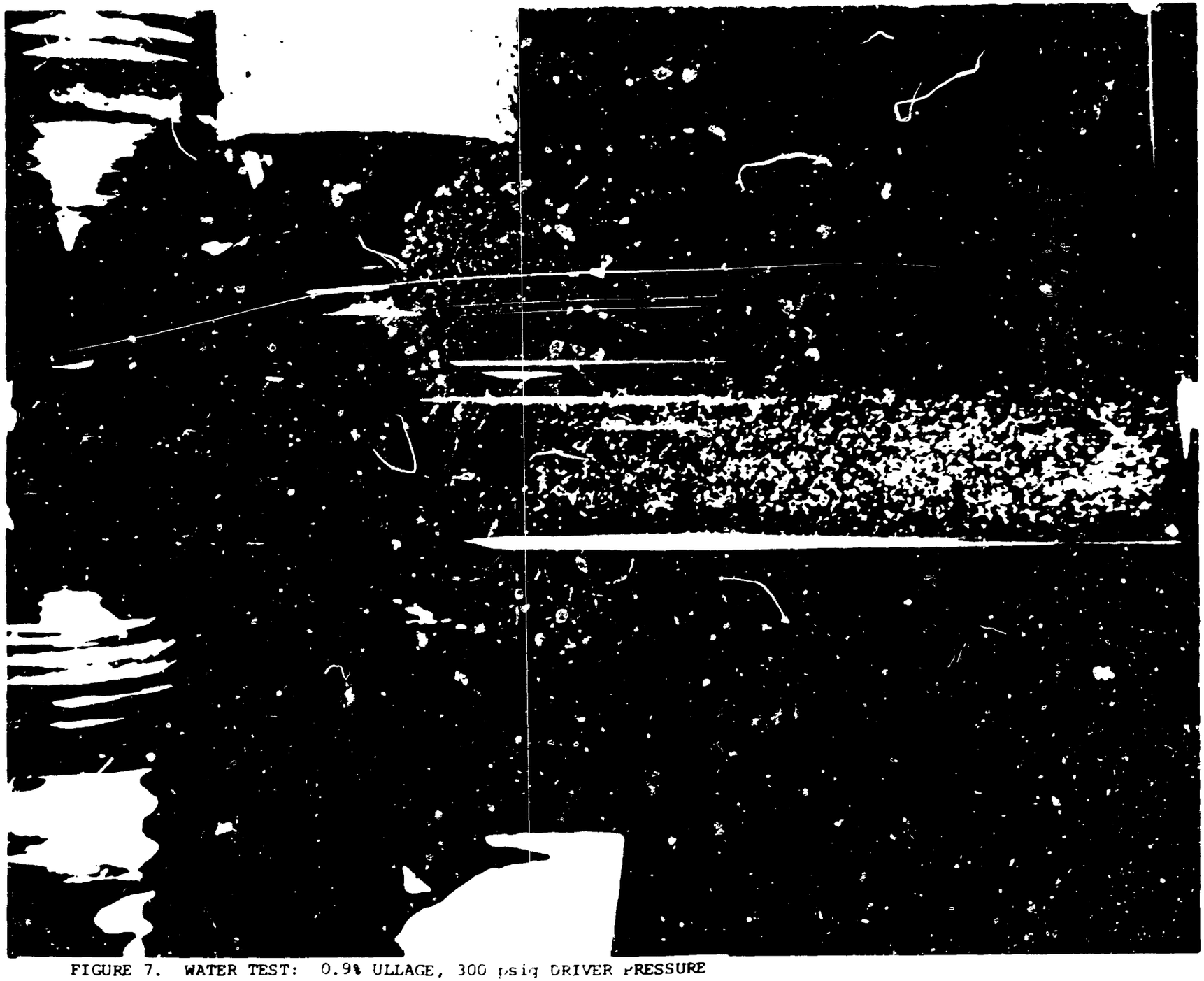

FIGURE 7. WATER TEST: 0.9% ULLAGE, 300 psig DRIVER PRESSURE

FIGURE 8. WATER TEST: 3.1% ULLAGE, 300 psig DRIVER PRESSURE.

photograph is taken, the "water hammer" pressure wave generated at the extreme right hand side of the liquid column by the slamming of the Projectile Piston against the End Plug has not yet propagated to the injection port location. Therefore the Poppet Valve is still in the open position, awaiting the pressure signal to propagate back through the liquid charge. Near the injection port, this cloud of vary fine bubbles is believed to be due to cavitation in the flow guide, producing bubbles of water vapor, which then rapidly condense and disappear further downstream. This cavitation phenomenon is not seen in the 0.9% ullage case (Figure 7). This could be due to the coincidence that the electronic strobe was discharged slightly later in time compared with the 0% ullage test, allowing vapor bubbles in the cavitation region to condense. The mean bubble diameter for the zero percent ullage case taken over a large enough sample of the bubbles downstream of the injection port, is 0.007 inch.

Figure 7 displays the bubble distribution for the case of 0.9% volumetric loading of air ullage. The mean bubble diameter for this case is 0.009 inch. By comparison of this case with the results of the zero percent ullage case, one could estimate that the zero ullage case may have about 0.1% of dissolved air and that this dissolved air tends to come out of the solution at the injector port where cavitation would take place. This is not surprising since de-aerated water is not used for the tests.

Figure 8 displays the bubble distribution for the case of 3.1% volumetric loading of air ullage. The mean bubble diameter for this case is 0.009 inch. Intense turbulent mixing can be seen in the vicinity of the injector port.

2.3.2 NOS-365 Liquid Monopropellant Tests

The first series of liquid monopropellant dynamic loading tests were conducted at a driving pressure of 300 psig with ullage volumes of 0%, 0.9%, and 3.1%. Figures 9a and 9b display oscillograph records of these propellant loading tests. The records of Figure 9b represent time expansions of the traces in Figure 9a in the neighborhood of the pressure spike. Propellant fill times, extracted from Figure 9a, are considerably less than corresponding fill times for water loading tests, i.e., ca. 20 msec for NOS-365 compared to 30 msec for water. Also, the spike pressure is increased to ca. 540 psig. A lower equilibrium pressure is attained in the propellant column, associated with a slightly increased Poppet Valve Spring compression.

Figures 10, 11, and 12 are photographs of the dynamically-loaded propellant column. These correspond, respectively, to 0%, 0.9%, and 3.1% volumetric loading of air ullage. The zero percent ullage case, Figure 10, shows results very similar to that of water, with intense cavitation action near the injector port and a mean bubble diameter in the column downstream of the injection port of approximately 0.008 inch.

(a) 0% Ullage

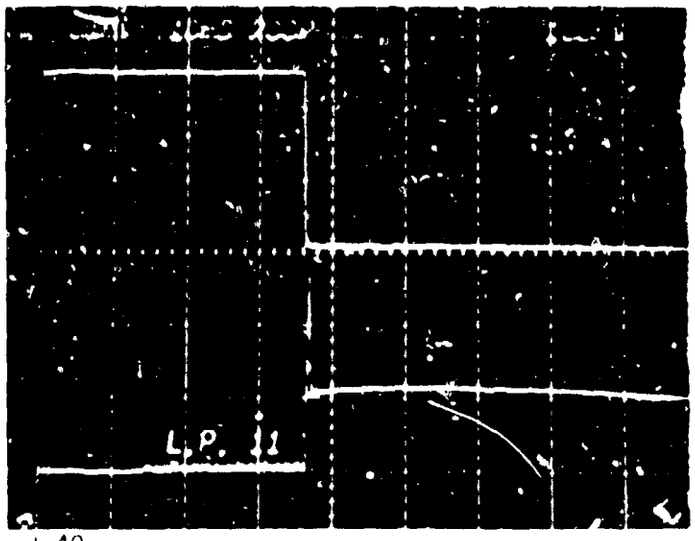

Strobe voltage

Liquid Pressure

200 psi/cm

40 msec

10 msec/cm

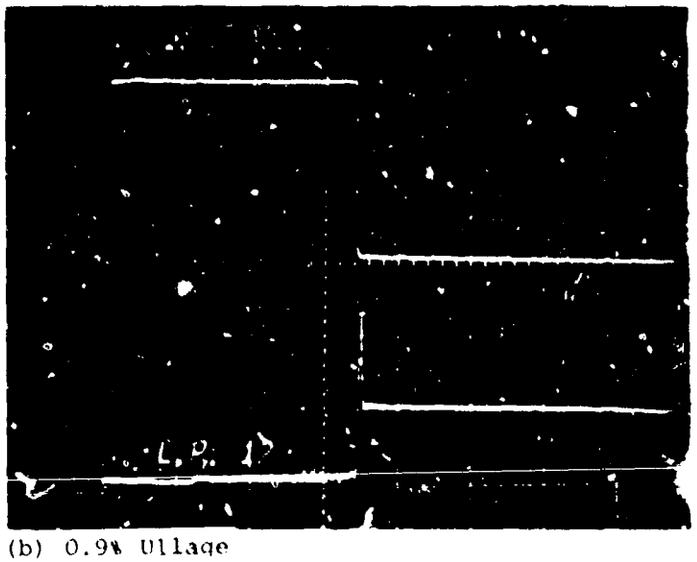

(b) 0.9% Ullage

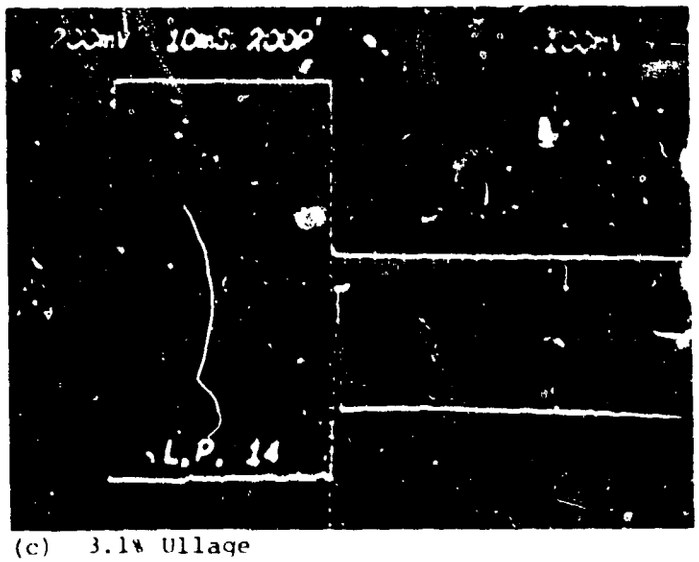

(c) 3.1% Ullage

FIGURE 9a. OSCILLOGRAPH RECORDS OF NOS-365 TESTS: 300 psig DRIVER PRESSURE

Strobe charged

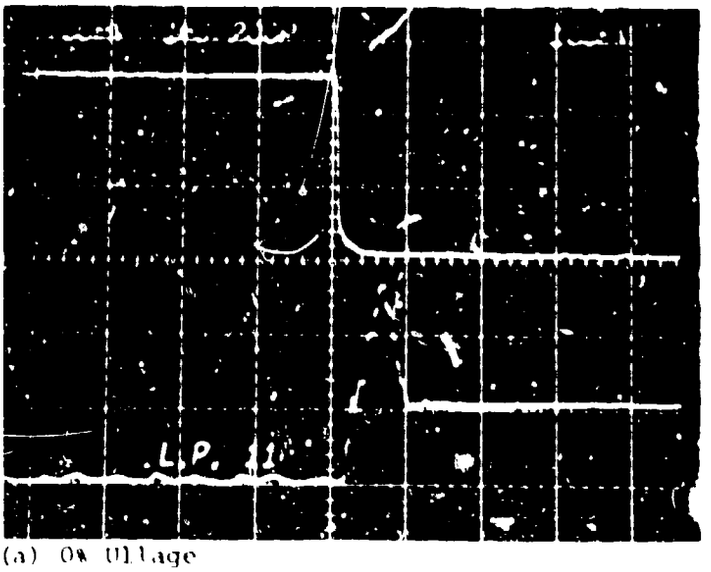

Strobe discharged

P_{spike} = 540 psi

P_{equil} = 210 psi

200 psi/cm

(a) 0% Ullage

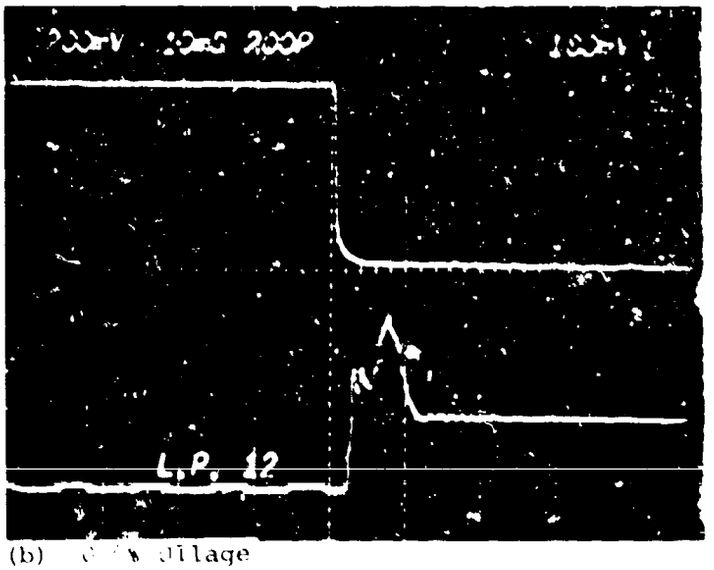

P_{spike} = 400 psi

P_{equil} = 200 psi

(b) [illegible] Ullage

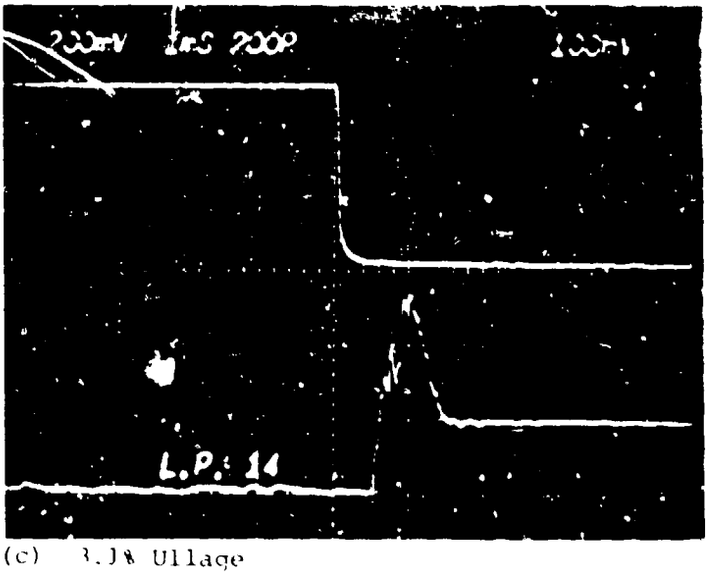

P_{spike} = 540 psi

P_{equil} = 200 psi

(c) 3.1% Ullage

Discharge of strobe

FIGURE 9b. EXPANSION OF OSCILLOGRAPH RECORDS

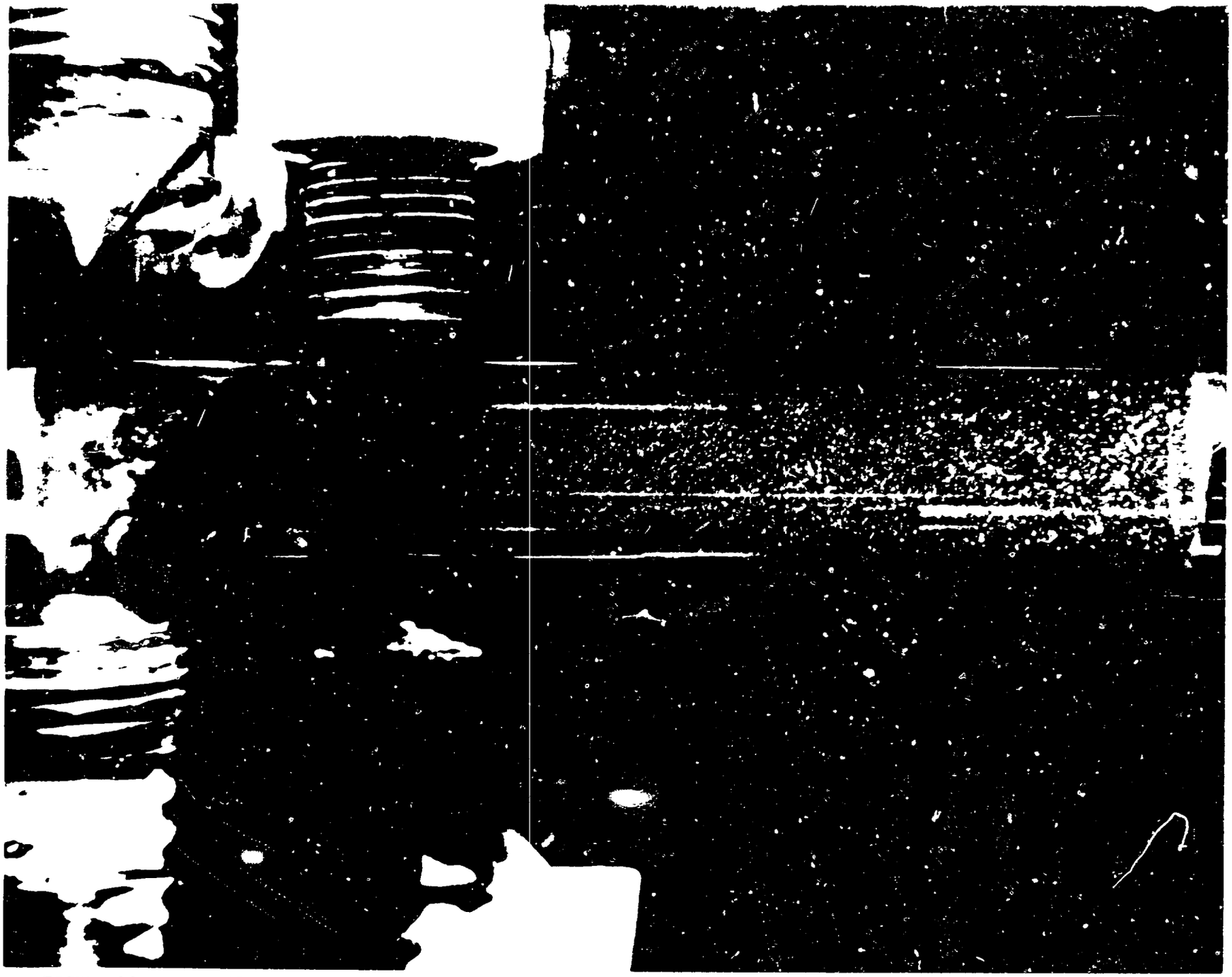

FIGURE 10. NOS-365 TEST: 0% ULLAGE, 300 psig DRIVER PRESSURE

FIGURE 11. NOS-365 TEST: 0.9% ULLAGE, 300 psig DRIVER PRESSURE

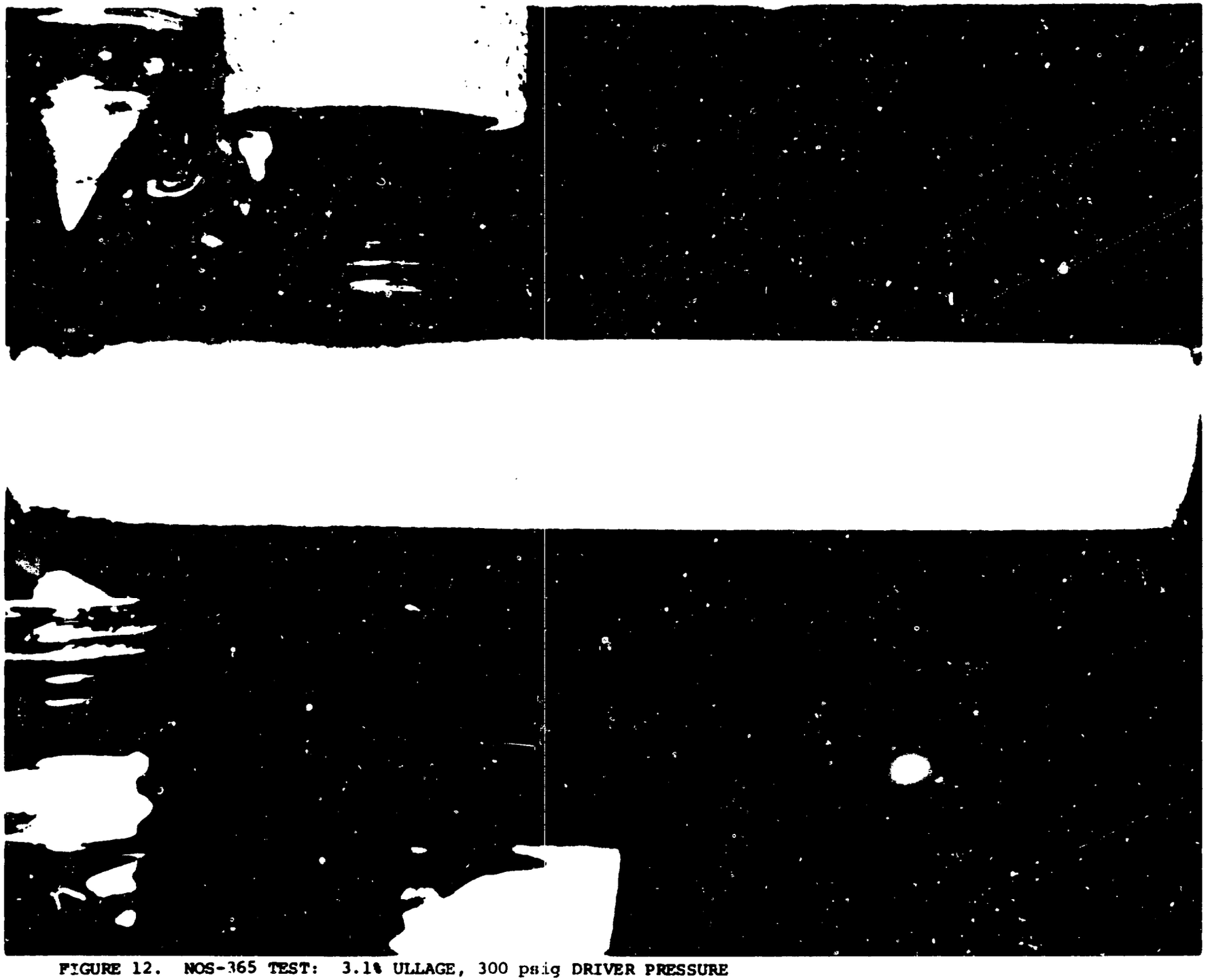

FIGURE 12. NOS-365 TEST: 3.1% ULLAGE, 300 psig DRIVER PRESSURE

Figure 11, depicting the physical condition of the dynamically-loaded propellant charge with 0.9% volumetric air loading, displays a "fog-like" appearance. The mean bubble diameter is less than 0.001 inch for this case.

Figure 12, the case of 3.1% volumetric air loading produces a "fog" that is nearly opaque. No bubbles of measureable diameter can be seen. It is reasonable to assume that the mean bubble diameter for this case is considerably less than 0.001 inch.

We can summarize these results as follows. Under identical conditions of ullage loading and driving pressure, the bubbles generated in NOS-365 liquid monopropellant are considerably smaller than those generated in water, by a factor on the order of 10. We suspect that surface tension plays a major contributing role in altering the ultimate size. It may be worthwhile for further experimentation to be performed with water and added surfactants and perhaps with more viscous liquids in order to understand more accurately the factors that determine the bubble size. This could be of immense practical importance as a means of ensuring that all bubbles created in a practical LPG fill procedure are smallest possible size(safest when considering compression-ignition sensitivity).

We anticipate that bubble size can be controlled by adjusting the driving pressure and hence the time of injection associated with the Pneumatic Load L.P. Cylinder. We expect that bubbles of finer or coarser diameter can be established by choosing either faster or slower fill times, i.e., higher or lower driving pressure. Two additional series of tests were conducted with NOS-365 liquid monopropellant with driving pressures of 500 psig and 150 psig. Note that the 150 psig driving pressure is just sufficient to drive the pneumatic piston and open the Poppet Valve, thereby injecting liquid into the Transparent Visualization Chamber.

Figures 13a and 13b display oscillograph records of propellant dynamic loading tests with a driving pressure of 500 psig. Table 2 contains information extracted from the oscillograph records on Visualization Chammer fill time, spike pressure , and equilibrium pressure in the liquid column. Figures 14, 15, and 16 are photographs of dynamically-loaded propellant column under a driving pressure of 500 psig. These correspond, respectively, to 0%, 0.9%, and 3.1% volumetric loading of air ullage. Figure 14, the zero percent ullage case, shows significant departure from the equivalent case at a driving pressure of 300 psig. Finer bubbles can now be observed, dispersed throughout the column. The mean bubble diameter is reduced to 0.004 inch, approximately one-half of that observed for the 0% ullage, 300 psig driving pressure case. Figure 15, the 0.9% ullage case at 500 psig driving pressure,shows remarkable similarity to the opaque "fog" produced in the 3.1% ullage, 300 psig driving pressure case. The mean bubble diameter is estimated to be considerably less than 0.001 inch. Increasing the ullage to 3.1% volumetric loading at a driving pressure of 500 psig results in a photograph (Figure 16) much like that of the 0.9% ullage case. The fineness of the ullage break-up into tiny bubbles cannot be resolved to any better than 0.001 inch.

(a) 0% Ullage

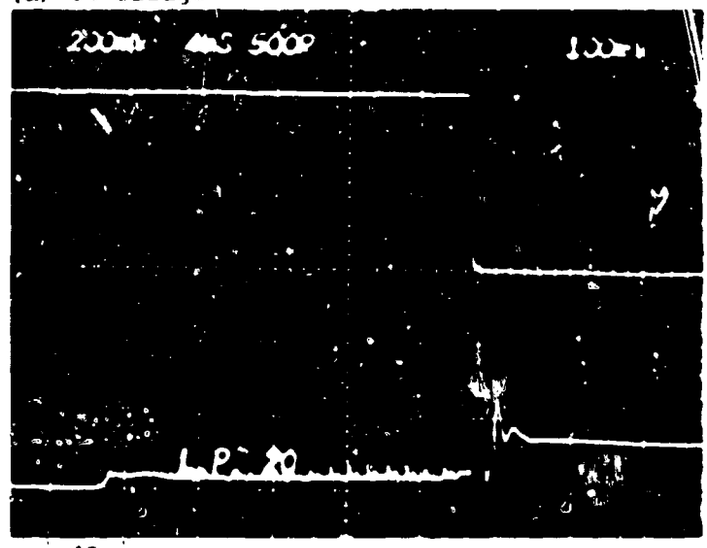

— strob voltage

— liqu d pressure

200 psi/cm

40 msec

4 msec/cm

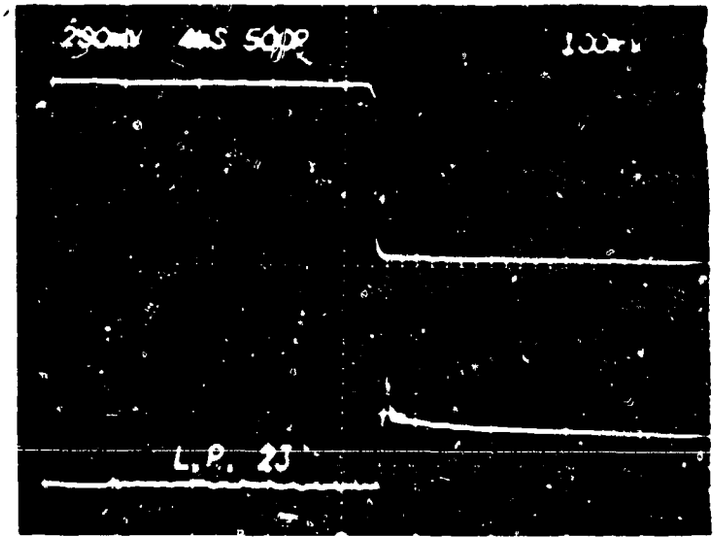

(b) 0.9% Ullage

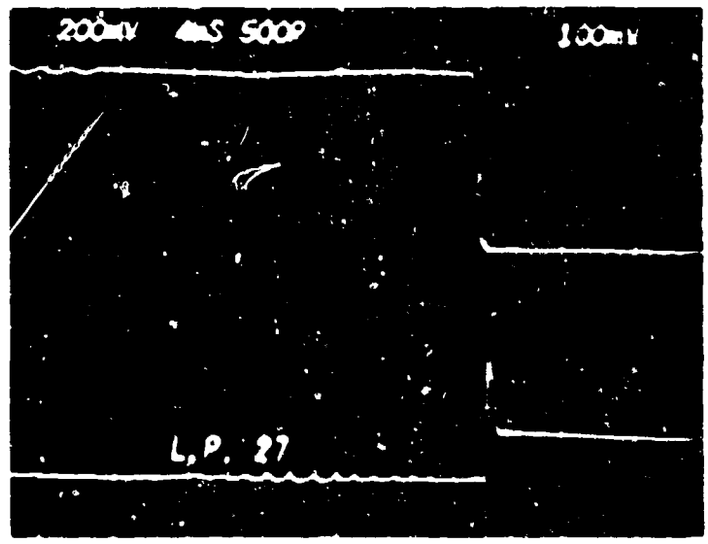

(c) 3.1% Ullage

FIGURE 13a. OSCILLOGRAPH RECORDS OF NOS-365 TESTS: 500 psig DRIVER PRESSURE

Strobe charged

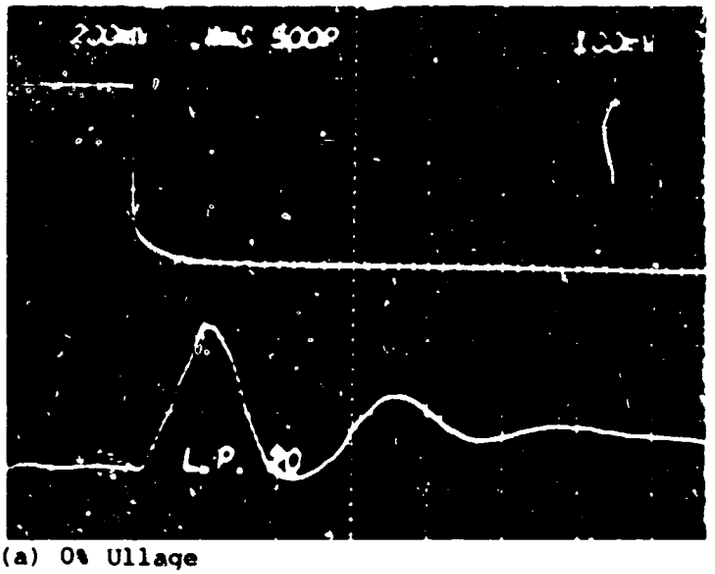

Strobe discharged

p_{spike} = 1100 psi

p_{equil} = 350 psi

200 psi/cm.

(a) 0% Ullage

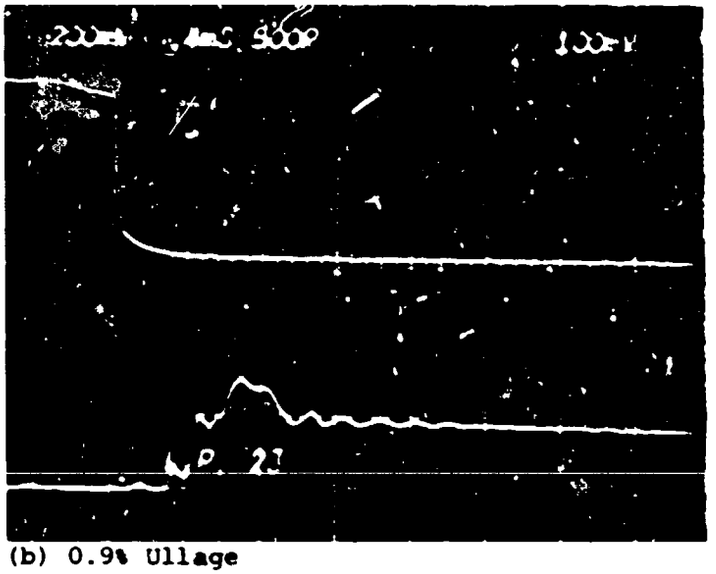

p_{spike} = 800 psi

p_{equil} = 400 psi

(b) 0.9% Ullage

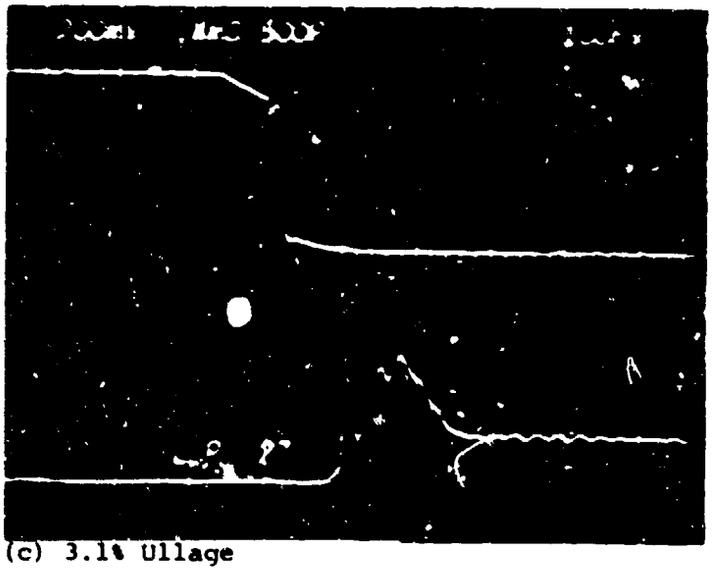

p_{spike} = 900 psi

p_{equil} = 300 psi

(c) 3.1% Ullage

FIGURE 13b. EXPANSION OF OSCILLOGRAPH RECORDS

DRIVING PRESSURE: 500 psig

RUN NO.	LIQUID TYPE	ULLAGE (VOLUME %, STP)	t_{fill} (msec)	P_{spike} (psig)	P_{equil} (psig)	d_{mean} (inch)
20	NOS-365	0.0	20.8	1100	350	0.004
23	NOS-365	0.9	22.0	800	400	< 0.001
27	NOS-365	3.1	16.0	900	300	< 0.001

TABLE 2. TABULATION OF RESULTS OF VISUALIZATION STUDIES CONDUCTED WITH NOS-365 LIQUID MONOPROPELLANT AT A DRIVING PRESSURE OF 500 psig.

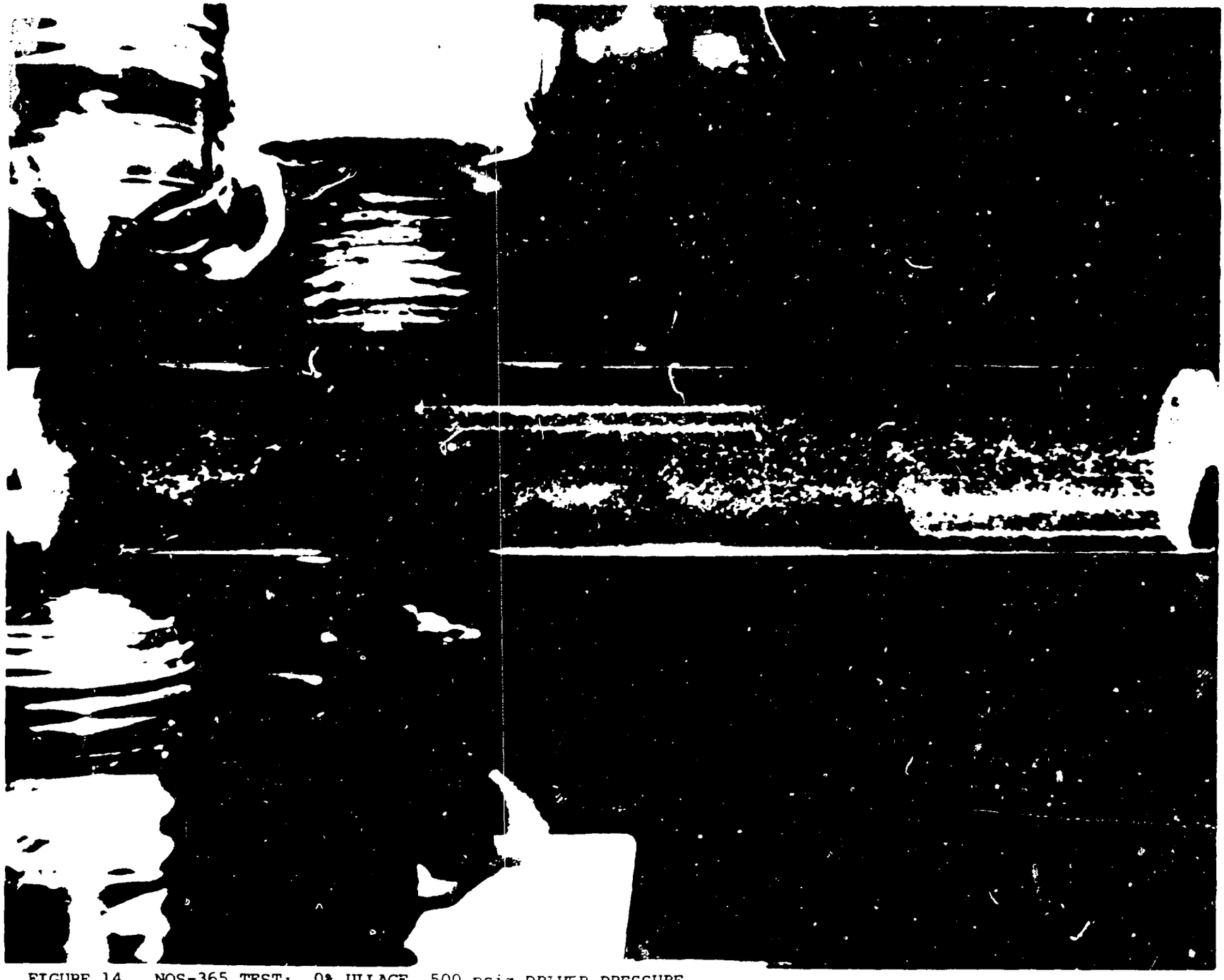

FIGURE 14. NOS-365 TEST: 0% ULLAGE, 500 psig DRIVER PRESSURE.

FIGURE 15. NOS-365 TEST: 0.9% ULLAGE, 500 psig DRIVER PRESSURE.

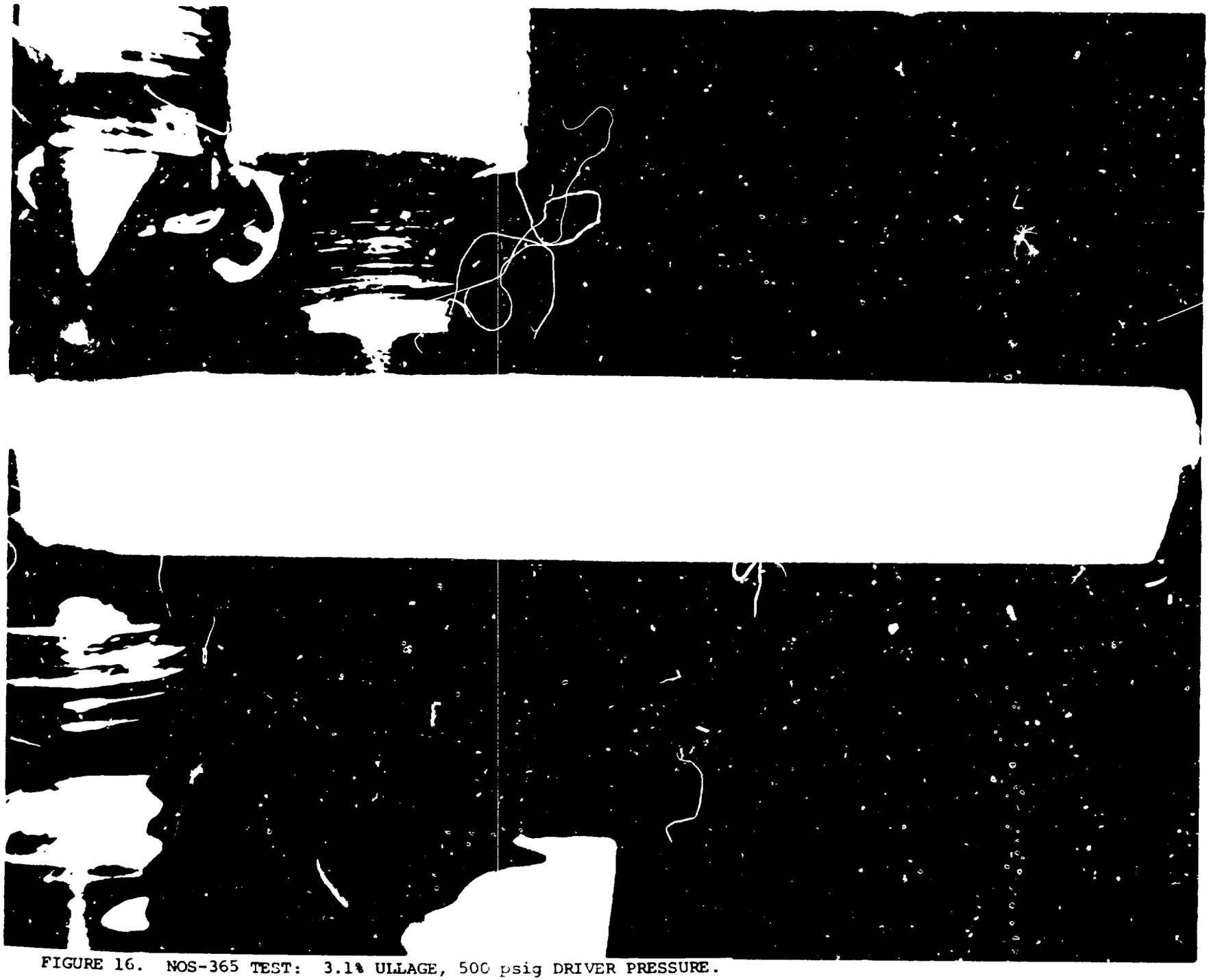

FIGURE 16. NOS-365 TEST: 3.1% ULLAGE, 500 psig DRIVER PRESSURE.

Photographs of the dynamic loading tests at a driving pressure of 150 psig are shown in Figures 17, 18, and 19 corresponding to 0%, 0.9%, and 3.1% volumetric air loading. Figure 17, the 0% ullage case, shows a liquid column relatively free of bubbles, indicating that the cavitation phenomenon is greatly reduced at this low driving pressure. The largest diameter bubbles can be seen in the center of the column length Bubbles with diameter as large a 0.023 inch can be observed. The effect of the low driving pressure on ullage break-up is more pronounced in Figure 18, the 0.9% ullage case. Large diameter bubbles and even undivided ullage can be seen superimposed on a field of well dispersed bubbles of mean diameter 0.009 inch. Bubbles with diameter as large as 0.045 inch can be seen in the column. Note that the "fog-like" quality of the liquid column observed in higher driving pressure tests, i.e., 300 psig and 500 psig, with NOS-365,and 0.9% ullage is not observed at this lower driving pressure. The subdivision of the original ullage loading in the flow guide and injector port is not as intense at low driving pressure. This same observation is borne out for the 3.1% ullage case, shown in Figure 19. The mean bubble diameter for this case is 0.006 inch, with bubbles well-distributed through the column length. The "fog-like" opaque liquid column as observed for the 3.1% ullage case at driving pressures of 300 psig and 500 psig is not observed at 150 psig driving pressure.

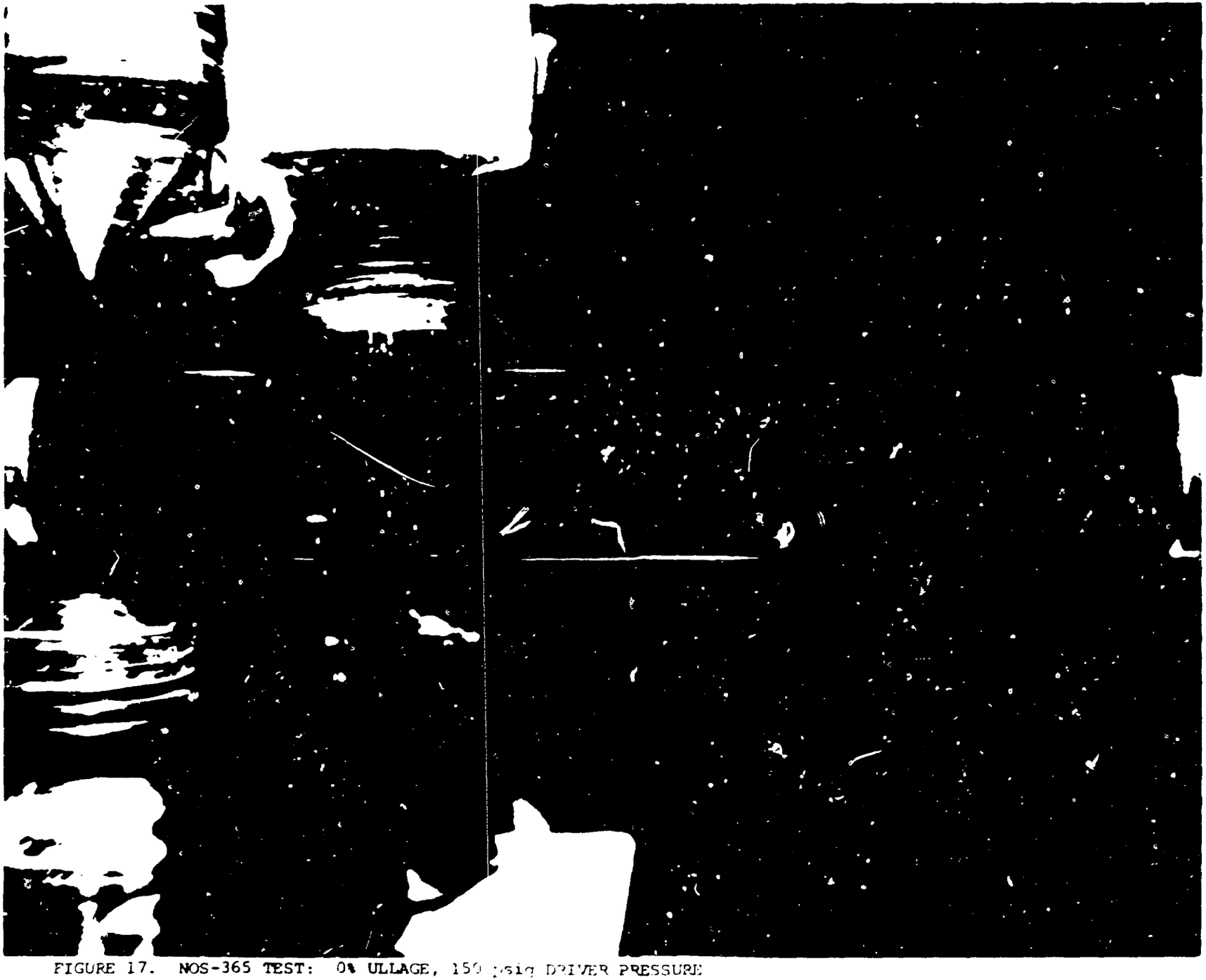

FIGURE 17. NOS-365 TEST: 0% ULLAGE, 150 psig DRIVER PRESSURE

FIGURE 18. NOS-365 TEST: 0.9% ULLAGE, 150 psig DRIVER PRESSURE

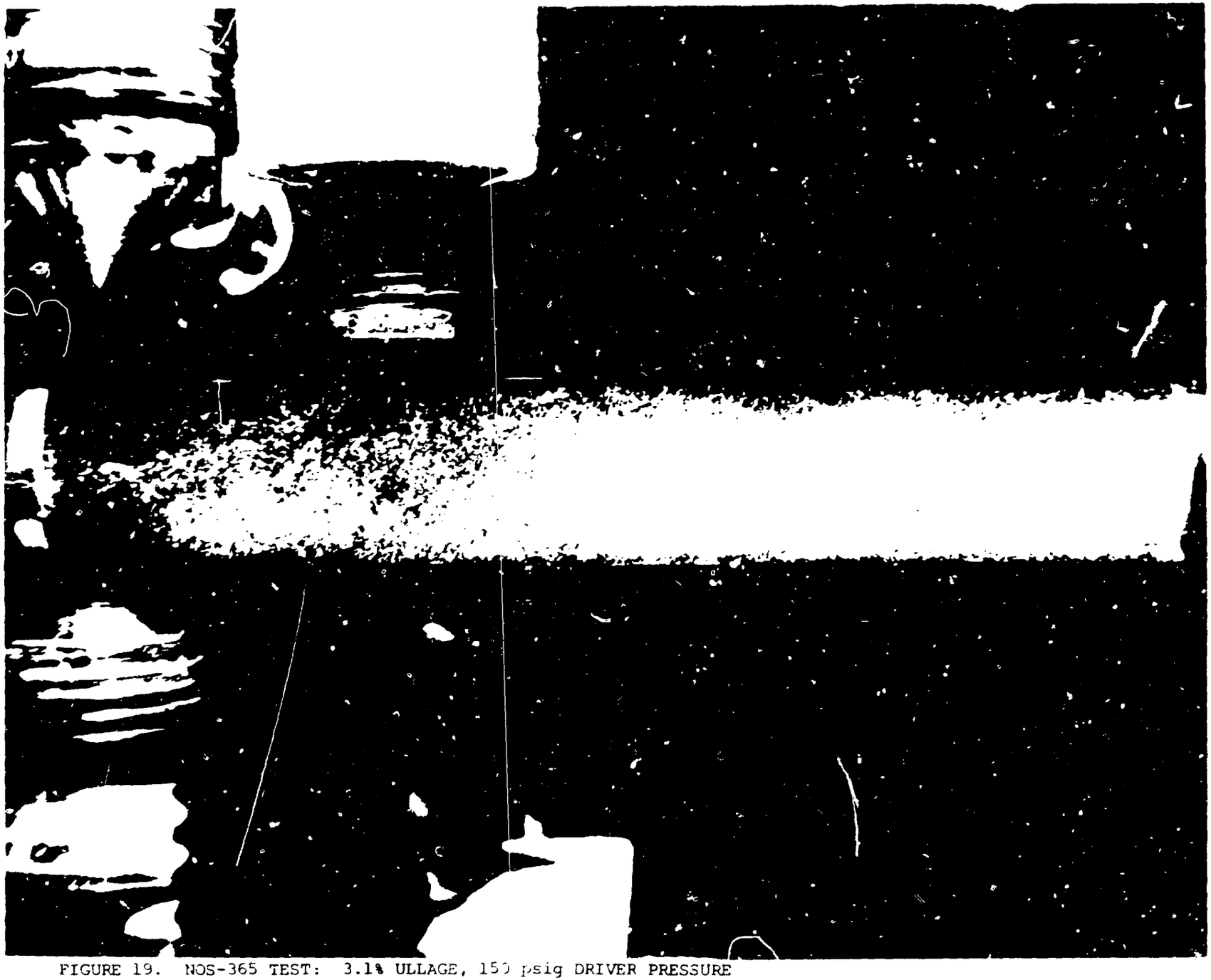

FIGURE 19. NOS-365 TEST: 3.1% ULLAGE, 150 psig DRIVER PRESSURE

2.4 Summary of Flow Visualization Test Results on Dynamic Loading Characteristics of a Liquid Charge.

1. The combination of Pneumatic Load L.P. Cylinder and Liquid Propellant Compression Chamber produces the desired physical state of the dynamically-loaded liquid propellant charge. A pre-compressed, multiple bubble, NOS-365 medium has been produced representing similar conditions found in other gun simulation studies.

2. The versatility of the system so designed has been established. Parameters under precise control are pre-compression liquid pressure level, fraction of initial ullage volume, mean bubble size in the dynamically-loaded column, and nature of the occluded gas.

3. The physical state of NOS-365 liquid monopropellant with varying fraction of air ullage, upon dynamic loading into the Transparent Visualization Chamber bore, is markedly different from that observed with inert (water) charges. In general, an opaque "fog-like" appearance of the NOS-365 column results with dynamic load, for driving pressures in the Pneumatic Load Cylinder greater than 300 psig. Subsequent compression-ignition analyses must take this physical observation into account.

4. The formation of bubbles in a dynamically-loaded "neat" propellant charge appears to result from cavitation effects in the flow guide and injection port. It is estimated that the resulting void volume may be as much as 0.1% of the total available chamber bore volume. At the "fire condition" of the compression-ignition sensitivity tests to be performed in the next phase of the project, it is anticipated that the cavitation vapor bubbles will not have returned to solution, since the time of "fire" is precisely the time that the photographic film was exposed.

5. Observed mean bubble diameter and distribution of bubbles in the dynamically-loaded liquid propellant column are quite repeatable in the 300 psig and 500 psig driver pressure tests. At low driving pressure, i.e., 150 psig, the nature of the ullage break-up is sensitive to the condition of the Pneumatic Load Cylinder bore surface and resulting "O"-ring friction. The subdivision of the initial ullage upon dynamic load is less reproducible at this extremely low driving pressure. It has been observed that pockets of gas are superimposed on a distribution of fine bubbles for low driving pressure tests. The characteristic "fog-like" appearance of the resulting liquid propellant column is not present at this low driving pressure.

6. It would definitely be worthwhile for experiments to be performed with water and added surfactants and with other liquid monopropellants, i.e., "LGP 1845", to understand the factors that determine bubble size and distribution in a dynamically-loaded column. It would also be instructive to alter the shape of the cavitation insert flow guide to purposefully alter the nature of the cavitation phenomenon. This, of course, all has a bearing on compression-ignition sensitivity of the resulting dynamically-loaded liquid propellant column.

3.0 Starter Charge Pressurization Rate Tests

In order to establish the threshold condition for runaway reaction in a liquid monopropellant leading to severe over-pressures and possible explosion, attention must first be directed toward control of the pressurization rate to which the dynamically-loaded liquid monopropellant column is subjected. Previous studies performed by Princeton Combustion Research Laboratories, Inc., Ref. 51,52, indicate that, for a given mean plateau pressure, the pressurization rate is an important parameter in determining sensitivity to compression-ignition. In those studies we found that the pressure-time start-up histories could be brought under precise control by varying the type of smokeless powder charge in the pressurizing chamber. In those studies the range of achievable pressurization rates was $1.25 \leq dp/dt$ (kpsi/msec) ≤ 150. Thus, the objective of this phase of the study was to establish "recipes", i.e., starter charge loading density and types of smokeless powders, to produce various pressure-time start-up histories to which the dynamically-loaded liquid monopropellant charge would be subjected for compression-igniton sensitivity analysis.

3.1 Description of Test Equipment

Figure 20 shows an assembly drawing of the Starter Charge Tester utilized in the Starter Charge Pressurization Rate Tests. The schematic drawing presented in Figure 21 identifies electrical connections for both instrumentation and firing circuit, vent gas, smokeless powder, and wadding locations. The Starter Charge Chamber is machined from a 3.5 inch diameter x 8 inch long bar of type 17-4PH stainless steel heat treated to condition H 1150 prior to machining. The chamber bore diameter is 1.00 inch. One end of the chamber bore has a 1 3/8-8N-2B internal threaded portion to accept the Electrical Primer Contact Assembly (P/N BUBBLE-1300). The other end of the chamber has a "neck"portion 1.3725 inch diameter and 1.250 inches long. This "neck" is machined with an O-ring groove for sealing purposes when the Starter Charge Chamber is mated with the Blind Chamber. A 0.88 inch length of the chamber body is machined with 3 1/2-8N-2A threads. These threads mate with the internal threads of the Chamber Coupling Collar to join the Starter Charge Chamber and Blind Chamber together.

The Blind Chamber (P/N BUBBLE-1005-A) was designed to allow calibration testing of the various starter charge mixes with an internal geometry that duplicates that of the more expensive and complex Liquid Propellant Compression Chamber. It, too, is machined from type 17-4PH stainless steel in the heat treated condition H 1150. The Blind Chamber is 3.5 inch in diamter by 2.5 inch long with a 0.95 inch length of 3 1/2-8N-2A external threads for mounting to the Coupling Collar. The central bore of the Blind Chamber , into which the "neck" of the Starter Charge Chamber fits, is 1.375 inch in diameter by 1.240 inch deep. A small bore 0.25 inch diameter by 0.50 inch long simulates the pressure communication passage between the Starter Charge Chamber and the isolated liquid column in the Liquid Propellant Compression Chamber. A PCB Type 119A piezoelectric gage is fitted into the Blind Chamber to monitor the pressure-time history within this passage due to the starter charge combustion. This P-t history is that which will be sensed by the Separator Piston compressing the liquid column during compression-ignition sensitivity testing.

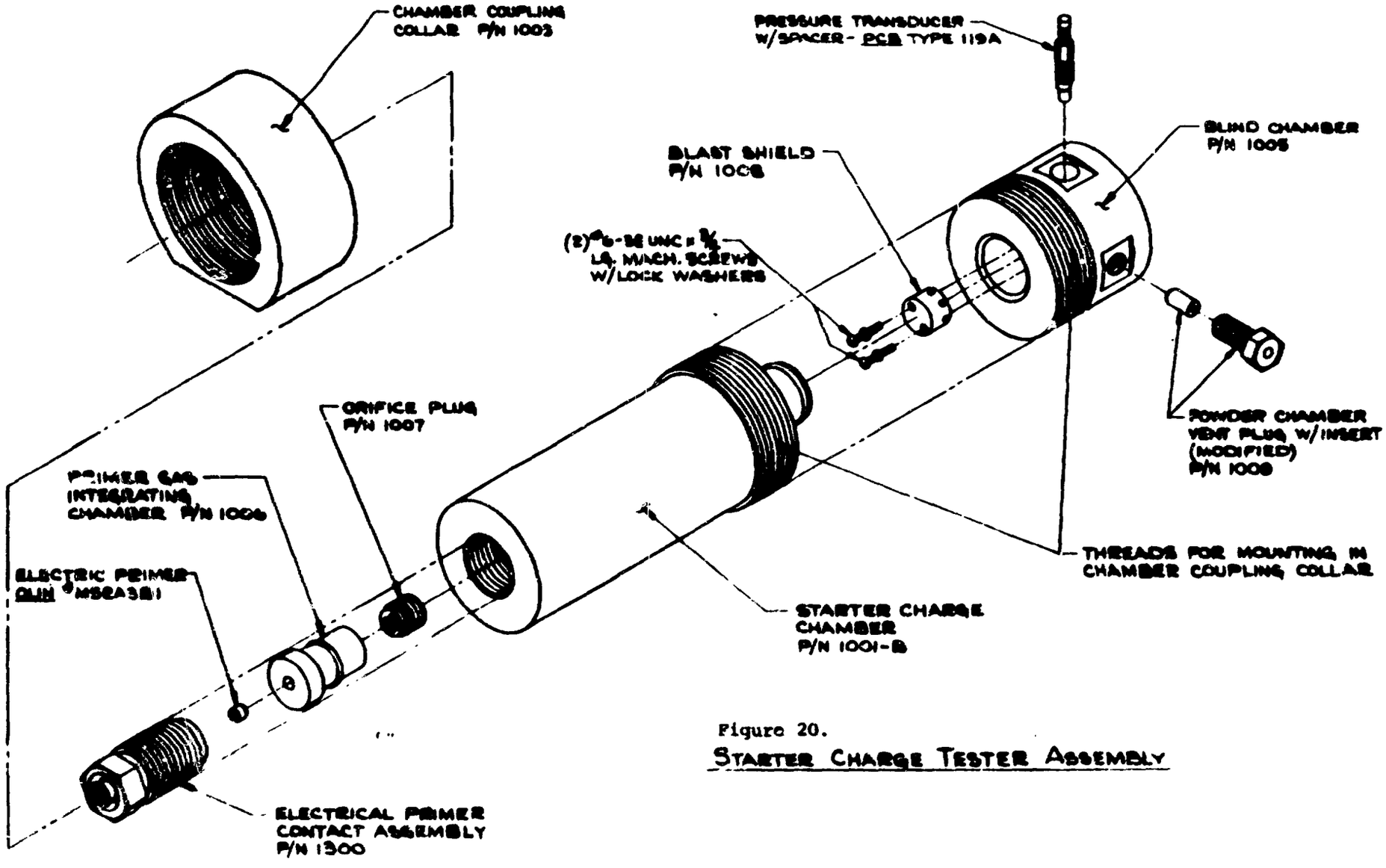

Figure 20.
STARTER CHARGE TESTER ASSEMBLY

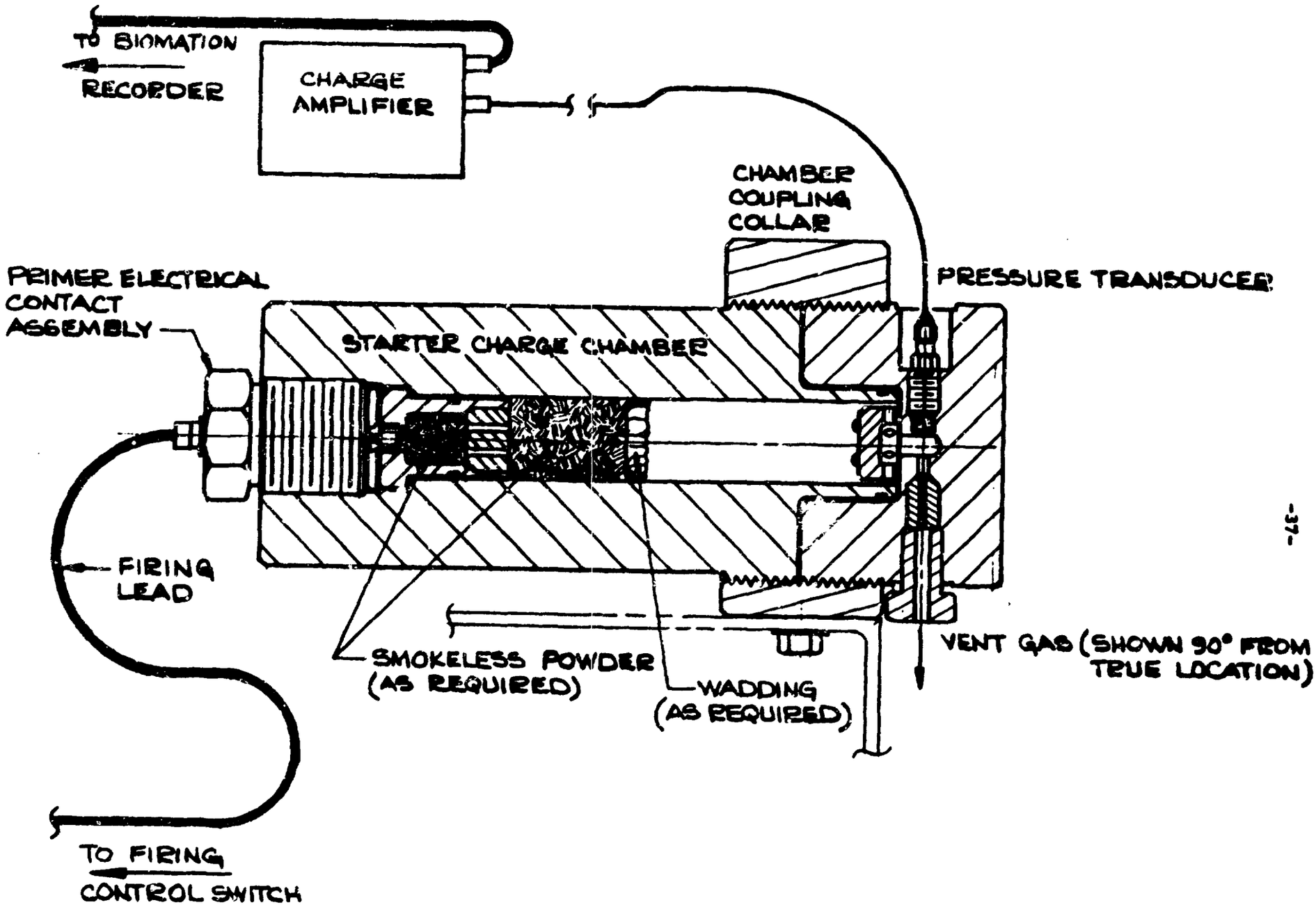

Figure 21. STARTER CHARGE TESTER SCHEMATIC
(SAFETY ENCLOSURE NOT SHOWN FOR CLARITY)

The Blast Shield (P/N BUBBLE-1008) fits over the 1/4 inch diameter pressure communication passage in the Blind Chamber and is designed to prevent the direct blast of burning powder and wadding from entering the passage. It is 0.87 inch in diameter by 0.50 inch high and machined from 17-4 PH stainless steel hardened to condition H 1025 after machining. Six 0.12 inch diameter holes are evenly spaced around the Shield periphery and connect to a center bore 0.375 inch in diameter by 0.25 inch deep. These holes allow gas pressure to communicate to the flow passage in the Blind Chamber. Two 0.152 inch diameter holes located 0.625 inch apart pass longitudinally through the Blast Shield to accomodate mounting screws.

The Chamber Coupling Collar (P/N BUBBLE-1003) is machined from a 2-inch thick plate of AISI 1020 carbon steel. It is 5 inches O.D. with 3 1/2-8N-2E threads spanning the 2" length of the collar. A milled flat with two 3/8-16 UNC-2B tapped holes located 1 7/8 inch apart provide a mounting surface for the collar. When the Starter Charge Chamber and the Blind Chamber are joined together and threaded into the Coupling Collar, the entire tester is supported by this mounting surface. The Chamber Coupling Collar provides a simple, high strength, fastening scheme for the chamber sections.

The combination of the Primer Gas Integrating (Fuse) Chamber (P/N BUBBLE-1006), the Orifice Plug (P/N BUBBLE-1007), and the Electric Primer (Olin #M-52A3B1) constitute the igniter assembly for the starter charge. When inserted into the Starter Charge Chamber, this assembly also provides a pressure seal for the chamber. The Integrating (Fuse) Chamber is machined from AISI 1020 carbon steel and is 1.63 inch long. One end has a machined bore to accept the electric primer. The M-52A3B1 primer is a center button contact, conductive mix type with a cup seal brass casing. The main body of the Integrating (Fuse) Chamber is 1.000 inch diameter with an "O"-ring groove machined 0.63 inch from the front edge. A shoulder 1.225 inch and 0.375 inch thick acts as a stop when the Integrating (Fuse) Chamber assembly is inserted into the Starter Charge Chamber. The main bore of the Integrating (Fuse) Chamber is 0.55 inch I.D. by 0.75 deep. The entrance bore is machined with 3/4-10 UN-2B threads for mounting the Orifice Plug.

The Orifice Plug is machined from a Grade 8 alloy steel 3/4-10 UN bolt. The plug is 0.55 inch long and has four (4) 0.0935 inch diameter thru holes located evenly spaced on a 0.3 inch diameter circle. These orifice holes meter the hot primer gases emerging from the Integrating (Fuse) Chamber into the main Starter Charge Chamber.

When threaded into the Starter Charge Chamber, the Primer Electrical Contact Assembly (P/N BUBBLE-1300) retains the Integrating (Fuse) Chamber assembly and provides the electrical current to the primer. The Contact Assembly is 2 1/4 inches long with a 1 1/4 inch wrench hex and 1 3/8-8N-2A threads. The Primer Electrical Contact Housing (P/N BUBBLE-1301) is made of AISI 1020 carbon steel rod and is machined to accept a BNC electrical connector at the hex end. A 0.076 inch diameter hole in the housing face allows the spring loaded Primer Electrical Contact Pin to make contact with the center button of the primer.

Combustion products of the smokeless powder starter charge are continuously vented from the chamber thru the Powder Chamber Vent Plug (P/N BUBBLE-1009).

The vent consists of an AISI 1020 carbon steel cylinder 0.410 inch diameter by 0.635 inch long. The sealing cone at one end is 88 degrees included angle. A 0.191 inch diameter by 0.50 inch long hard copper insert is press fit into the bore in the steel body. The copper carries a 0.053 inch diameter thru hole which serves as the vent hole. Copper is used because of resistance to high temperature erosion. A 1/2-13 hex bolt with a 3/16 inch diameter thru bore retains the vent in the Blind Chamber.

A photograph of the assembled Starter Charge Chamber and Blind Chamber is shown mounted in the test stand in Figure 22 .

3.2 System Operation

The Integrating (Fuse) Chamber is first loaded with smokeless powder. In all cases DuPont IMR 4198 was used. The mass loading can be varied, depending on the nature of the start-up pressurization history desired in the main Starter Charge Chamber. It has been our experience that pressurization rate delays (a pre-pressurization "stew") can be achieved with such an igniter configuration by decreasing the charge loading in the Integrating (Fuse) Chamber. This will be discussed further in the next section.

Once the Integrating (Fuse) Chamber is loaded, the Orifice Plug is threaded in place. The gas mass flow into the main Starter Charge Chamber can be precisely metered by appropriate choice of Orifice Plug. A thin layer of cellophane tape is used to cover the orifice holes to retain the powder. The Integrating (Fuse) Chamber and Electric Primer Contact Assembly are then fitted into the Starter Charge Chamber. Finally the remaining loading of smokeless powder is introduced into the bore of the chamber and retained with wadding. The complete Starter Charge Tester Assembly Procedure is presented in Appendix D.

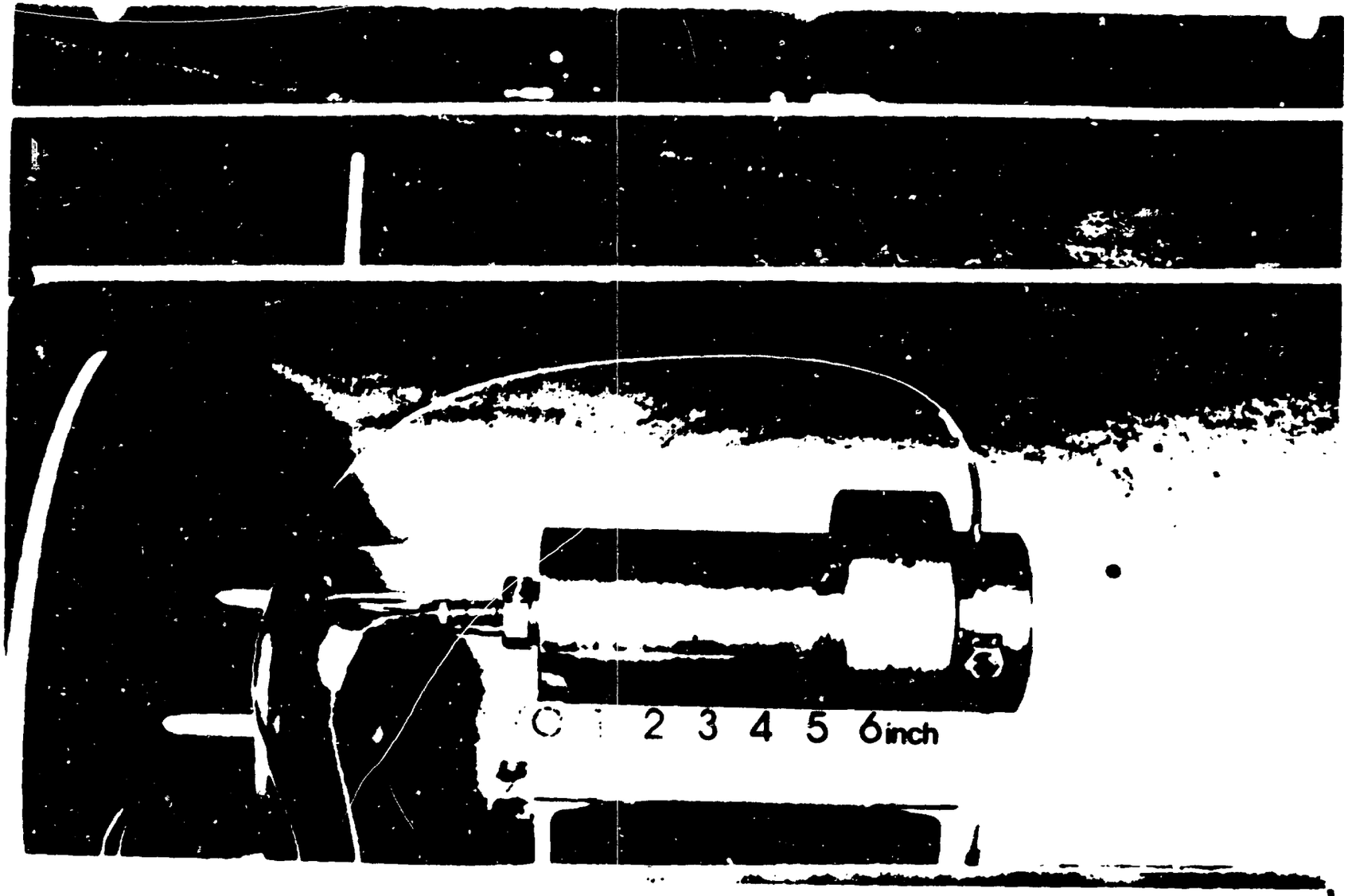

PRINCETON COMBUSTION RESEARCH LABORATORIES, INC.
1041 U S HIGHWAY ONE NORTH / PRINCETON, NEW JERSEY 08540

Figure 22. Photograph of Starter Charge Chamber and Blind Chamber Mounted in Chamber Coupling Collar for Starter Charge Pressurization Rate Tests.

3.3 Results of Starter Charge Tests

A cautious approach was taken in the starter charge test series in order to assure proper functioning of the starter charge chamber with associated electric primer assembly, fuse section, and orifice plug. Supporting thermochemical equilibrium calculations for DuPont IMR 4198 Smokeless Powder were performed with the "BLAKE" computer code to establish peak chamber pressure as a function of loading density in the chamber. The results of this computation are shown in Figure 23 , a plot of predicted equilibrium chamber pressure vs. loading density. Starter charge tests were performed for $\bar{\rho}$ = 0.075, 0.125, and 0.165 g/cc. In all cases 2.60 g of IMR 4198 powder were loaded into the Integrating (Fuse) Chamber. Resulting peak pressures, as sensed by the piezoelectric gage in the Blind Chamber, are plotted in Figure 23 , represented by open circles. The firing test resulting in a peak chamber pressure of 25 kpsi corresponds to a total of 10.15 g of DuPont IMR 4198 Smokeless Powder loading. By reducing the loading of the powder charge in the Integrating (Fuse) Chamber the onset of rapid chamber pressurization can be delayed. This corresponds to a low pressure pre-compressive interval in the p-t history, the duration of which is a function of the powder loading in the Fuse section. Likewise, a faster burning smokeless powder, such as Herco Shotgun Powder or Herco Pistol Powder will result in a more rapid chamber pressurization.

A summary plot of p-t start-up histories for various starter charges and loading densities is shown in Figure 24 . The range of achievable pressurization rates is seen to be 25 $\leq$ dp/dt (kpsi/msec) $\leq$ 100. The fastest pressurization rate, i.e., 100 kpsi/msec, is obtained with Herco Pistol Powder in the main chamber and an IMR 4198 fuse (Curve E). The slowest pressurization rate, i.e., 25 kpsi/msec, is obtained with 0.65 g of IMR 4198 and 10.57 g of IMR 4198 in the main chamber (Curve A). Curve A also displays a low pressure pre-compression interval, lasting approximately 2.5 msec prior to rapid pressurization.

Starter charge pressurization rate tests were limited to mean peak chamber pressures of 25 kpsi, although the apparatus has been designed to withstand testing with a mean peak chamber pressure of 50 kpsi. It was felt that all the phenomena of interest would be present at 25 kpsi mean peak chamber pressure. Also, since large excursions from the mean pressure can be anticipated in the liquid propellant compression chamber if explosion were to occur, it was felt it necessary to confine sensitivity testing to 25 kpsi mean peak chamber pressure in order to assess the magnitude of any pressure spikes.

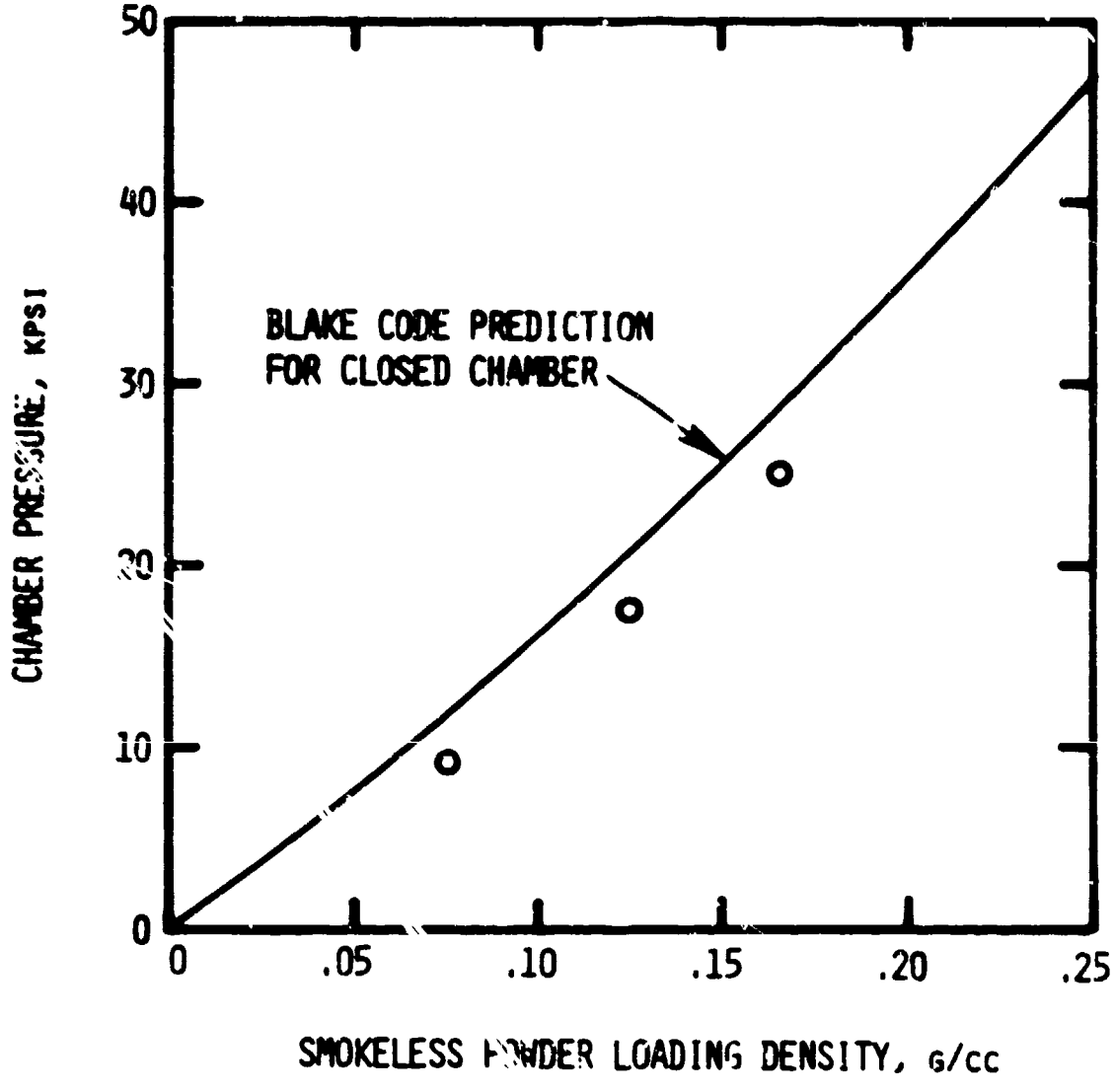

Figure 23. COMPARISON OF CHAMBER FIRINGS WITH DuPONT IRM 4198 SMOKELESS POWDER AND THERMOCHEMICAL EQUILIBRIUM CALCULATIONS.

STARTER CHARGE LOADINGS		
	INTEGRATING CHAMBER (FUSE SECTION)	MAIN CHAMBER
A	0.65g DuPont IMR 4198	10.57g DuPont IMR 4198
B	1.30g DuPont IMR 4198	9.92g DuPont IMR 4198
C	2.60g DuPont IMR 4198	7.55g DuPont IMR 4198
D	2.60g DuPont IMR 4198	7.00g Herco Shotgun Powder
E	2.60g DuPont IMR 4198	6.50g Herco Pistol Powder

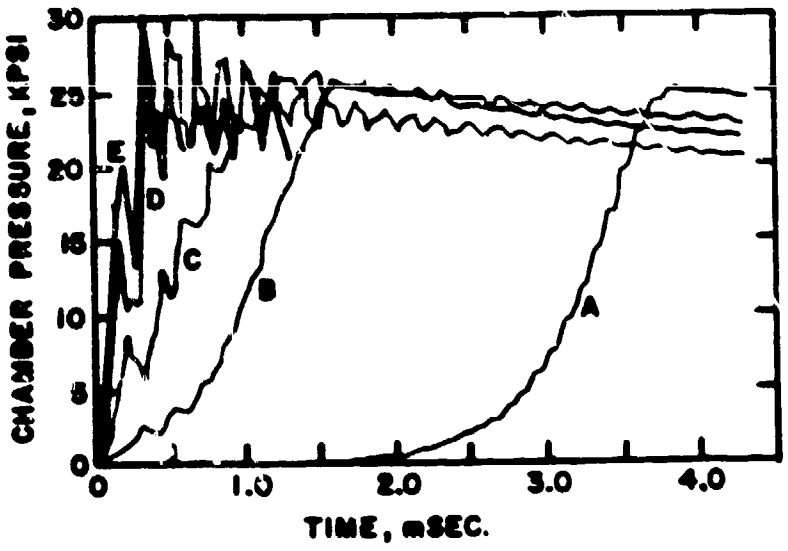

Figure 24. Pressurization Rate Histories for Various Starter Charge Mixes.

4.0 Compression-Ignition Sensitivity Studies of a Dynamically Loaded Liquid Propellant Charge

4.1 Description of Test Equipment

Figure 25 shows an assembly drawing of the L.P. Compression-Ignition Sensitivity Tester used in the experimental studies. Functional components such as valves, gas lines, liquid fill and discharge lines, gas vent, and electrical connections are presented in the schematic drawing Figure 26 . A complete description of the Starter Charge Chamber and associated components is given in Section 3.1 . The L.P. Compression Chamber (P/N BUBBLE-1002-C) mates with the Starter Charge Chamber via the Chamber Coupling Collar. The Compression Chamber is machined from type 17-4PH stainless steel in the H 1150 heat treated condition and measures 3.5 inch in diameter by 7 3/16 inch long. The main bore of the chamber is 0.4382 inch diameter and carries the Separator Piston (P/N BUBBLE-1100-A) and the Projectile Piston (P/N BUBBLE-1013). The Separator Piston prevents hot combustion gases from the Starter Charge Chamber from igniting the liquid propellant charge in the Compression Chamber bore. The Projectile Piston is utilized to facilitate chamber filling under dynamic loading and provides the trigger to actuate the ignition of the Starter Charge. The Vent Plug (P/N BUBBLE-1009-A) mounts in the Compression Chamber and provides continuous venting of starter charge combustion gases through its 0.053 inch diameter copper orifice. Hard drawn copper is used for the vent orifice insert because of its resistance to hot gas erosion.

The extreme end of the chamber is machined to accept the aluminum Shear Disc (P/N BUBBLE-1015) and the Disc Retainer (P/N BUBBLE-1016-A). The Shear Disc acts as a stop for the Projectile Piston during dynamic loading and, in the event of an overpressure (exceeding 65 kpsi) due to L.P. combustion, the Projectile Piston will shear thru the disc and allow the chamber to empty and depressurize rapidly. Mounted on the Disc Retainer is the Micro-switch Assembly which fires the electric primer when dynamic loading is complete. The L.P. Compression Chamber also contains a Bleed Valve for flushing residual ullage from the system prior to dynamic loading of the liquid propellant charge. The injection port is designed so as to accept various Flow Guides to alter the cavitation dynamics of the injected liquid.

The Pneumatic Load L.P. Cylinder (P/N BUBBLE-1004) is machined from type 416 stainless steel heat treated to Rockwell C30/38. The 0.50 inch diameter bore contains a Pneumatic Piston (P/N BUBBLE-1021) which transfers the liquid propellant charge through a Poppet Valve into the injection port of the L.P. Compression Chamber. The Pneumatic Load L.P. Cylinder acts as a liquid syringe to control the dynamic loading process. A regulated supply of N_2 gas fed through a Solenoid Valve provides the driving pressure for acceleration of the Pneumatic Piston. The injection time is controlled by this driving pressure, for a fixed volumetric loading of liquid propellant. The Poppet Valve controls the steady state (equilibrium) pressure in the L.P. Compression Chamber by adjusting the Poppet Valve Spring compression. The Pneumatic Load L.P. Cylinder contains a Silicon Rubber Septum through which a Gas Ullage Syringe passes to introduce a precise loading of air ullage (volume percent, STP). Liquid propellant is introduced into the Pneumatic Load L.P. Cylinder through a fill port equipped with a tube fitting and valving.

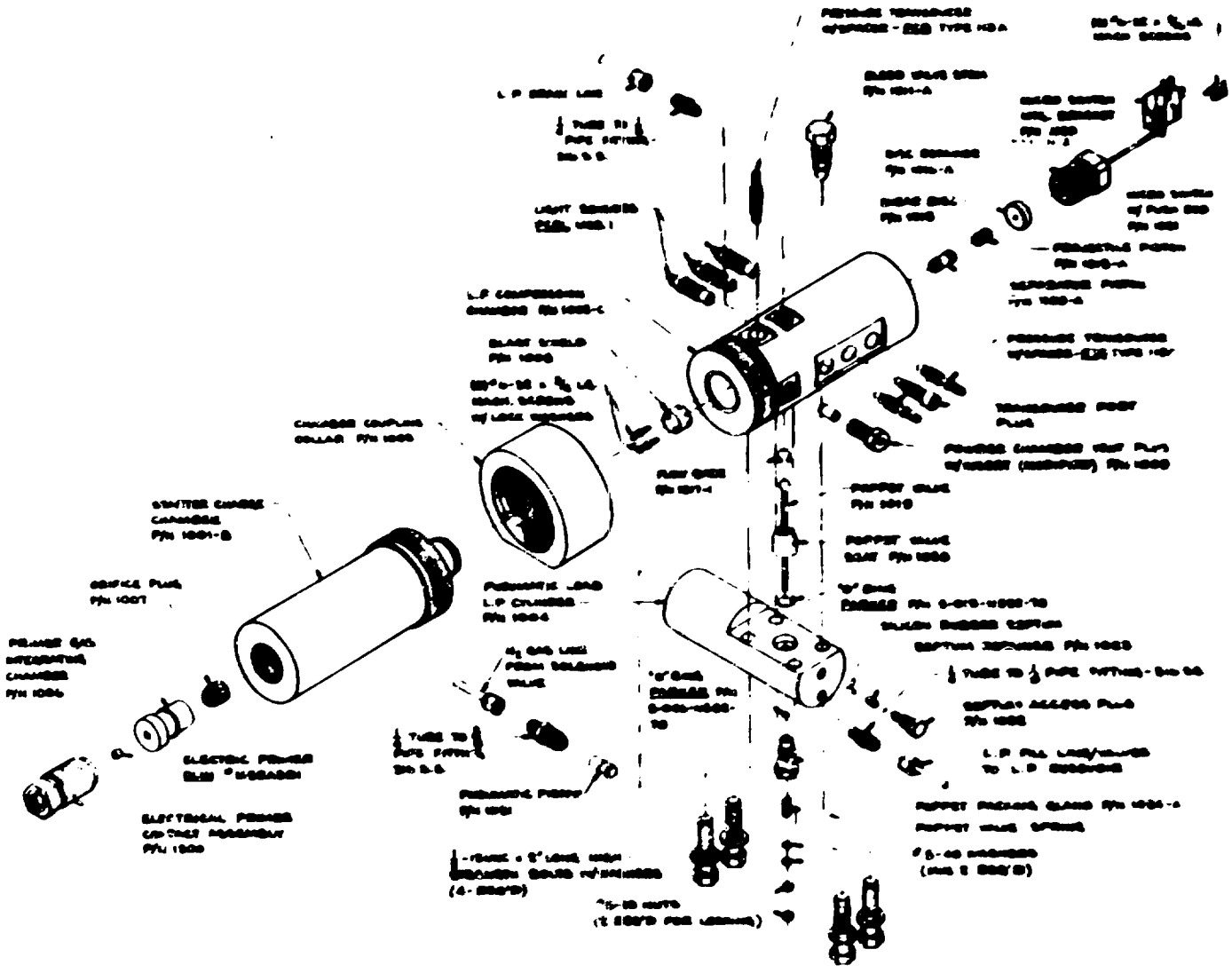

Figure 25. L.P COMPRESSION IGNITION SENSITIVITY TESTER ASSEMBLY

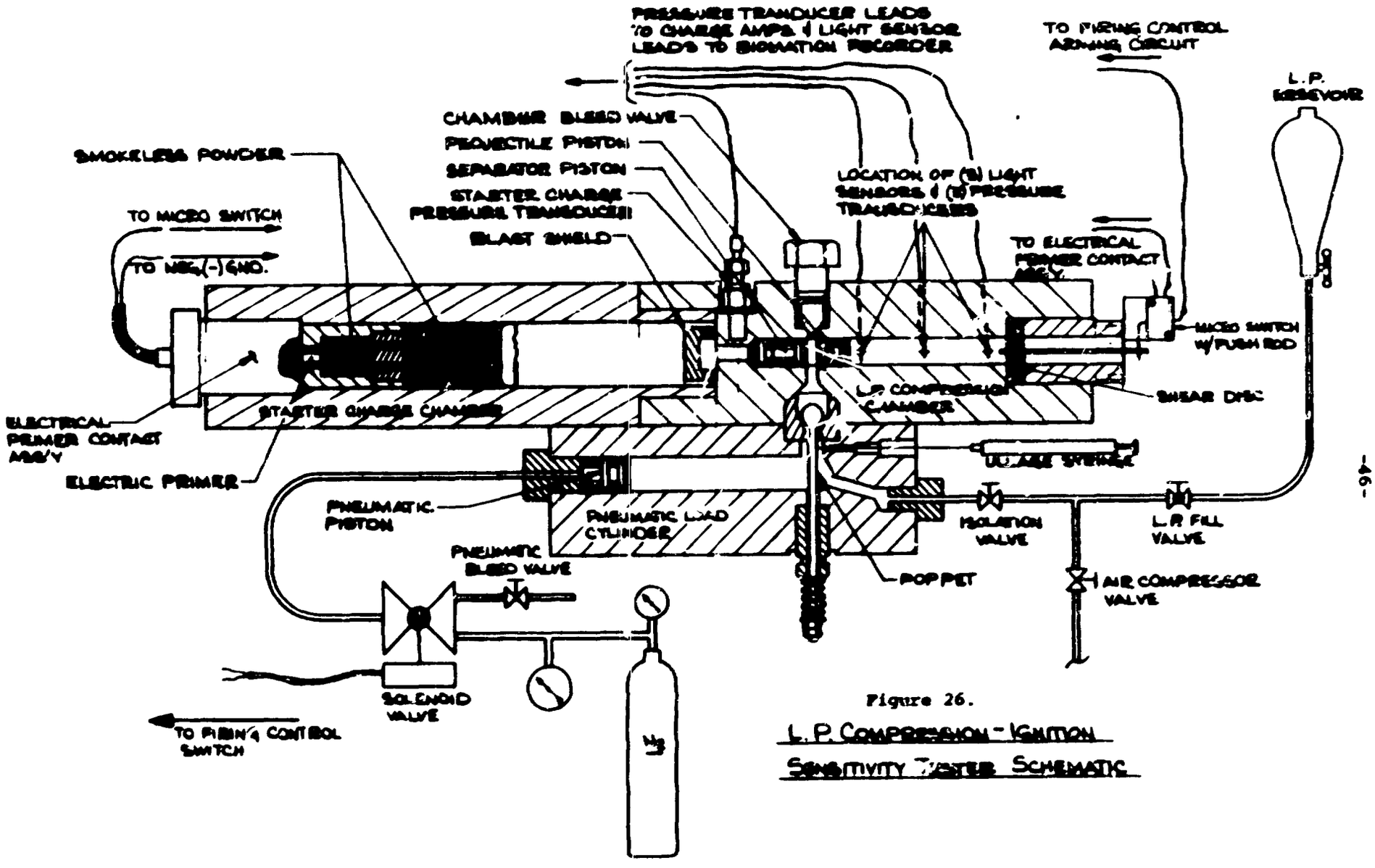

Figure 26.

L. P. COMPRESSION - IGNITION
SENSITIVITY TESTER SCHEMATIC

Four PCB type 119A quartz pressure transducers, ruggedized to withstand hydraulic pressures to 200 kpsi, are mounted in the L.P. Compression Chamber to record pressure-time histories during a compression test. One pressure transducer is located in the pressure communication passageway between the Starter Charge Chamber and the L.P. Compression Chamber to measure the driving p-t history sensed by the liquid propellant charge. Three pressure transducers and three light sensor assemblies are mounted 180° apart and 1.0 inch on centers along the Compression Chamber bore.

A photograph of the assembled Starter Charge Chamber, L.P. Compression Chamber, and Pneumatic Load L.P Cylinder is shown in Figure 27.

4.2 Phototransistor Light Sensor Assemblies

Three phototransistor light sensor assemblies, PCRL MOD 1 design, have been incorporated in the Liquid Propellant Compression Chamber design. Use of such a light-sensing system which is capable of detecting ignition of the liquid propellant charge is a useful diagnostic tool for these compression-ignition studies. The design provides for (i) easy insertion and removal in the chamber, (ii) a seal against pressure and protection of the sensitive phototransistor element; and (iii) no ablation or cracking of the viewing (sealing) sapphire window when subjected to the high pressure, hot gas environment.

The light sensor assembly has two major components: (1) the phototransistor housing which contains the active light sensing element and (2) the high pressure window housing which protects the phototransistor from the high pressure (25-50 kpsi), hot gas environment in the compression chamber by means of a small sapphire window.

The phototransistor housing has an overall length of 1.28 inch with half this length threaded 10-32 UNF, terminating in a Microdot female connector. The opposite end of the phototransducer housing is open with the phototransistor lens recessed for protection.

The high pressure window housing is 1.50 inch in length and has ¼-20 threads for mounting into the combustor housing. The window housing has 1/2 inch wrench flats for tightening. It contains an internal bore with threads to accept the phototransducer and a 0.04 inch diameter x 1/2 inch long sight hole to admit light from the sapphire window to the phototransistor.

The phototransistor employed is a Texas Instruments LS-400 N-P-N Planar Silicon Phototransistor. The rise-time and decay-time of this transistor are 1.5 μsec and 16 μsec, respectively. The phototransistor elements are contained in a hard glass, hermetically-sealed case with a hemispherical-shaped lens. The operating temperature range with elements exposed is -65 C to 125 C. The device requires 9mW/cm^2 of incident radiation to fully saturate. The outer dimensions of the phototransistor are 0.6 inch in length and 0.08 inch diameter. The collector and emitter connections are accomplished by means of two fine copper wires.

In the phototransistor housing, the collector wire is soldered to a brass female Microdot connector after being fitted with heat shrink tubing. Two small Teflon sleeve collars insulate the female Microdot for the phototransducer housing. The brass grounding bushing presses the emitter lead to the housing when the phototransducer is finally assembled. The phototransistor element is potted into the housing using General Electric silicone rubber RTV-108.

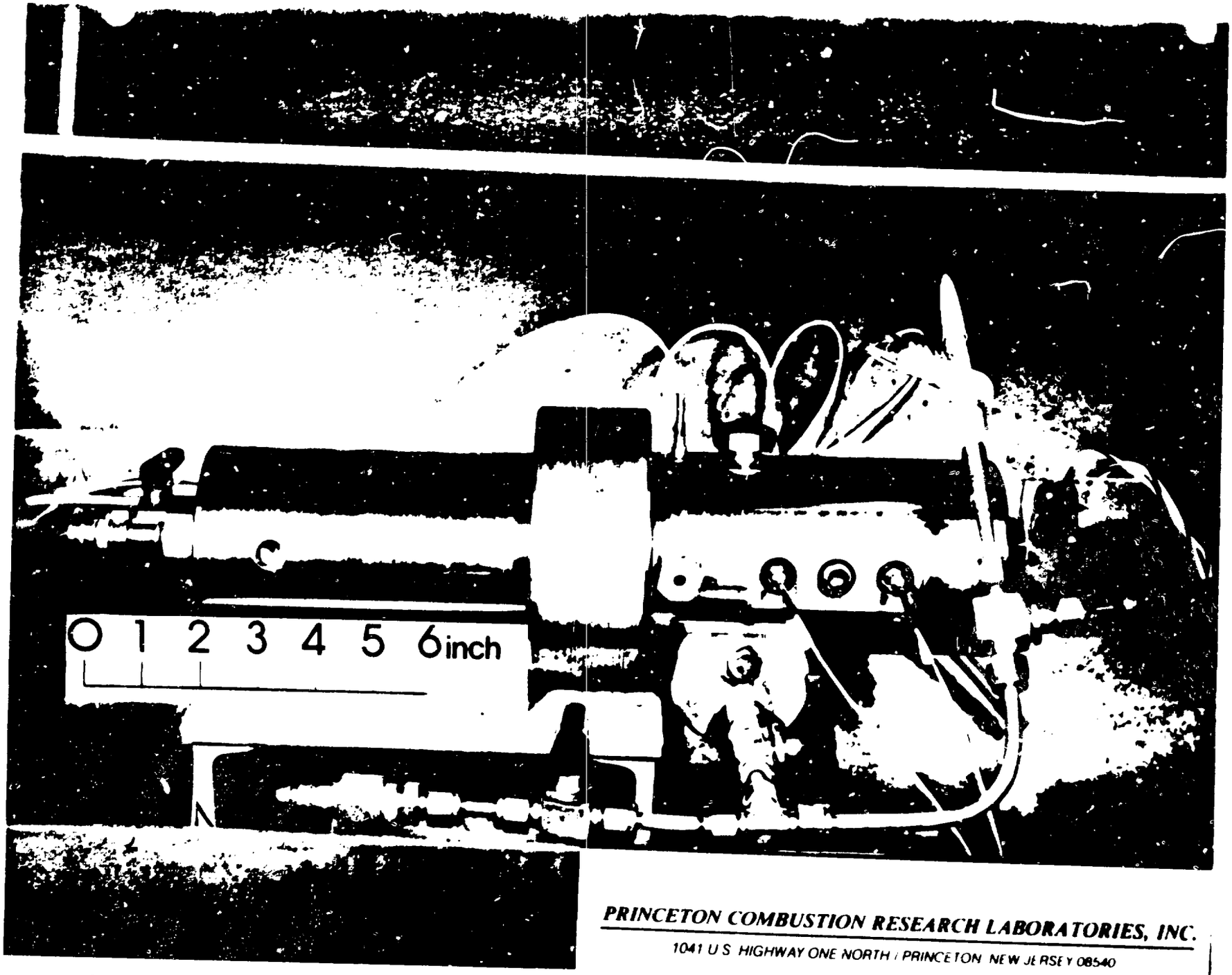

Figure 27. Photograph of Assembled Compression-Ignition Sensitivity Apparatus

A lock nut is tightened to hold the phototransducer in place. The sapphire window, which measures 0.125 inch diameter by 0.200 inch long and is manufactured by Adolf Meller Co., has optically polished faces for optimum light transmission. The window is placed into the high pressure housing from the pressure side and is sealed by means of a Parker No. 5-17B-N552-90 "O"-ring in a dove-tail groove in the housing face.

The relative spectral response of the LS 400 phototransistor is shown in Figure 28 , with the response of the human eye, output of a 2870 K Tungsten source, and output of GaAs sources displayed for comparison.

4.3 System Operation

Following the complete assembly of the L.P. Compression Chamber and the Pneumatic Load L.P. Cylinder, the Starter Charge Chamber is fitted with an electric primer and loaded with the prescribed smokeless powder mix. The Starter Charge Chamber and the L.P. Compression Chamber are then joined together with the Chamber Coupling Collar on the test stand. The liquid propellant filling procedure can now begin.

The Pneumatic Load L.P. Cylinder and the L.P. Compression Chamber are first bled to remove residual unwanted air. This is accomplished by first positioning the Separator Piston and the Projectile Piston with ends on either side of the Compression Chamber fill port, thereby forming a 5/32 inch wide passageway for flow of liquid from fill port to Bleed Valve. The Poppet Valve is then manually held in the open position as a gravity-fed supply of liquid propellant flows into the Pneumatic Load L.P. Cylinder, through the Poppet Valve, Flow Guide, fill port, the 5/32 inch slice of Compression Chamber bore, and out the Bleed Valve. In this manner the entire system including the initial bore volume between the two Compression Chamber pistons can be flushed. With the Poppet Valve released, free to return to its normally closed position, a prescribed volumetric loading of gas ullage is introduced into the Pneumatic Load L.P. Cylinder with the gas syringe. The displaced liquid propellant volume is permitted to flow out through the Isolation Valve. All valves are then closed. The liquid propellant reservoir is removed from the test area, all electrical connections completed, and the safety enclosure closed. Upon enabling the instrumentation to record, the system is ready to fire.

The ignition circuit which ultimately initiates the electric primer is energized by first closing the Ignition Circuit Safety Interlock key switch and then the Ignition Circuit Arm switch on the control panel (Refer to Figure 29 , Firing Circuit Schematic.) This applies +500 VDC to the open leg of the microswitch. The firing voltage is not sent to the electric primer until the microswitch is closed at the completion of dynamic loading.

A liquid propellant load circuit is now energized by closing the Load System Safety Interlock key switch. Refer to the schematic drawing, Figure 29 , for the following description. The dynamic loading sequence is initiated by closing the Load System Firing Switch. This action opens the Solenoid Valve which releases the driving N_2 pressure into the Pneumatic Load L.P. Cylinder to accelerate the Pneumatic Piston. The motion of the Pneumatic Piston forces the liquid propellant and its gas ullage past the Poppet Valve once the force balance establishes Poppet Valve opening. The

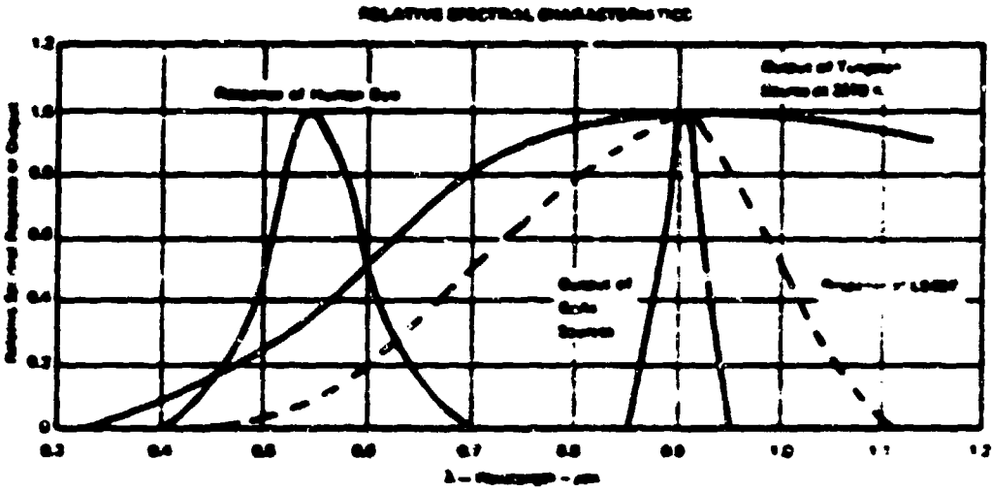

Figure 28. Relative Spectral Response Characteristics of LS 400 Phototransistor.

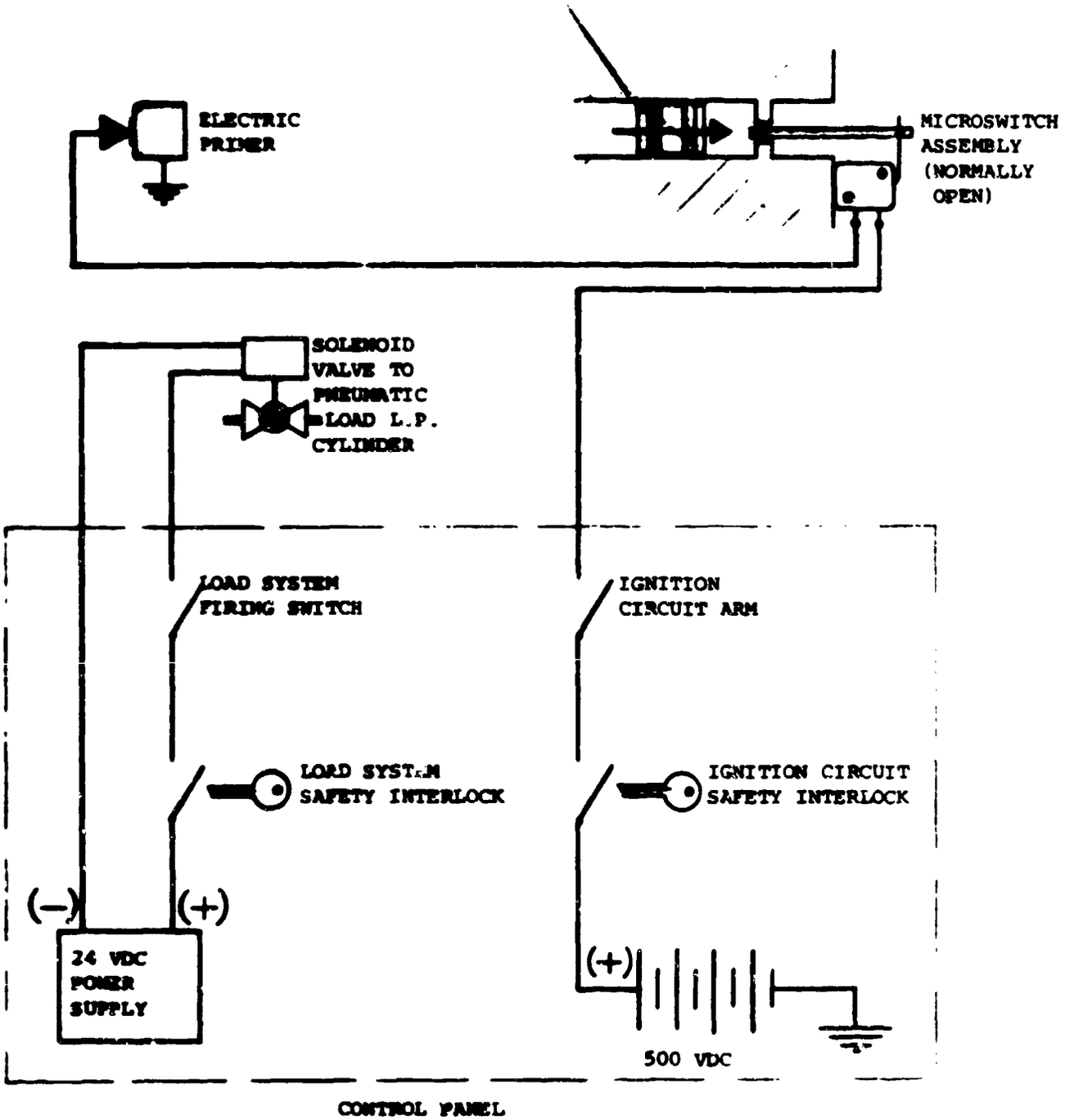

Figure 29. Firing Circuit Schematic

liquid propellant and its gas ullage flow through the Flow Guide, possibly resulting in cavitation depending on the nature of the orifice, into the bore of the L.P. Compression Chamber. The Projectile Piston is then driven to the right allowing the charge to fill the bore until the maximum stroke is achieved. The contact of the Projectile Piston with the pushrod of the Microswitch Assembly closes the microswitch and applies the + 500 VDC to the Electric Primer in the Starter Charge Chamber. The resulting pressure generated by the combustion of the starter charge mix is sensed by the Separator Piston which is free to move in the Compression Chamber bore. As the pressure in the Starter Charge Chamber rises, the Separator Piston accelerates compressing the liquid propellant charge along with its bubble distribution. The nylon portion of the composite Separator Piston expands radially outward to the bore to prevent hot gases from reaching the liquid propellant charge. This is a high pressure seal. We rely on "O"-rings fitted to the Separator Piston for low pressure sealing. Combustion gases from the starter charge are continuously being vented through the 0.053 inch diameter orifice in the Vent Plug. If the compression cycle does not produce an explosion of the liquid propellant charge, the Separator Piston will return to its original position as Starter Charge Chamber pressure declines. If, however, the liquid propellant charge undergoes runaway reaction at some point in the compression cycle, the Projectile Piston will shear through the aluminum Shear Disc when the bore pressure exceeds 65-70 kpsi. As the Projectile Piston emerges from the bore, the combustion gases from the liquid propellant charge are vented out though the bore hole in the Disc Retainer bolt. The venting is so rapid that a positive pressure gradient between the Starter Charge Chamber and the L.P. Compression Chamber drives the Separator Piston from the bore also. Both the Separator Piston and the Projectile Piston must be replaced in the event of a liquid propellant explosion.

4.4 The Data Acquisition System

Princeton Combustion Research Laboratories', Inc. data acquisition system includes a Biomation Waveform Recorder, Model 1015, Tektronix Model 7704A Oscilloscope, DATAcap Coupler Model B403, and Texas Instruments Model 733 ASR Electronic Data Terminal.

The Biomation Waveform Recorder records four simultaneous analog input signals, with resolution of each input signal being one part in 1024 (better than 1/10 percent). The four input signals recorded are : Channel 1: Starter Charge Chamber pressure, p_c; Channel 2: Light sensor output, L1; Channel 3: Liquid Compression Chamber pressure, p_1; Channel 4: Liquid Compression Chamber pressure, p_3. The recorder is operated in the Pre-trigger Mode. This mode of data recording permits the recording of the event prior to the trigger signal, if desired, and the subsequent signal history. This is accomplished by having the unit record continuously until the trigger is received, then using the trigger to stop the recording process, freezing the data that was recorded prior to triggering in memory. Each of the four channels stores 1024-10 bit words. The sampling rate utilized is 100 KHz (0.01 msec/word), resulting in a data recording window of 10.24 msec. The window is quite adequate to capture the events of interest. The

waveform recorder is operated in the pretrigger mode with a trigger delay of 900 sample intervals. The trigger signal utilized is the external voltage associated with the Starter Charge Chamber pressure transducer response. When the trigger circuit of the waveform recorder detects the external voltage signal of 0.6 V (or 6000 psi), it records 900 words of ensuing data. This provides for sufficient resolution of the rapid pressurization portion of the p-t start-up history.

The stored data in the waveform recorder can be output to an oscilloscope for visual display and photographic recording, and/or to the printer of a teletypewriter, and/or directly to a data file on the time-sharing computer (IBM 370-158) for subsequent output in tabular form and/or Calcomp plots. In order to accomplish the two latter means of digital data display, a DATAcomp Coupler and Texas Instruments Electronic Data Terminal are required.

The DATAcomp Coupler, Model B403, is an integrated circuit unit specifically designed to interface the Biomation Waveform Recorder to various recording and computing units, by providing the circuitry and cable necessary for connecting the digital output of the waveform recorder. The coupler is set up to accept the digital data from the waveform recorder on a manual (command-type) basis. Digital data is streamed from the waveform recorder into the DATAcomp Coupler and then onto a cassette tape on the Texas Instruments 733 ASR Electronic Data Terminal. When the entire data file has been stored on magnetic tape it is then streamed to a file on an IBM 370-158 time-sharing computer for subsequent calibration, tabulation, and plotting.

4.5 Functional Testing: Inert Simulant (Water) Tests

Functional Tests of the system were performed with water to determine that all aspects of system operation checked out. These functional tests with water also provided a baseline for comparison of compression-igniton sensitivity studies performed with MOS-365 liquid monopropellant. In all functional tests the line pressure to the Pneumatic Load L.P. Cylinder was 300 psig and "neat" liquid was dynamically loaded in the Compression Chamber. Two different pressurization p-t start-up curves were employed, Type C and Type E.

A verification of the system response to the pressure loadings generated by Type C and Type E starter charges was obtained by exercising the "SUPER-SCEPTRE" Computer Program 54 for a liquid spring/mass system with physical properties, e.g., density and sound speed, representative of MOS-365 liquid monopropellant.

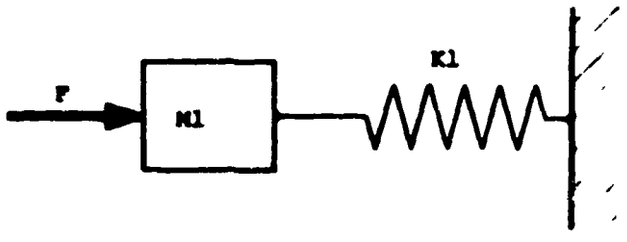

In this simplified approach, no account is taken of system damping and the liquid is assumed "neat". The mass of the liquid charge is lumped with the mass of the Separator Piston, the sum being M1. The applied pressure produced

by the starter charge acting on the cross-sectional area of the Separator Piston results in the driving force F, input to the computer program. The spring constant Kl for the neat liquid monopropellant charge is obtained as follows:

The isentropic bulk modulus of the liquid is given by:

$$B \equiv \left(\frac{dp}{d \ln \rho}\right)_s$$

$$\sim \frac{\Delta p}{\Delta V/V} = \frac{\Delta p}{\Delta l/l}$$

The spring force for a "linear spring" is given by:

$$dF = k\, dl$$

or

$$k = \frac{\Delta P \cdot A}{\Delta l}$$

$$= \frac{BA}{l}$$

Now, $B_{HOB-365} = (c^2\rho)_{HOB-365}$

$$= (1.893 \times 10^5 \text{ cm/sec})^2 \ (1.398 \text{ g/cc})$$

$$= 0.502 \times 10^{11} \text{ dynes/cm}^2$$

or

$$k = 7.364 \times 10^9 \text{ dynes/cm} \equiv Kl$$

where $V = 6.402 \text{ cm}^3$
$l = 6.604 \text{ cm}$

Figure 30 shows the predicted force in the liquid monopropellant "spring" in response to the driving force loading associated with starter charge pressurization curve Type R. Large amplitude oscillations are predicted in the liquid "spring". In fact, the liquid is in tension at t ~ 0.68 msec. Of course, the response of the real system includes the effects of damping. Therefore the force, or pressure, excursions in the liquid are not anticipated to be as violent. Similarly, Figure 31 shows the predicted force in the liquid spring in response to the driving force loading associated with starter charge pressurization curve Type C. Notice that the predicted liquid pressure response is less violent, the amplitude of the force excursions being significantly reduced. Also, the liquid is always in compression, i.e., a negative pressure(tension) does not result.

Results of the functional tests are identified in Figures 32 and 33 as "INERT RUN 2" and "INERT RUN 3". In all cases a mean peak chamber pressure, p_c, of 25 kpsi is obtained. These figures display digitized firing records of the pressure-time history in the Starter Charge Chamber,

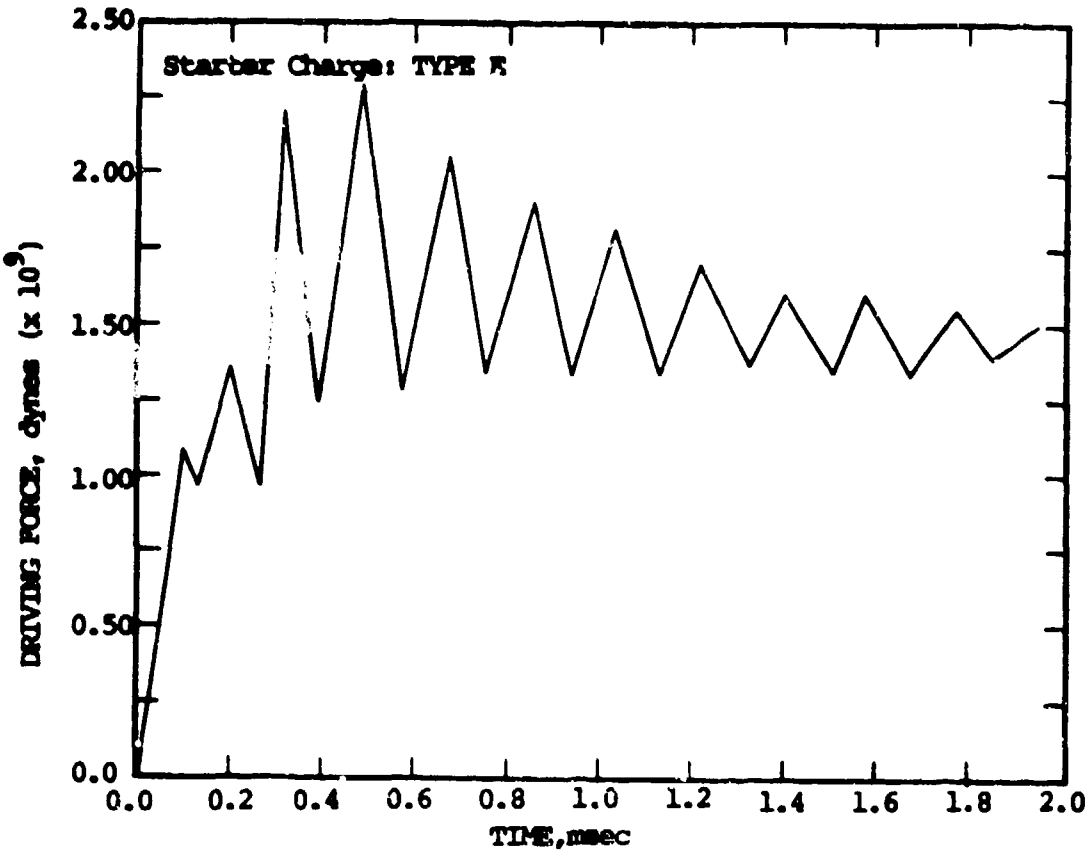

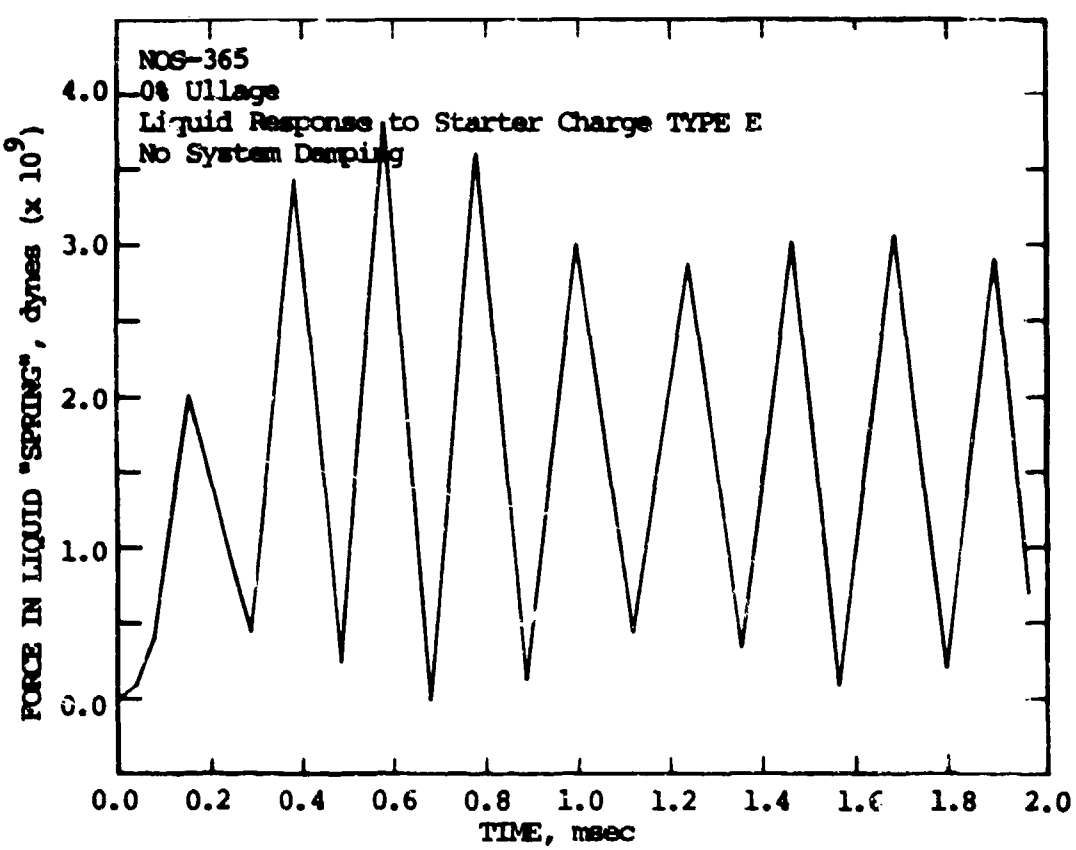

Figure 30. Predicted Liquid Response to Starter Charge Type E.

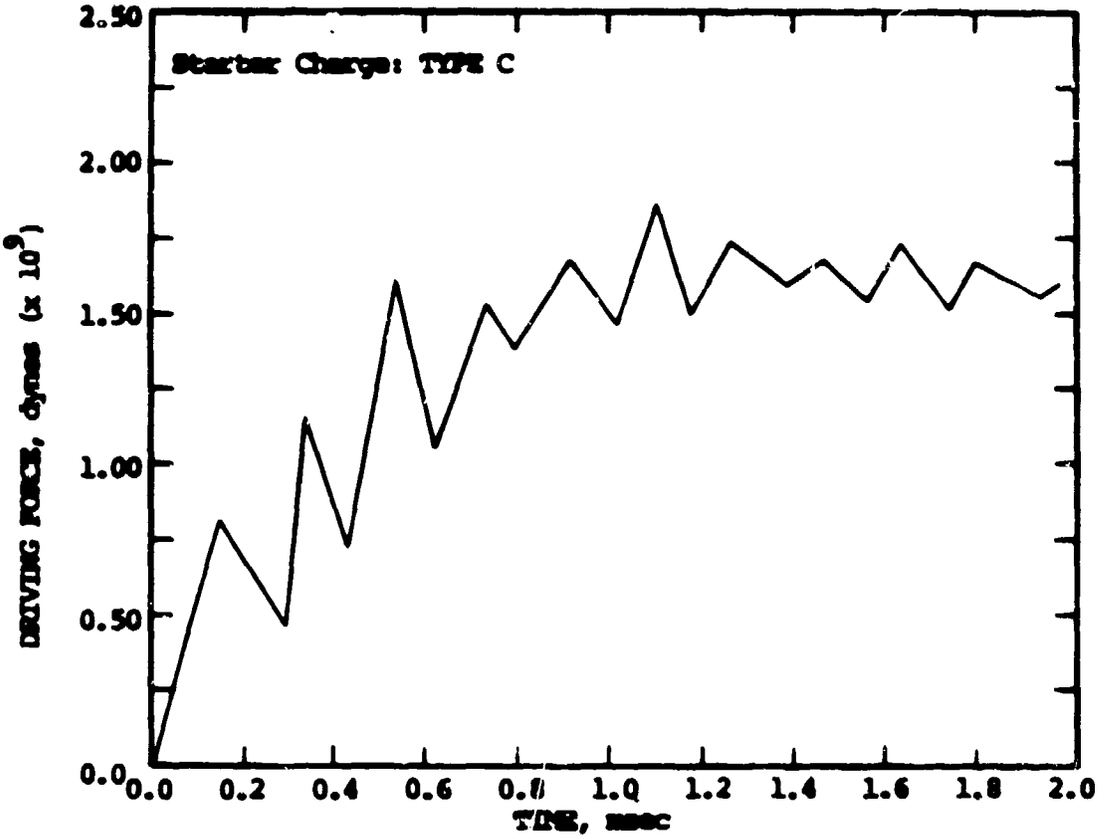

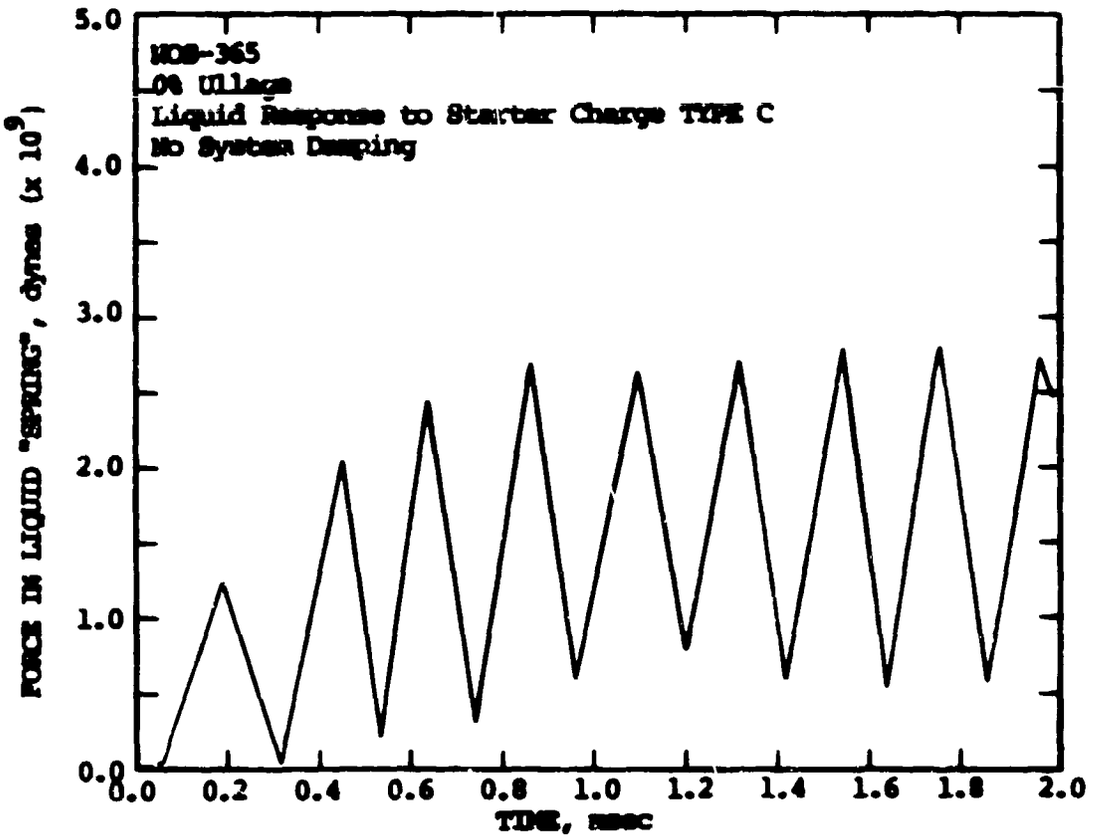

Figure 31. Predicted Liquid Response to Starter Charge TYPE C.

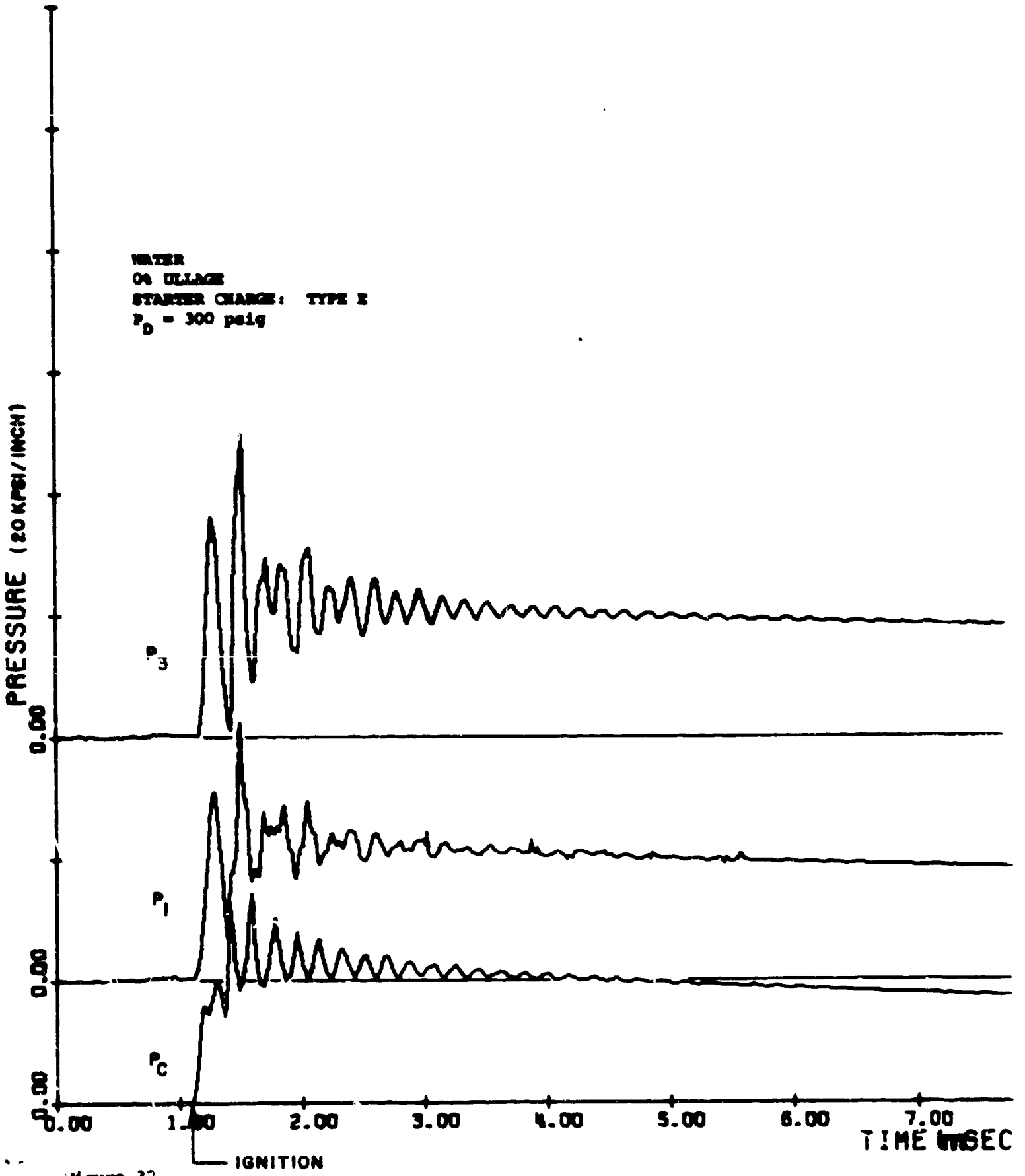

Figure 32.

INERT RUN 2

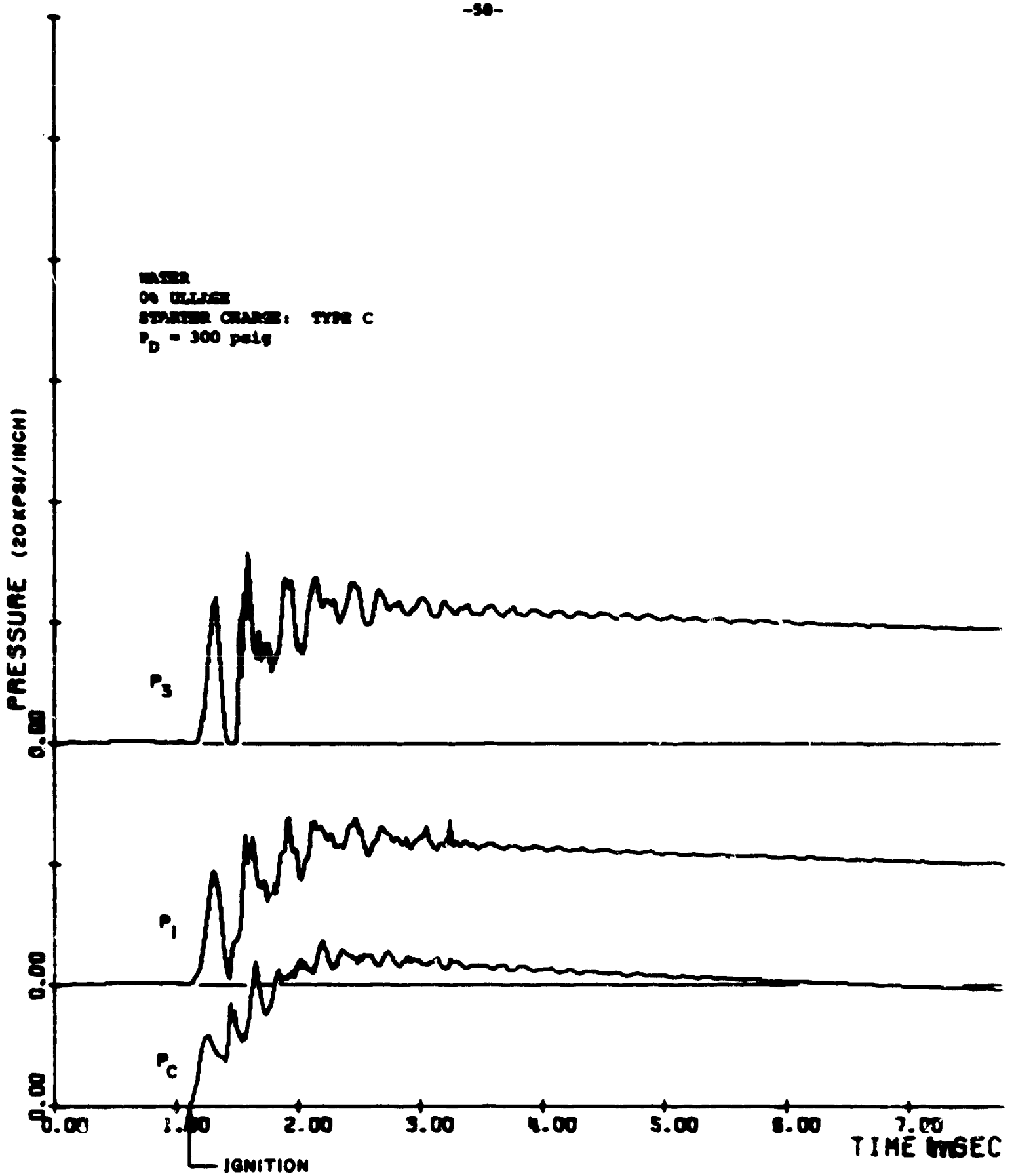

Figure 33.

INERT RUN 3

$p_c(t)$, and in the bore of the L.P. Compression Chamber, $P_1(t)$ and $P_3(t)$. Pressure transducer p_1 is located 0.60 inch from the rear face of the Separator Piston and p_3 is located 2.00 inches downstream of p_1. The vertical scale in these figures is 20 kpsi/inch, with shifted baselines for each pressure record. The oscillation frequency of 5000 Hz in the p_c-t record is associated with excitation of the fundamental acoustic mode of the starter charge chamber due to the combustion process. The liquid response, p_1 and p_3, (essentially a damped spring-mass system) to the driving pressure p_c associated with starter Type E displays rather large amplitude pressure excursions of the same frequency. Although the mean peak liquid pressure is seen to be 25 kpsi, a pressure wave of 50 kpsi amplitude is generated in the dynamically-loaded liquid column, at the location of p_3. Notice that the magnitude of the pressure spikes in the liquid column are not as severe for "INERT RUN 3" since the pressure excursions developed by the smokeless powder starter charge Type C are less severe. This was predicted by the system response calculations of the "SUPER-SCEPTRE" Code.

In both of these inert loading tests system components and instrumentation functioned perfectly. The integrity of all seals was established. As anticipated, all light sensors remained on baseline for the duration of the inert loading test, indicating that compression-ignition of the dynamically loaded neat water charge did not result. Compression-ignition sensitivity studies with MOS-365 liquid monopropellant are discussed next, in Section 4.6.

4.6 MOS-365 Liquid Monopropellant Tests

Compression-ignition sensitivity studies of dynamically-loaded MOS-365 liquid monopropellant were performed with the apparatus previously described. The pressurization rate to which the liquid propellant charge with associated ullage is subjected is an important parameter in determining the threshold for runaway reaction and, therefore, the safe operating limits of start-up pressurization. The matrix of tests performed is presented in Table 3 . Figures 34 thru 41 display firing records of the sensitivity tests performed. In each case starter charge chamber pressure and two liquid propellant compression chamber pressures are displayed as a function of time on a staggered baseline scale. The timewise response of the phototransistor light sensors in the compression chamber bore is shown as an insert in each figure.

Firing tests "BUBBLE" RUN NO'S 1, 2 and 4 were performed with neat propellant and a dynamic loading driver pressure of 300 psig. In all cases the mean peak starter charge pressure was 25 kpsi. The pressurization rate was varied between tests, corresponding to those associated with start-up curves Type C, E and D respectively. Figure 34 displays test results of "BUBBLE RUN 1". The response of the dynamically-loaded neat propellant charge to a pressurization rate given by TYPE C start-up charge is benign. This can be seen by inspection of the p-t history in the liquid charge, a comparison of these records with those associated with test "INERT RUN 3", and by the lack of response of the phototransistor light sensors.

Figure 35 displays test results of "BUBBLE RUN 2". The response of the dynamically-loaded neat propellant charge to a pressurization rate given by TYPE E start-up curve, a faster pressurization rate than TYPE C curve, is an explosion. Light sensor L2 detects combustion in the liquid charge at approximately 0.60 msec after ignition of the starter charge (onset of chamber pressurization), followed by a response of L1 at t = 0.70 msec and then L3 at t = 0.85 msec. The pressure-time histories in the liquid charge show large scale oscillations with peak pressures in excess of 60 kpsi. Charge amplifier gains were increased in subsequent tests in order to capture the exact pressure peak. Several points are worth noting: (i) the departure of the liquid pressure response from that of an inert loading test, i.e., Figure 32 "INERT RUN 2", occurs in the neighborhood of t = 0.50 msec after ignition of the starter charge, and (ii) at approximately t = 1.0 msec after pressurization onset the shear disc ruptures and rapid depressurization of the liquid propellant compression chamber bore results. This was our first indication that the design of the pressure relief blow-out system would ensure the integrity of the compression-ignition test apparatus as a result of an explosion.

"BUBBLE" NO.	START-UP CURVE	PERCENT ULLAGE (VOLUME %)	DRIVER PRESSURE (psig)	SYSTEM RESPONSE
1	C	0	300	BENIGN
2	E	0	300	EXPLOSION
3	C	3.1	300	BENIGN
4	D	0	300	EXPLOSION
5	D	3.1	300	EXPLOSION
6	D	0	500	EXPLOSION
7	C	0	500	BENIGN
8	C	3.1	150	EXPLOSION

TABLE 3

Tabulation of Compression-Ignition Sensitivity Tests with Dynamically-Loaded NOS-365 Liquid Monopropellant Charge.

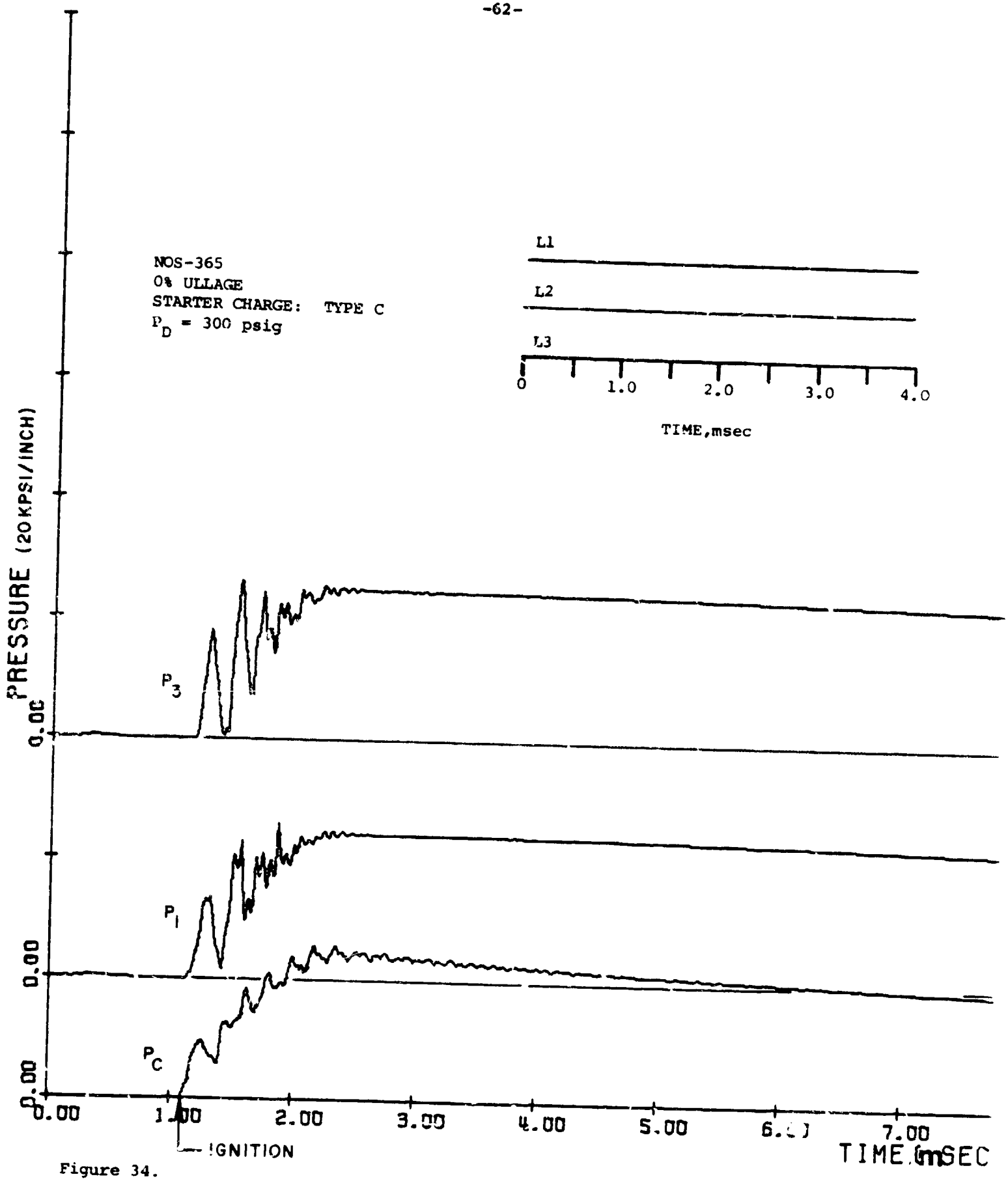

Figure 34.

BUBBLE RUN 1

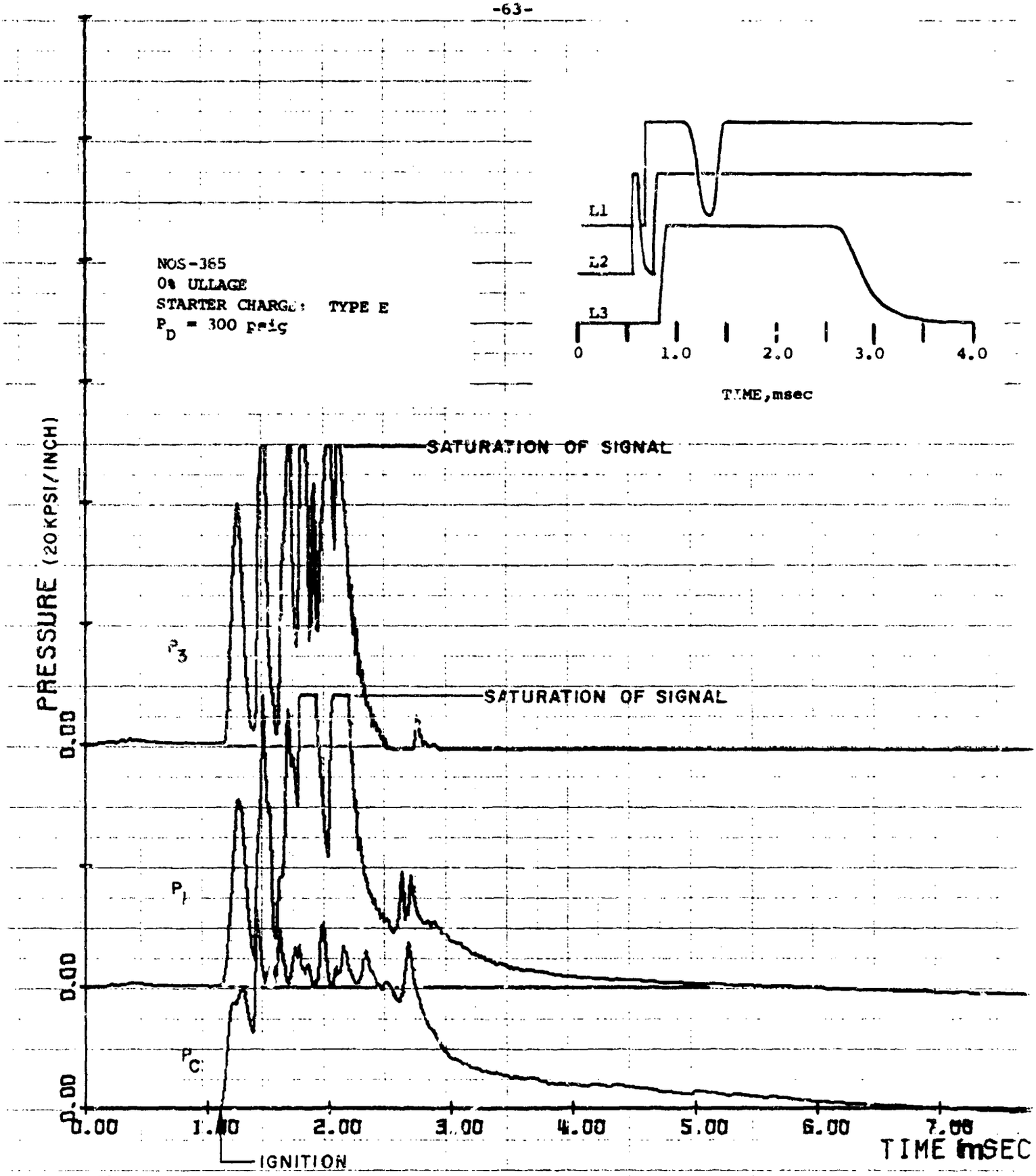

Figure 35.

BUBBLE RUN 2

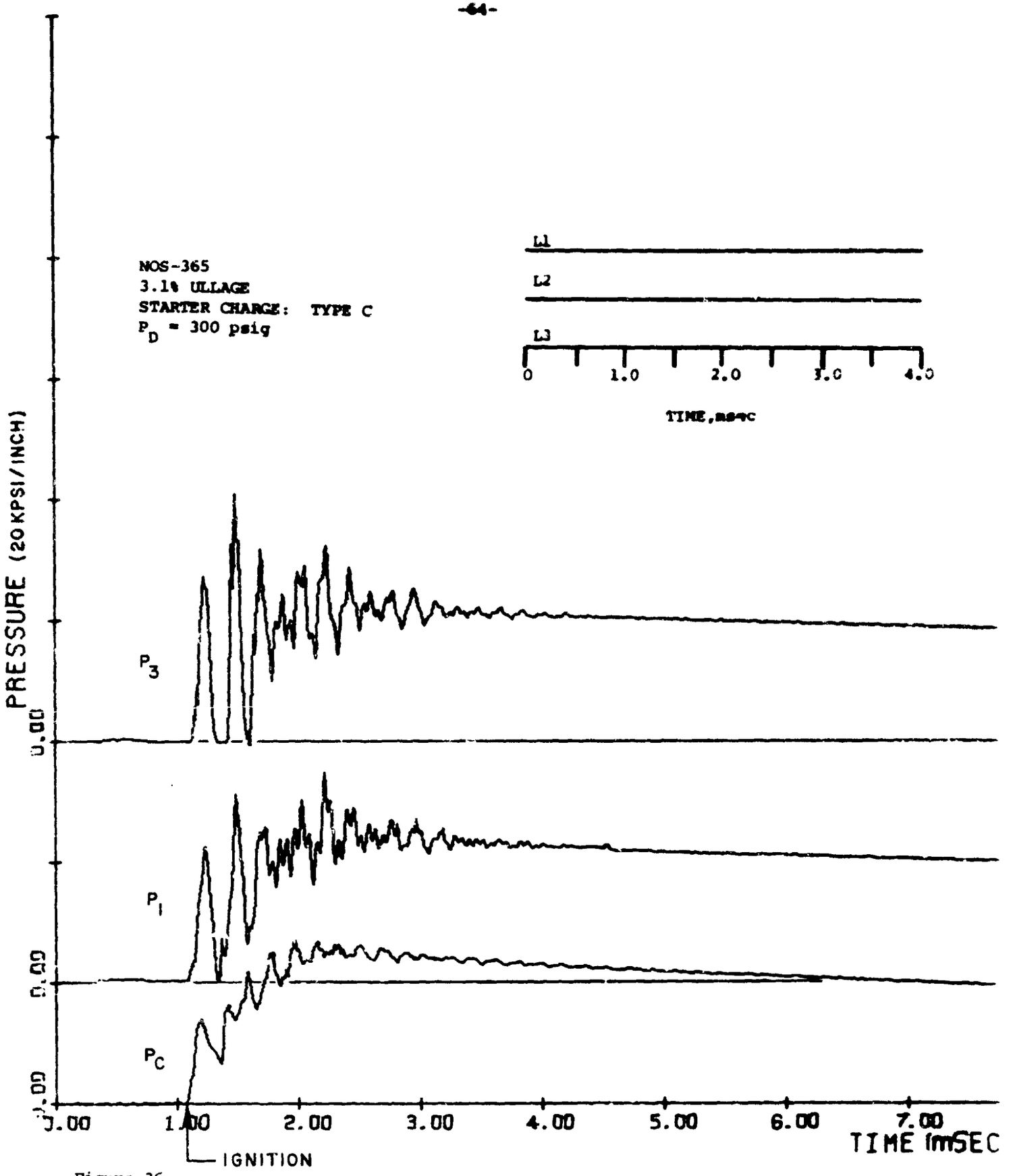

Figure 36.

BUBBLE RUN 3

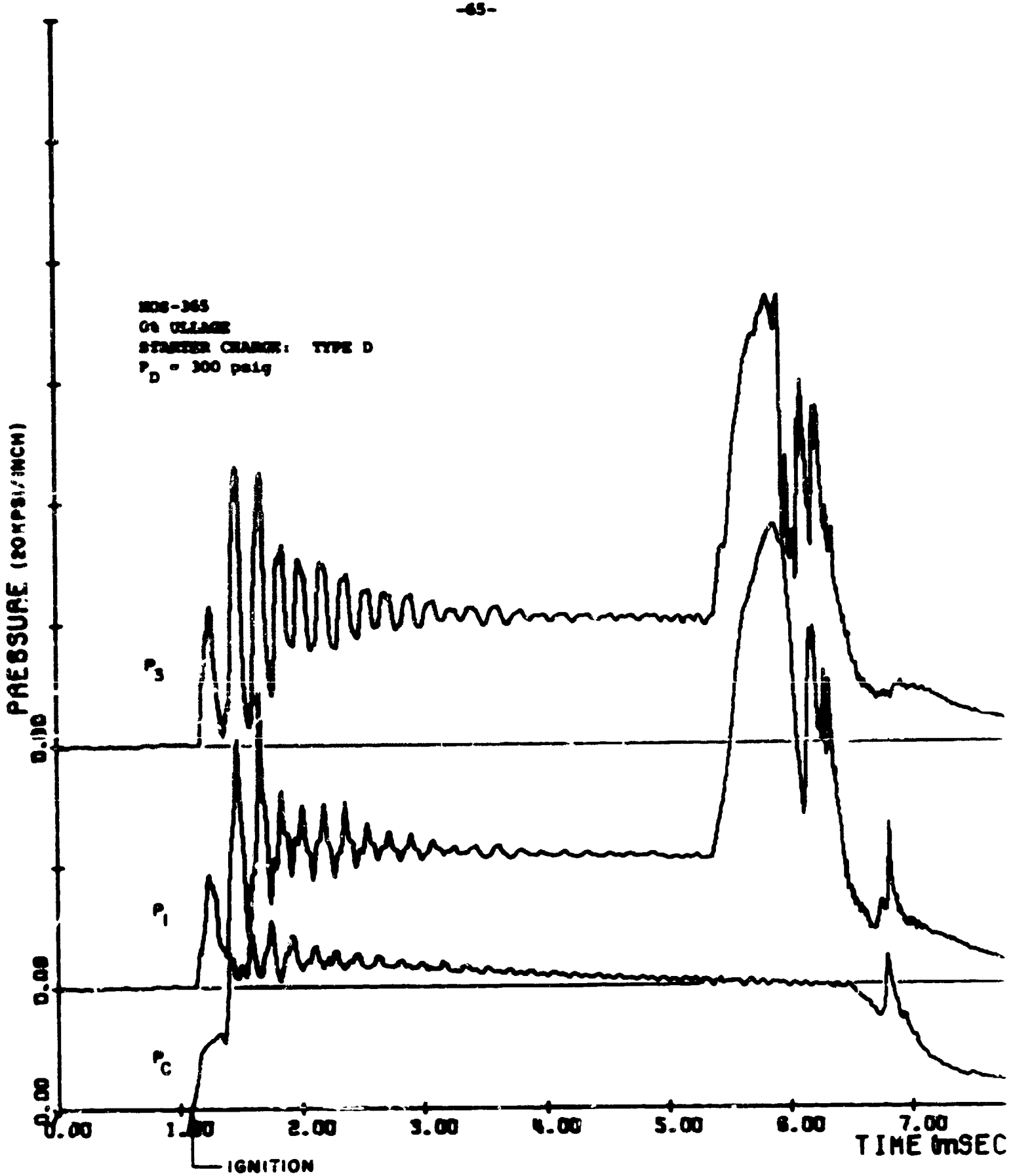

Figure 37.
BUBBLE RUN 4

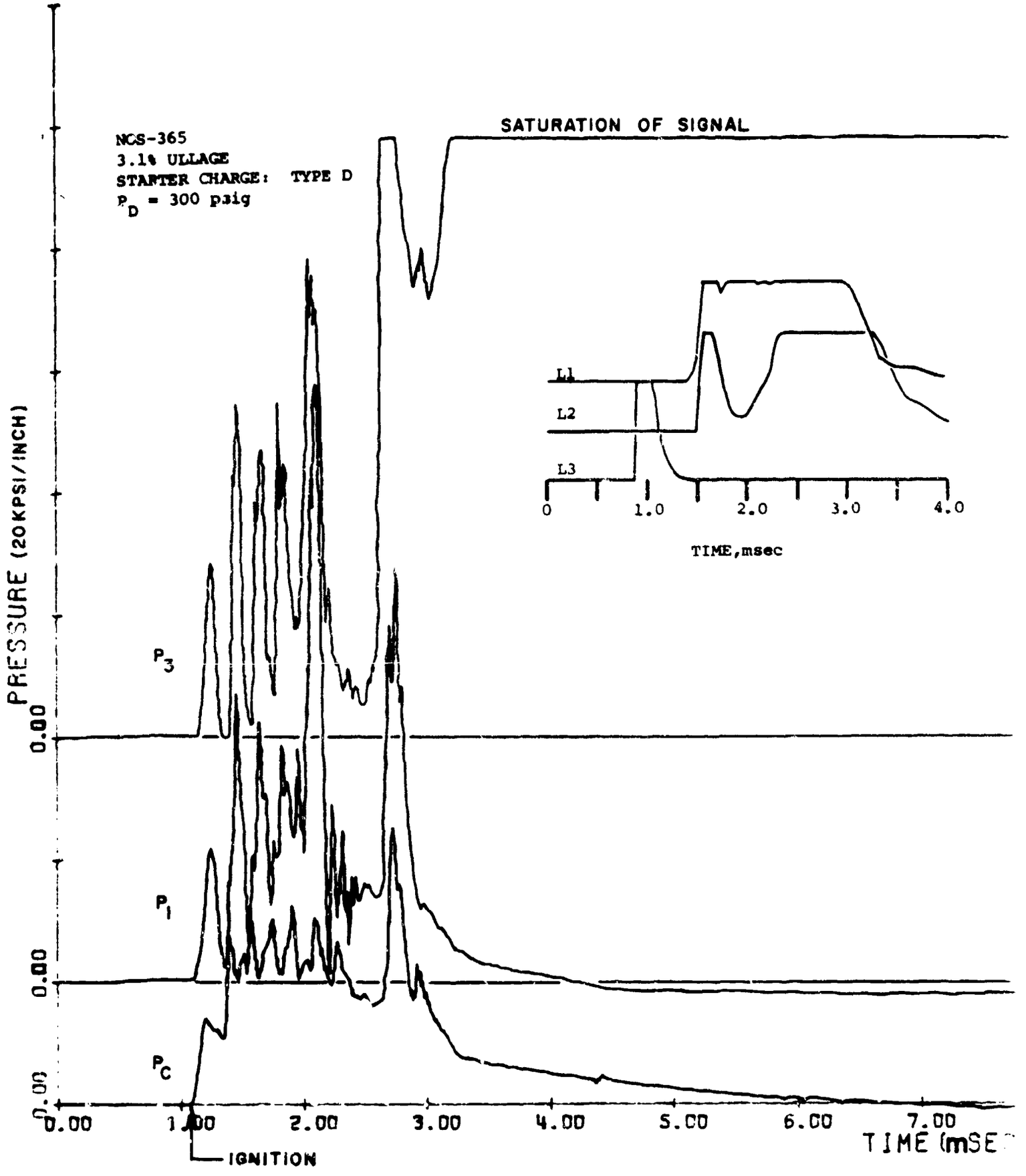

Figure 38.

BUBBLE RUN 5

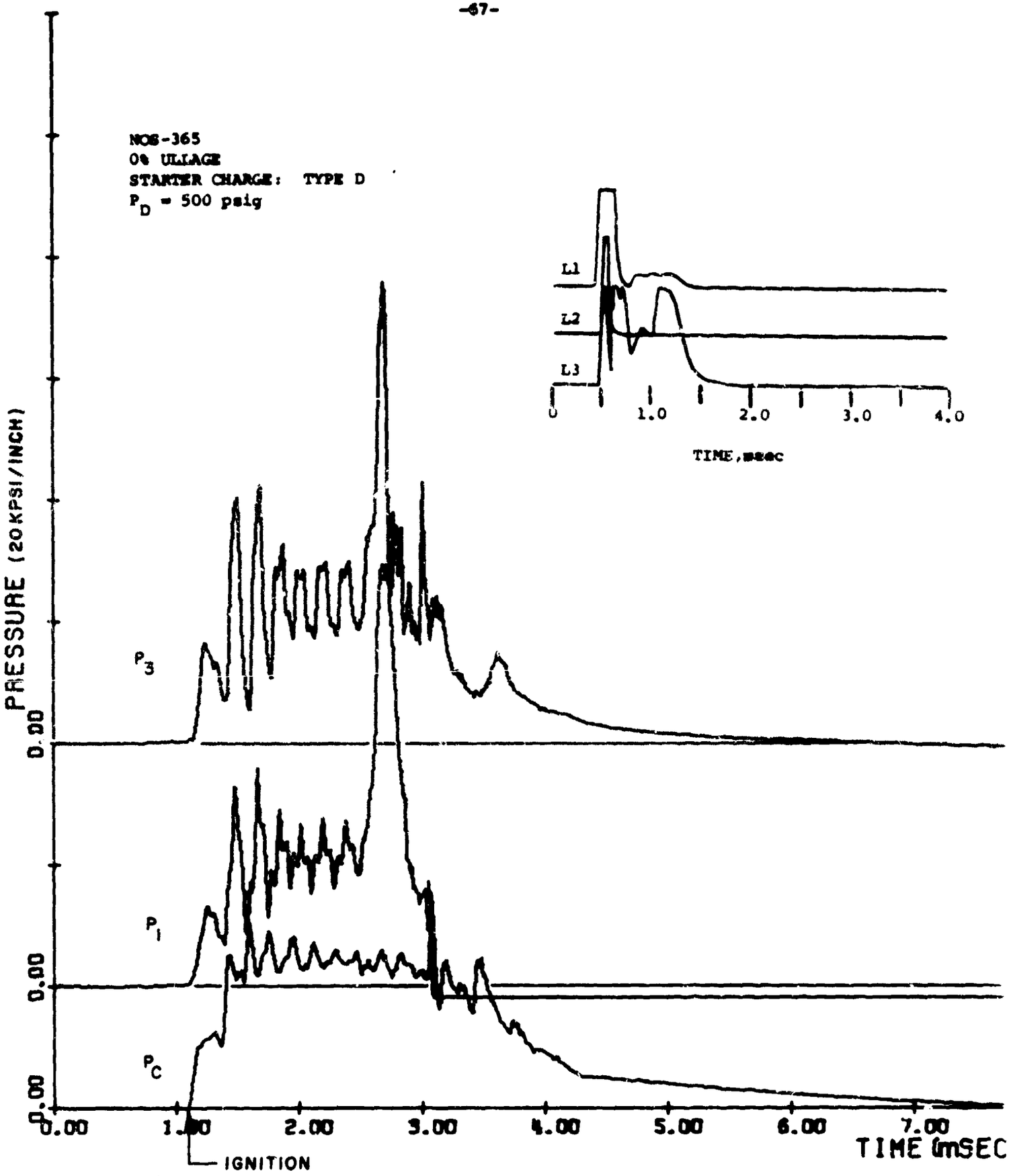

Figure 39.

BUBBLE RUN 6

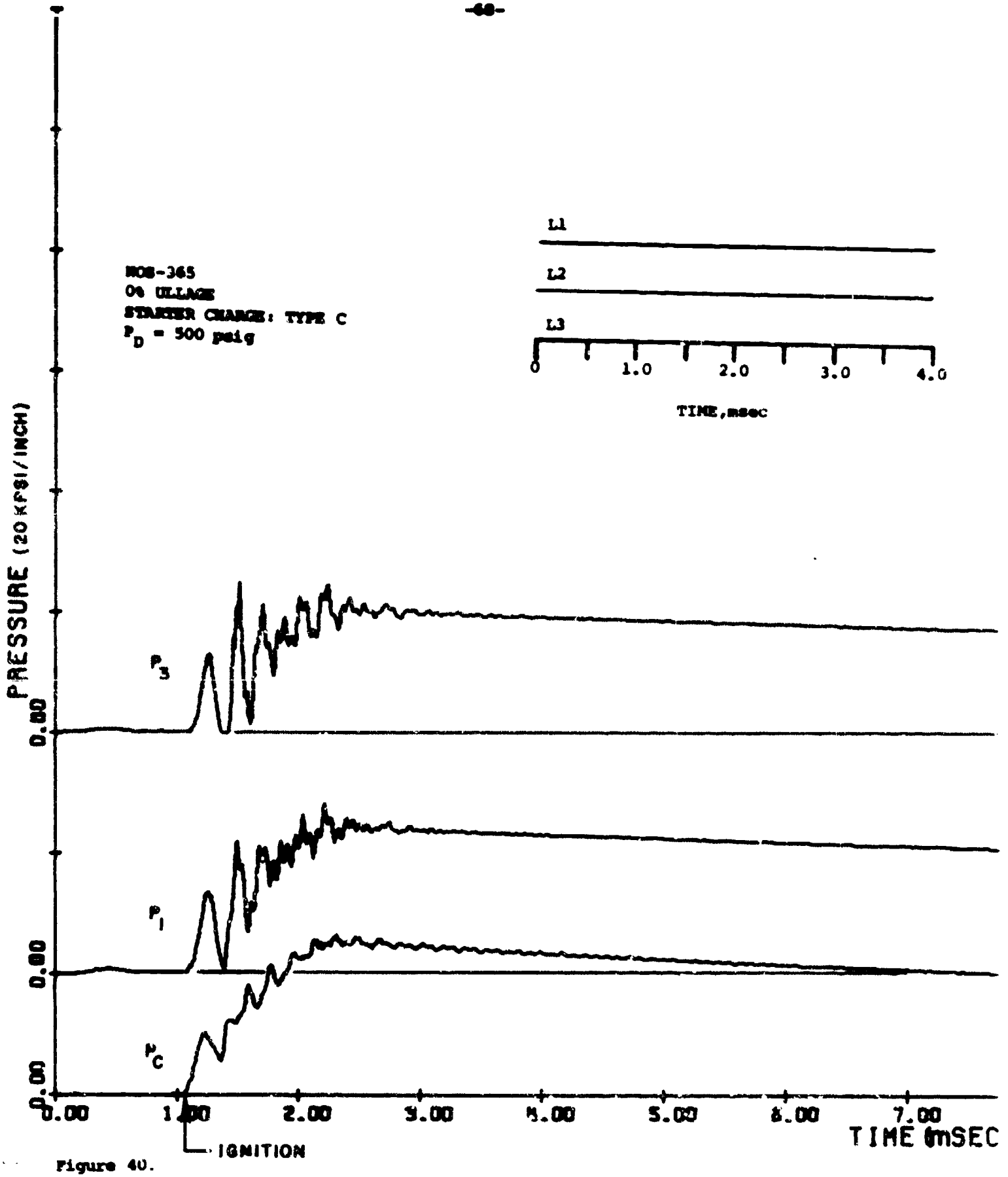

Figure 40.

BUBBLE RUN 7

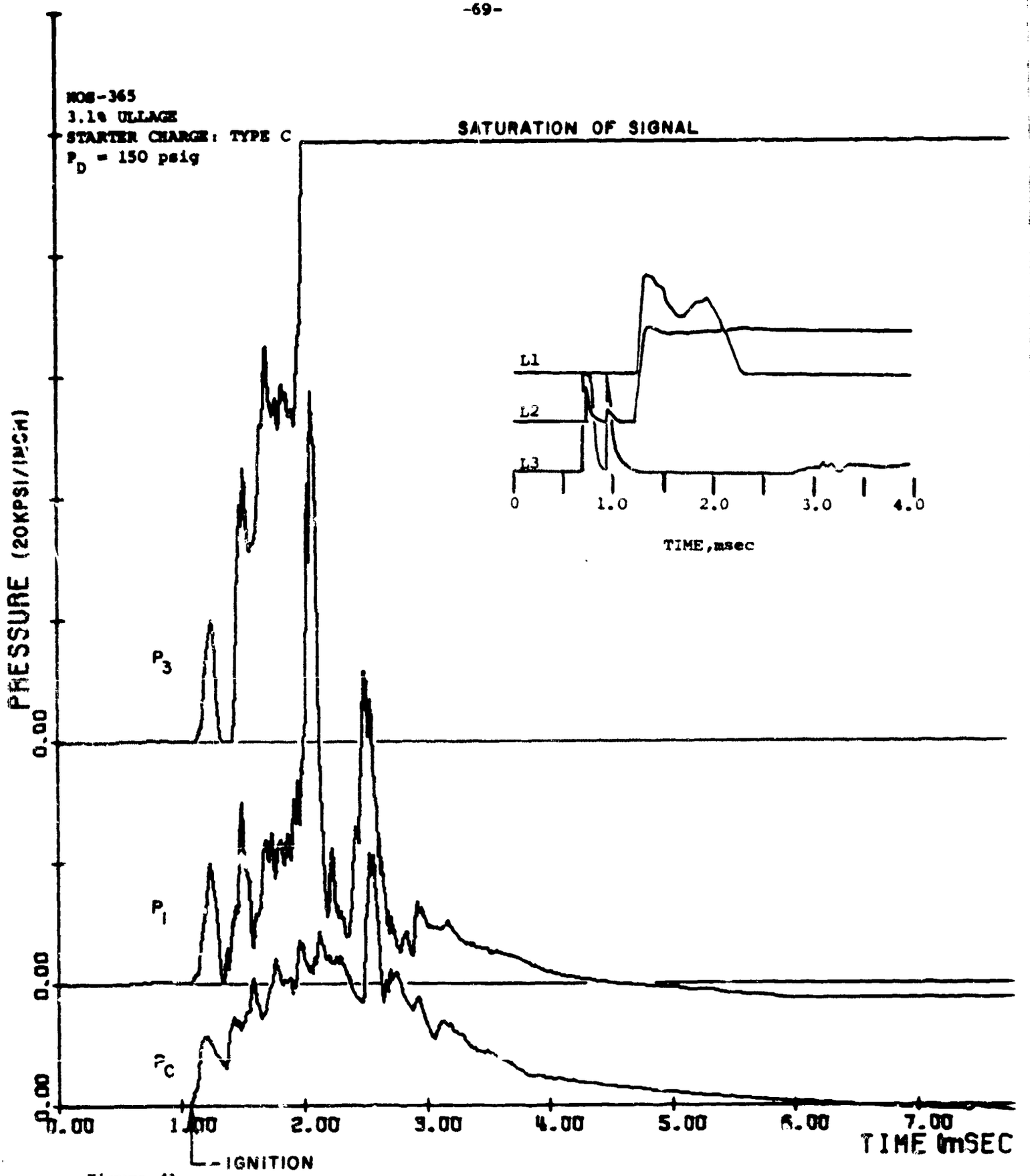

Figure 41.

BUBBLE RUN 8

Figure 37 displays test results of "BUBBLE RUN 4", an intermediate pressurization rate case corresponding to TYPE D starter charge. The dynamically-loaded neat propellant charge undergoes delayed runaway reaction, approximately 4.25 msec after starter charge ignition. The response of the liquid propellant charge is essentially benign up to this point. Unfortunately, no light sensor output data was obtained due to the delayed liquid response. This delayed explosive response of the liquid propellant suggests that a critical threshold condition for compression-ignition has been achieved. For pressurization rates less than that associated with TYPE D starter charge, the liquid response is benign; for faster pressurization rates, explosion results.

Figure 42 is a summary plot displaying the corridor for safe start-up operation of the dynamically-loaded neat propellant charge.

The next sequence of compression-ignition sensitivity tests performed was directed at determining the effect of deliberately introduced air ullage (3.1% by volume) on the tendency toward explosion. These tests, identified as "BUBBLE RUN 3" and "BUBBLE RUN 5" were performed with a dynamic load driver pressure of 300 psig and pressurization rates given by starter charge TYPE C and TYPE D respectively. Figure 36 displays digitized firing records of "BUBBLE RUN 3". The response of the dynamically-loaded MDB-365 propellant charge with its associated bubble distribution to a pressurization rate given by TYPE C start-up curve is benign. Again we note the lack of response of the phototransistor light sensors indicating the absence of compression-ignition.

Figure 38 displays digitized firing records of "BUBBLE RUN 5". The response of the propellant charge with associated ullage to a faster pressurization rate given by TYPE D start-up curve is an explosion. Light sensor L3 detects combustion in the liquid charge at t = 0.90 msec following ignition of the starter charge. The delay time to explosion is considerably reduced by the introduction of 3.1% ullage as compared to the neat liquid response to TYPE D starter charge pressurization. The pressure generated in the liquid column is seen to be in excess of 100 kpsi (charge amplifier signal saturation). Rapid depressurization of the propellant compression chamber bore is seen to begin 1.6 msec after the onset of pressurization. Also notice that pressure transducer p_3 shorted during the firing due to the excessive pressure. This transducer was scrapped after the firing due to diaphragm rupture.

The next group of tests was performed with a dynamic loading driver pressure of 500 psig and a neat propellant charge. At this high driver pressure the cavitation phenomenon is anticipated to be more severe than the 300 psig driver case, but the resulting bubbles (from cavitation and residual ullage in liquid) tend to be smaller in diameter. Figure 40, "BUBBLE RUN 7", shows the benign response of the dynamically-loaded neat propellant charge subjected to TYPE C starter charge pressurization history. Again the light sensors show no sign of compression-ignition in the charge. However, as shown in Figure 39 for "BUBBLE RUN 6", explosion results when the neat propellant charge is subjected to the start-up pressurization history given by a TYPE D curve.

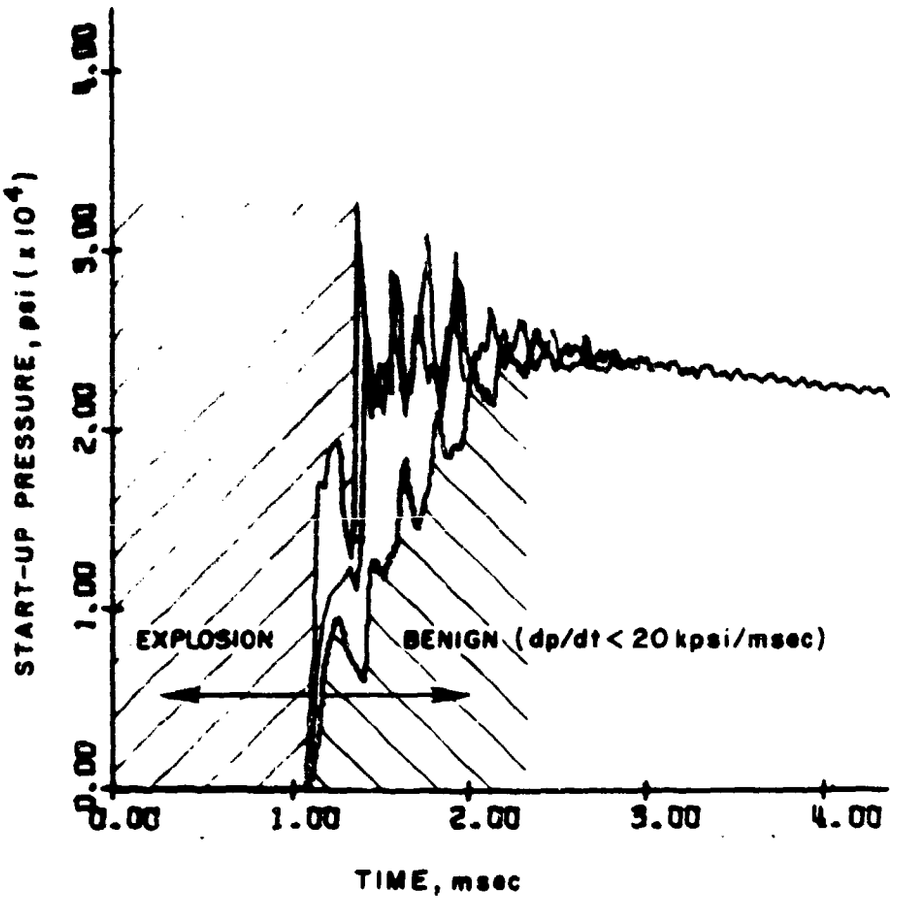

Figure 42. Corridor for Safe Start-Up Operation of a Dynamically-Loaded Neat NOS-365 Liquid Monopropellant Charge.

In all of the above-referenced compression-ignition tests, the dynamically-loaded liquid propellant charge displayed a benign response to the pressurization rate given by starter charge TYPE C. It was felt that explosion could be produced by compression-ignition by reducing the dynamic load driver pressure to 150 psig thereby increasing the mean bubble diameter distributed through the liquid propellant charge. The results of the Flow Visualization studies, discussed in Section 2.3, indicate that large bubbles are created with this low driver pressure. It is our experience that larger diameter bubbles are more sensitive to compression-ignition than smaller diameter ones. Therefore "BUBBLE RUN 8" was conducted with a liquid charge containing 3.1% by volume air ullage. As anticipated, explosion ensued. Light sensor L3 detected combustion in the bore of the liquid propellant compression chamber at t = 0.70 msec after the onset of starter charge pressurization. The pressure-time history in the liquid charge indicates severe pressure peaks (p > 100 kpsi) at approximately 1.00 msec after starter charge ignition. The severe overpressure at axial location P3 resulted in the rupture of another transducer diaphragm.

4.7 Interpretation and Discussion of Compression-Ignition Sensitivity Studies

In considering whether rapid compression of a liquid monopropellant charge with associated ullage can lead to secondary ignition sites (hot-spot ignition) and resulting explosion of the charge, we have to consider the detailed processes that may initiate a runaway exothermic chemical decomposition reaction. Heat produced by the compression process in the neighborhood of a collapsing bubble is believed to the triggering agent, not the pressure itself.

When the liquid monopropellant is rapidly compressed to ca. 50 kpsi an estimate of the temperature rise shows that, if the liquid is debubbled (de-aerated) and if the compression process is taken to be isentropic, it can be as much as 10 to 20 °C, with some uncertainty in the calculation due to lack of precise data on compressibility and thermal expansion coefficient, among other properties. A completely bubble free monopropellant is therefore unlikely to explode under sudden compression.

However, with one or more small bubbles in the liquid, a "hot spot" can be generated by the adiabatic compression of the bubble, either air or vapor, and if the bubble in initially large enough and if the compression process is rapid enough, the sharp local rise in temperature can cause the bubble to retain its heat long enough to initiate exothermic chemical reaction. The resulting rapid gas generation, which can lead to rupture of a gun chamber or to a gun breech blow if it is rapid enough or if the volume expansion does not accommodate the gas production, leads to rupture and expulsion of the specially designed shear disc assembly from the liquid propellant compression chamber bore in the PCRL experiments.

The following summarizes the results of the compression-ignition studies:

(1) For pressurization rates less than 20 kpsi/msec a dynamically-loaded neat HGB-365 liquid monopropellant charge is benign. For pressurization rates in excess of this threshold condition, explosion of the liquid monopropellant charge results, whether it be neat or containing purposefully introduced distributed ullage. This establishes the domain of safe start-up for practical dynamic load LPG systems.

(2) The severity of the explosion and associated delay time to explosion in a confined liquid monopropellant charge appears to be proportional to the space density of the bubbles.

(3) For a given pressurization rate, ca. 20 kpsi/msec, bubble size plays a dominant role in determining the tendency toward explosion. When the mean bubble diameter is increased by an order of magnitude, from 10^{-3} inch to 10^{-2} inch, the threshold for runaway reaction shifts. The dynamically-loaded liquid monopropellant charge is no longer benign when subjected to pressurization rates of 20 kpsi/msec for distributed bubbles of mean diameter 10^{-2} inch. This is of practical significance. Line (fill) pressure in a dynamic-load rapid-fire LPG can be controlled so as to produce the maximum bubble break-up. Also volumetric content of residual ullage can probably be minimized to the range considered in the aforementioned tests.

(4) No detonations have occurred in the compression-ignition sensitivity studies.

(5) It is apparent that explosion does not occur during the first pressure pulse on start-up. Runaway exothermic reaction ensues as early as 0.50 msec after pressurization onset to as late as 4.00 msec. This suggests that bubble collapse time compared to heat retention (or escape) time during the pressurization cycle is key to understanding compression-ignition.

(6) Management of the start-up pressurization history is of paramount importance from the standpoint of compression-ignition sensitivity analysis.

5.0 Theoretical Approach to Initiation of Explosion by Dynamic Compression of Liquid Explosive with Bubbles

5.1 Four Hypothetical Situations to be Considered Theoretically

A comprehensive theoretical analysis of the sensitivity problem due to bubbles should take into account at least four different physical situations. One is the case of the bubble-free or neat liquid. This might be considered the baseline case. As a result of its non-zero compressibility, the liquid takes up energy in a rapid compression, and this energy manifests itself as heat or temperature rise. This rise is on the order of a few tens of degrees C, not enough for most propellants to cause a runaway reaction in the milliseconds of gun cycle time. However, a container of neat liquid can, if the applied rate of pressure rise is tailored appropriately, (e.g., a sharp compression pulse to plateau) cavitate during the traverse of a reflected expansion wave. Such cavitation bubbles can contain air drawn out of solution as well as the propellant vapor. It requires detailed fluid mechanical analysis plus consideration of finite-rate cavitation theory in order to estimate theoretically the time delay required for the appearance of cavitation bubbles of a size sufficient to initiate the runaway reaction. This question of a safe non-cavitating pressure rise profile has not been investigated for a neat liquid to the stage of deciding just what the safe limits are, to our knowledge.

A second case of importance is that of undistributed air ullage, a large cavity or "bubble". It can be shown by analysis that a cavity of as little as 1% of a large caliber LP gun chamber volume constitutes a large bubble in the context of this theoretical discussion, that is, one whose collapse time is comparable to the applied pressure rise time and whose heat retention time is also long compared with the pressure onset time. In other words, a large bubble is one extreme of the hot-spot initiation theory, and undistributed ullage usually fits that case.

The third case for theoretical consideration is that of the isolated small bubble, initially perhaps 0.1 to 0.01 cm in size, or even smaller. In the gun chamber compression process, the bubble can "implode" to a diameter as small as a few microns, creating pressure levels within the bubble and in the immediately surrounding liquid enormously higher than the field pressure in the LP chamber, and reaching temperatures in the range of many thousands of degrees Kelvin. This is the case treated here. The bubble is taken as filled with both air and vapor; we have ignored for simplicity the dissolution of the air in the surrounding liquid but we have explicitly taken into the analysis the finite rate of evaporation and condensation of vapor in the bubble. The general conclusion can be anticipated, that a runaway reaction can be provoked by a combination of conditions: a large enough bubble, a rapid enough compression, and a sensitive enough propellant. The formulation of the equations is such as to admit the possibility of runaway exothermic reaction in either the vapor phase or the liquid phase. It should be noted that monopropellants composed of water solutions of inorganic explosive compounds that do not vaporize cannot produce explosive vapors in the bubble, so it must be inferred that the runaway reaction in such cases takes place only in the liquid phase. If so, the theory would suggest that the reaction goes most

rapidly right at the bubble-gas interface, where the temperature reaches the highest levels. If the liquid charge in the gun chamber contains many bubbles, a realistic assumption, caused by break-up and scattering of the unavoidable air ullage introduced in the filling process or brought out of solution by cavitation, then the question can be asked, whether the isolated bubble theory is applicable. It can be shown theoretically that the most important effects of the bubble in causing a runaway reaction are contained within a few radii of the bubble, so that if the ullage is less than 1%, there is a good chance that most of the bubbles can be treated by single-bubble theory.

This brings up the fourth case, that of bubble clusters. No theory is offered here for this case. Obviously, it can become the dominant case when the amount of ullage is more than 1%. A bubble cluster can lead to runaway reaction more readily than the isolated bubble, since it can create a situation in which a small field of propellant is surrounded by heat sources, thus being heated more rapidly to decomposition temperature levels than by a single central heat source. But, unless the ullage is large (which ought to be corrected in the design), the number of such clusters would be much smaller than the number of single-bubble reaction sites, and so clusters may not be the dominant problem. However, the cluster situation does deserve analysis. It has never been treated, to our knowledge.

5.2 Scope of the Present Work: Fundamental Processes and Theoretical Considerations

With the preceding discussion as background, the present work was initiated simply as an entry into the problem. Limitations of contract time and very severe limitations of contract funding precluded more than a definition of the problem and an indication of the manner of solution. For the reasons given above, attention was focused on the single-bubble problem.

Many of the ideas that underlie the following theoretical formulation were drawn from the extensive work that has been done on the theory of bubble dynamics ever since the pioneer work of Rayleigh[1], most of it with an eye on application to cavitation damage. Our problem differs from the cavitation work in one important respect: the liquid is an explosive medium that can decompose rapidly and exothermically when initiated by a collapsing bubble serving as a hot spot.

Before entering into the analysis, it is worthwhile to discuss the physical picture. We visualize a small air bubble at some moderate initial pressure, containing some vapor, perhaps one millimeter in diameter or even less, located in the middle of a field of liquid monopropellant. At the starting instant, the applied pressure comes on, not simply as a step, but as an arbitrary function of time, rising to its operating level of ca. 50 kpsi in a time of the order of 1 msec. The "wavelength" of the applied pressure is much larger than the diameter of the bubble, so that it is legitimate to treat the liquid field around the bubble as having a uniform value of "pressure at infinity", which is taken to vary with time in the manner of the applied pressure.

An "implosive" motion of the liquid ensues and the bubble starts to contract. Due to the momentum acquired by the liquid in its inward motion, the pressure in the bubble can reach levels on the order of a million atmospheres. The adjacent liquid reaches similar pressures. The temperature of the gas in the bubble can reach peaks on the order of tens of thousands of degrees Kelvin. At the severe pressures in the micro-domain around the compressed bubble, the liquid must be taken as compressible. This moderates enormously the bubble pressure that would have been predicted on the basis of incompressible liquid theory; and correspondingly, the gas temperature in the bubble is moderated enormously by the introduction of compressibility. One of the examples given below shows that the gas temperature decreases by a factor of five when the compressibility is introduced. A numerical example shows that as much as 95% of the energy of the implosion resides in the compression work absorbed by the compressible liquid, at the moment of peak bubble pressure, and only the other 5% in the compressed gas. Conduction of heat from the hot bubble gas to the surrounding liquid also moderates the pressure rise and the temperature rise during the collapse. This non-adiabaticity is difficult to predict in the absence of information about the motion of the gas in the tiny collapsing bubble. In the present work, it is assumed that the gas is simply in radial contracting motion and that the pressure is approximately uniform, i.e., that the bubble wall Mach Number is much less than one. The formulation for heat loss rests therefore on molecular heat conduction in a contracting (moving) gas. A similar formulation is used to describe the heat conduction in the surrounding liquid.

The heat conduction processes within the bubble and outside the bubble are incorporated in the general energy equation of the fluid in each case. It will be noted that each energy equation includes a chemical reaction term to describe the dependence of the exothermic reaction heat generation on the local temperature, that is, the formulation allows the possibility of reaction in both the gas (vapor) and the liquid. Associated with the question of the flow of heat from the bubble into the surrounding liquid is the rate of vaporization of the liquid to form vapor in the bubble. In the present work, finite-rate vaporization kinetics is included. In some other published work, especially in the cavitation theory literature, it has been commonplace to take the vapor density in the bubble as being in thermodynamic equilibrium with the surrounding liquid surface temperature. We have reviewed the supporting order-of-magnitude arguments and we are not convinced. Accordingly, the finite-rate evaporation-condensation equations are introduced.

One of the most interesting features of the problem arises from consideration of the time scales inherent in the problem. Five can be identified: (1) The induction time for chemical reaction in the vapor phase, determined at the high temperature at the moment of peak bubble pressure; (2) The corresponding chemical reaction time in the liquid phase; (3) The duration of heat retention in the bubble (heat conduction time); (4) The rise time of the imposed pressure "ram"; (5) The collapse time of the bubble in response to the imposed pressure field.

It is possible to anticipate some of the theoretical results. If the chemical reaction induction time is long compared with the heat retention time (i.e., slow kinetics and tiny bubbles) there is a good chance that the runaway reaction can be avoided. This effect was demonstrated in the PCRL compression initiation tests reported in 1978 (Ref. 51).

Consideration of the relative times of bubble collapse and pressure rise leads to an interesting theoretical problem that, as far as we can find, has not been treated in the literature but has a very important bearing on our problem of explosion avoidance. It can be shown theoretically that the collapse time of a typical bubble, at driving pressures on the order of 1 or more kpsi, is only on the order of a few microseconds. On the other hand, realistic pressure rise times (an LPG system or a warhead explosive subjected to setback forces) are generally on the order of one or more milliseconds. Thus, there are hundreds and perhaps thousands of cycles of bubble collapse, rebound, and collapse again within the rise time. The heat retention time is generally also long compared with the collapse time. This means that each successive collapse introduces more and more compression heat into the bubble, so that the danger point for runaway reaction would be well along in the rise of pressure, perhaps even after the applied pressure has reached the highest level, and thus the point of interest would be after some hundreds of cycles. Despite this observation, previous theoretical work has been aimed at computing the pressure, temperature, and reaction rate trajectories of a bubble during the first cycle only, usually be a vary painstaking numerical procedure on a computer. This seemed to give plausible results, but only because it was commonly assumed that the question of time scales was an unimportant one and that the pressure rise could therefore be taken to be instantaneous. It was thought that a sudden jump is just as good a model as any other pressure rise function. This is not so. The control of pressure rise rate is probably the most practical way to avoid explosions. The many-cycle model must not be ignored, but this means that the theoretical methodology has to be altered. It is simply not feasible to compute at length the entire history of the bubble through all the hundreds and perhaps thousands of cycles required to reach the theoretical explosion point. Some approximate method for summing all the effects of successive cycles is needed. More on this problem and possible approaches is given in Section 9.0 .

As pointed out at the beginning of this section, the original limited task specified in the contract was to develop a methodology for solving the system of equation developed below. Although not simple, it seemed straightforward at the time the Statement of Work was written. We conclude from the above arguments that, for a ramp-type pressure rise or for any other time function of practical nature, a new method has to be sought. Straightforward computation of the problem is not applicable to real LPG systems or to the important problem of explosion avoidance.

6.0 Literature Analysis

6.1 Collapse of Bubbles in Inert Liquids

The collapse of a cavitation bubble was first analyzed by Rayleigh[1], who addressed the problem of a spherical, evacuated bubble in an infinite liquid domain. Neglecting viscosity, surface tension and heat transfer, as well as liquid compressibility, Rayleigh used the momentum equation to derive the equation for bubble surface motion:

$$R\, d^2R/dt^2 + \frac{3}{2}(dR/dt)^2 = [p(R) - p_0]/\rho \tag{6.1}$$

Where R(t) denotes the bubble surface, P_0 = const is the driving pressure at infinity, and $p(R) = p_B^0$ = const is the bubble pressure. The mass continuity for the incompressible liquid leads to

$$u/U = (R/r)^2 \tag{6.2}$$

where U = dR/dt, which was used in the derivation of the bubble surface equation. The time for collapse was shown to be

$$t_{COL} = 0.915\, R_0(\rho/p_0)^{\frac{1}{2}} \tag{6.3}$$

expressed in terms of the initial bubble radius.

Considering the final bubble surface velocity, Rayleigh also introduced the effect of a permanent gas in the bubble, undergoing isothermal compression during collapse and calculated the conditions for rebound, as a certain maximal pressure is reached. In a concluding remard, Rayleigh mentioned the effect of liquid compressibility, noting that a satisfactory theory of collapse should include it at the early stages of development.

Addressing the original problem considered by Rayleigh, namely constant bubble pressure and incompressible liquid, Poritsky[2] investigated the effects of liquid viscosity and surface tension upon bubble collapse. He has shown both effects to enter only through the bubble surface balance, (viscosity in the liquid vanishes under the assumptions of incompressibility and irrotational flow). Incorporation of viscosity at the bubble surface results in the balance of pressures,

$$p_B^0 = p(R) + 4\mu(dR/dt)/R \tag{6.4}$$

and the bubble surface equation is

$$R\, d^2R/dt^2 + \frac{3}{2}(dR/dt)^2 + \frac{4\mu}{\rho}(dR/dt)/R = \frac{p_B^0 - p_0}{\rho} \tag{6.5}$$

where μ is the liquid viscosity, and the added term is clearly one of viscous damping.

The effect of surface tension further modifies the balance of pressures at the bubble surface,

$$p_B^0 = p(R) + 4\mu(dR/dt)/R + 2\sigma/R \tag{6.6}$$

so that the forcing term on the right hand side of Eq. 6.5 becomes:

$$(p_B^0 - 2\sigma/R - p_0)/\rho \ . \tag{6.7}$$

Clearly surface tension is important when the bubble radius is small, and tends to accelerate collapse and decelerate expansion. Viscosity, on the other hand tends to slow down the process of collapse as well as rebound. Within the range of parameters considered, Poritsky[2] shows a reduction in both collapse and rebound times by a factor ~O(10). The results were obtained by numerical integration of Eq.6.5 after transformation.

Shu[3], in a note following the analysis of Poritsky obtained asymptotic relations describing the behavior of bubble undergoing collapse or rebound, through the phase plane (U - R plane) analysis. The results point out the fundamental importance of viscosity and surface tension in the problem considered. It should be stressed, however, that both analyses are for constant bubble pressure and hence apply most closely to the cavitation bubble problem and not to the case where the cavity contains permanent gas, in which case the driving pressure difference is time dependent, and oscillatory collapse-rebound motion is anticipated. Further, the consideration of compressible liquid would have necessitated the incorporation of viscosity in the liquid momentum equation, resulting in a much higher degree of analytical complexity.

The formation, expansion and collapse of vapor bubbles in a cavitating liquid, upon passage over an ogive shaped body in a water tunnel were the subject of an analysis by Plesset.[4] This work combines experimental observations, involving pressure measurements along the body and high speed photography of the bubble motion, with analysis of the bubble surface equation. The following assumptions were employed in the analytical model: (1) incompressible liquid, (2) pure-vapor bubble (no air or permanent gas), with $p_B = p_B^0 = p_v$ = const, where p_v is the vapor pressure, (3) the bubble radius is small compared to the length scales associated with longitudinal and radial pressure gradients, (4) bubbles are carried with the local (approximately constant axial) liquid velocity, i.e., no velocity slip between the cavity and the liquid, and (5) bubble is outside of the boundary layer. These assumptions allow consideration of a vapor bubble within an "infinite" but time-dependent pressure field, with $p_0 = p_0(t)$ determined by the observed (stationary) pressure field and the longitudinal liquid velocity component. Thus the relationship of Eq.6.1 has been used, with the prescribed forcing term

$$\frac{p(R) - p_0}{\rho} = \frac{p_v - 2\sigma/R - p_0(t)}{\rho} \tag{6.8}$$

which includes the surface tension effect. In addition to the aforementioned $p_0(t)$ variation, R_{max}, the maximal bubble radius observed experimentally, is used as an input; numerical solutions were obtained, and comparison with experimental data regarding R versus t was good.

It should be mentioned that at the pressures considered (p_0 up to 8 psia) and the typical bubble radius, $R_{max} \sim O(0.1)$in, the characteristic collapse time is ~O(1)msec, and comparable to the time over which $P_0(t)$ varies. Interestingly, the plotted results show that the instant of maximal radius (full expansion) lags appreciably behind that of minimal $p_0(t)$, and occurs somewhat prior to the attainment of maximal pressure. However, no attempt was made to calculate the pressure field about the bubble, and the extent to which it influences the pressure profile about the immersed body.

Several important aspects of cavitation bubble dynamics were discussed in a further study by Plesset.[5] Actual solutions were not included in this work; rather, the physics of the cavitation problem were illuminated through comparison of characteristic scales. Dynamics of vapor-bubbles and of bubbles containing permanent gas are treated separately, and the (secondary) importance of rectified diffusion in the gas, (where mass exchange between the phases is considered) was pointed out. The questions of uniformity of the temperature field within the bubble, and limiting asymptotics of isothermal (at the low and the high frequency limits of bubble oscillations) and adiabatic (intermediate frequencies) bubble processes were discussed in terms of the thermal diffusion scales.

The question of stability of the spherical bubble shape was addressed as well; using linearized small perturbation reasoning, it was shown that the stability results for a planar phase interface are reversed for the case of a spherical cavity, namely, that if the surface is accelerated outward (into the liquid) the surface shape perturbation term approaches a constant or zero, while it tends to grow out of bounds in an oscillatory manner if acceleration is in the direction of the gas (as in collapse), and $R \to 0$.

The question of stability of the spherical bubble shape was addressed as well. Using linearized small perturbation reasoning, it was shown that the stability results for a planar phase interface are reversed for the case of a spherical cavity, namely, that if the surface is accelerated outward (into the liquid) the surface shape perturbation term approaches a constant or zero, while it tends to grow out of bounds in an oscillatory manner if acceleration is in the direction of the gas (as in collapse), and $R \to 0$. This reasonong is repeated with greater analytical detail in the review by Plesset and Prosperetti[6] leading to the conclusion that collapsing bubbles are in general unstable (converging streamlines in incompressible flow) and would result in shape distortion and subsequent breakup. Bubbles containing sufficient amounts of permanent gas (relative to liquid vapor) would tend to be more stable in this respect, on the premise that they might not reach very small radii at the fully compressed state.

These observations have led to the statement that the onset of instability during violent collapse of vapor bubbles occurs before the effects of liquid compressibility, viscosity, surface tension or heat transfer become important, thereby justifying analysis of the events leading to bubble breakup through the classical Rayleigh equation.[5] However, two major caveats should

be raised regarding the preceeding stability results: (1) The linearized analysis naturally breaks down as amplitudes of the perturbational harmonic components exceed some small value compared to R(t). Thus the final events remain unresolved, since nonlinear coupling, such as lare variations of R itself during collapse, viscous effects or heat transfer could become important and counteract to indefinite amplitude growth. Yet the very same effects were intrinsically neglected to facilitate linearization. (2) The effect of liquid compressibility was precluded in the analysis, yet it seems to become important at least at the same extents of bubble compression as those associated with instability, for driving pressures $p_0 >> 1$ atm are considered. Admittedly, the convergent streamlines during compression would enforce a meta-stable process at best, but the (particularly sensitive) high pressure region near the bubble surface would tend to be stabilized by $\partial p/\partial t \neq 0$, as some of the liquid mass displaced inward is taken up in accumulation.

Most treatments of liquid compressibility were associated with the formation and propagation of hydrodynamic shocks in the liquid, and hence relate to processes following complete collapse of vapor bubbles or underwater explosions. In the latter context the subject was extensively treated in a book by Cole[7], who summarized the knowledge accumulated from research prior to and during World War II. An exceptionally successful approximation due to Kirkwood and Bethe[8] has been advanced, under the assumption that the entropy change in the liquid, $\partial S = 0$, (unlike the enthalpy change, density change, pressure jump, etc.). This leads to the explicit expression of the conservation of total enthalpy along an outgoing (radial) characteristic line, viz.,

$$r(h + u^2/2)_I = \text{const.}$$

where I denotes the characteristic. This approximation forms the basis of a theory by Gilmore [9], and was later compared favorably with numerical solutions of the compressible equations of motion (concerning continuity and momentum, neglecting viscosity and heat transfer) by Hickling and Plesset.[10] These authors considered the problem of a bubble containing permanent gas undergoing compression and their rebound. Upon rebound, a compression wave is sent into the liquid, steepening into a weak shock within a distance comparable to the original bubble radius R_0, and with decreasing strength due to spherical dilatation. Numerical solutions were obtained by the method outlined by VonNeumann and Richtmyer [11], for the equations in Lagrangian form. The solutions were not pursued beyond wave steepening, as numerical instability was encountered.

Heat transfer from a collapsing gas bubble, provided the initial radius is small enough, has a primary effect on sonoluminescence considered in an analysis by Hickling.[12] The major effect of heat loss from the compressed bubble gas to the liquid is that of decreasing the emitted light intensity. The phenomenon itself results from subjecting a liquid with dissolved gas to cavitation by a sound field. The luminescence emanates from cavitation bubbles. The different emittance properties associated with various gases were explained in the analysis on basis of differences between their thermophysical properties. Interestingly, the equations of motion for the bubble gas contain

(beside continuity and energy) a momentum equation with an internal pressure gradient, despite indications made in a scale-analysis. At the initial pressure ratios considered, $p_B^0/p_0 \simeq 1/40$, with $p_0 = 3$ atm, it would seem important to compare the effect of liquid compressibility on the maximal temperatures attained (the effect could be comparable to that due to heat loss from the gas by conduction).

Heat transfer was also considered by Plesset and Zwick[13], in their treatment of vapor bubble growth in an initially uniformly superheated liquid, and later by Skinner and Renkoff[14] in a similar treatment with general, spherically symmetric temperature fields. The latter authors also published a second report concerning a binary liquid, and added a species conservation equation to the liquid model. In both instances the pressure within the bubble was considered uniform and constant, equal to the vapor (or vapor mixture) pressure. This and many other aspects of bubble dynamics were treated in a unified analytical discussion by Hsieh[15], where a rather complete formulation of the problem was derived.

The excellent review by Plesset and Prosperetti[6] illuminates many of the physical processes involved and serves as a good source of references on the various subjects associated with bubble dynamics. An additional general explanation to the process of cavitation is provided in the book by Batchelor[17].

6.2 Hot Spot Initiation Theory

Thermal initiation of explosives can be obtained in several manners: uniform heating (imposing a constant temperature on the sample surface), heating by shocking the explosive (heating behind a propagating shock wave in the substance) and by formation of hot spots.

In the first instance, a constant temperature is applied to an explosive sample surface. Depending on the shape (slab, cylinder or spherical) and a characteristic length of the sample, as well as on the thermochemical and thermophysical properties of the explosive, runaway reaction may occur for a surface temperature beyond a typical critical value. The criterion is simply whether a particular temperature (and history) would allow a self-sustaining exothermic reaction at some inner location. A study of this form of initiation was made by Zinn and Mader[18] covering all three sample geometries mentioned above, and four typical explosives. Theoretical analysis involves solution of the nonsteady Fourier heat transfer equation with an exothermic reaction term of first order overall, for which solutions were generated numerically. Theoretical predictions were compared with experimental measurements on a plot of time to explosion versus inverse surface temperature and show good agreement in general (except for TNT, where the decomposition kinetics were uncertain). The authors identify three parameter groups which determine the explosive behavior upon initiation, along with the geometry:

$$a^2 \frac{(\rho\lambda/C_c)}{\lambda_c}, \quad \frac{a^2}{\lambda_c} \quad \text{and } E$$

where α_c and C_c are the thermal diffusivity and specific heat of the propellant respectively, Q, A and E are the heat of reaction, the pre-factor and activation energy respectively and a is the characteristic sample dimension.

Shock initiation of explosives was discussed recently by Walker and Wasley[19] of Lawrence-Livermore Laboratory, presenting a unified model for solid, liquid and gaseous explosive substances. The model draws from a large number of published works on the subject, both theoretical and experimental, as well as from experiments performed by the authors. Three stages in shock initiation were proposed as follows:

(1) Production of ions, radicals and free atoms either by the mechanical shear effect of the shock or by thermal heating behind the shock front through molecular collisions, or by combination of shear and collisions. The first applies mostly to solids, where molecular motion is limited, the second to gases where the translational energy gain behind a shock is substantial, and the combination to liquids which have more molecular freedom than solids but also have more intermolecular structure than gases. These reactions involve usually very small activation energies.

(2) Formation of statistically random reaction sites where exothermic reactions are sustained. The number of these areas of concentrated reaction was found directly proportional to the shock strength or pressure jump.

(3) Input of critical energy flux is required, for the distributed exothermic reaction sites to grow into an explosion or detonation. In a previous article[20], the authors derived a correlation for the critical energy flux, based on energy conservation relationships:

$$J_{CRIT} = \frac{t_s \Delta P^2}{\rho u_s}$$

where t_s is the shock pulse duration, ΔP the mean shock pressure rise, ρ the density in the unshocked explosive and u_s the shock front speed. Obviously, this critical energy input is from the shock itself and, except for the relation to explosive density and shock velocity, contains no detail of the actual reaction considered, unlike the surface heating model discussed previously.[18] In this respect, only a posteriori estimates can be made for given shock conditions leading to explosion in experiments, and the correlation of Eq. 6.9 does not offer predictive capability outside of a tried explosive formulation.

A simplified explanation of hot spot initiation of explosives was given in a short analysis by Zinn[21], considering a spherical region of radius a

at a uniform elevated temperature T_i, with a single, first order overall exothermic chemical reaction. The nonsteady heat transfer equation is,

$$\partial T/\partial t + \alpha \nabla^2 T = (Q/C_p)\, Y A \exp(-E/R_u T) \tag{6.10}$$

with $Y \approx 1$ to approximate ignition. A cooling time, during which $T \simeq T_i$ within the sphere of radius a can be established,

$$t_c^* = 0.04\, a^2/\alpha \tag{6.11a}$$

due to diffusion in absence of reaction, by letting $A = 0$ in Eq. On the other hand, a heat-up or induction time can be calculated, during which temperature remains unchanged until the onset of rapid heating by reaction,

$$t_H^* \approx \left(\frac{C_p}{Q}\right)\left(\frac{R_u T_i^2}{E}\right) \exp\,(E/R_u T_i) \tag{6.11b}$$

obtained by neglecting thermal diffusion, letting $\nabla^2 T = 0$ in Eq. 6.10. If $t_c^* \simeq T_H^*$, ignition is possible. This is the basis for the calculation of a critical (minimal) radius of the hot spot.

$$a_{CRIT} \simeq \left[25\left(\frac{C_p}{Q}\right)\left(\frac{R_u T_i^2}{E}\right) \alpha \exp\,(E/R_u T_i)\right]^{1/2} \tag{6.12}$$

The author's calculated result (numerical solutions of Eq. 6.10 and a species equation where molecular diffusion was neglected) agree well with the result of Eq. 6.12, namely ignition was found possible when $a > a_{CRIT}$. However, conditions for ignition could not ensure propagation. Indeed Rosen[22] has shown that unless $E \ll 30$ kcal/mole, the reaction in the problem formulated above would extinguish due to heat losses exceeding the gain due to exothermicity.

Although the analysis gives a clear physical picture, the results seem strongly dependent upon the hot spot model, involving a sharp temperature fall at $r = a$ (outside of which $T = T_0 < T_i$ is kept) initially, leading to abrupt cooling. A more realistic model may involve a Gaussian initial temperature distribution with T_i being the peak temperature and the radius a taken at some mean value between T_i and T_0. Of course, enhanced analytical complexity can be expected.

A treatment of shock-bubble interaction in gases (neon bubble in helium and vice-versa) was presented by Evans, Harlow and Meixner[23]. The details of the two-dimensional finite difference algorithm used were given in a previous report by Harlow.[24] The results depict the process of bubble collapse upon shock passage, and the deformation caused to the initially planar shock: for the neon bubble in helium, shock velocity in the bubble is smaller than in the helium outside, and hence the shock curves locally backward; the bubble shape (initially spherical) is compressed from front

to back. The reverse is shown for helium bubble in neon. Isotherm plots show high temperature regions within the deformed bubbles and outside, after shock passage. A high degree of internal non-uniformity in temperature is indicated. Calculations with nitromethane (liquid) containing an air bubble apparently resulted in numerical instability.

Hot spot initiation of explosives by interaction between shock and inhomogeneities in the explosive (such as bubbles) was recognized and investigated in a preliminary work by Mader.[25] The calculations were aimed at correlating available experimental detonation times in nitromethane, liquid TNT and single crystal PETN which were ~O(1)μsec after the shock passage. The one-dimensional analysis (formulation was not reported) was concerned with two types of prescribed hot spherical spots, in the domain behind the planar shock, as follows: (1) thermal hot spot, in which temperature was initially elevated uniformly over the hot spot region, while density was taken equal to that of the surrounding (shocked) material, and (2) pressure hot spot, which in addition to the elevated temperature included a density increase. The elevated temperature in both cases was prescribed such that decomposition would occur at a much faster rate in the hot spot region than in the surrounding explosive (~1400K for nitromethane). Thus, unlike the treatment by Evans et al,[23] no attempt was made to assess the formation of the hot spot itself. Several distinct equations of state were considered, for the different hydrodynamic regions, e.g., for the undetonated explosive, for the detonation products (gas), for the mixture of detonation products and unreacted explosive. The work also addressed the simpler problem of uniform heating behind a shock in homogeneous explosive. In both instances good agreement with the experimental data of Campbell, Davis and Travis[26] was demonstrated, regarding both induction times and critical hot spot diameters. Mader concluded that (1) the one-dimensional (homogeneous) shock initiation model was successful and (2) that transport of heat from hot spots under shock interaction occurs primarily by hydrodynamic flow (i.e., convection) with thermal diffusion negligible, as indeed indicated by the short induction times.

This work was criticized by Enig and Petrone[27], who questioned the validity of the model predictions on grounds of (1) use of two incompatible (e,p,ρ) equations of state to describe the same unreacted explosive region, and (2) use of unreasonable values for thermophysical parameters in the equations of state, which seemed necessary to obtain agreement with the experimental detonation delay times. The parameters in question were C_{p_0} and

$$\alpha_0 = -\frac{1}{\rho_0}(\partial\rho/\partial T)_p^0$$

for the unreacted explosive, being the isobaric specific heat and the thermal expansion coefficient respectively. Mader[25] assumed these were constant in the process, i.e., $c_p(T) = C_{p_0}$, etc., and also that the specific internal energy of the explosive is $e = C_v T$ with $C_v = C_{v_0}$ = const. Enig and Petrone[27] argue that if realistic experimental values were substituted, agreement between the model results and experimental predictions would break down. The reply by Mader follows these comments.[28]

The bubble-shock interaction problem was addressed again by Mader[28], extending the previous one-dimensional model to two dimensions. The particle-in-cell method of Harlow[29] was used for finite difference approximation, modified to incorporate exothermic reaction in the liquid (represented by Arrhenius kinetics). In contrast to the previous model[25], this work is concerned with the process of hot spot formation. To include also the possibility of shock interaction with density inhomogeneities in the explosive, the study incorporates an aluminum cylinder in place of the bubble as well. The results are generally in agreement with the predictions of the one-dimensional model. For the particular case of the bubble, with a shock strength of 85 kbar and 1200K, temperatures of 4000K were found in the compressed bubble. Mechanisms of detonation-failure were discussed, with the possibility of rapid cooling by the expanding flow (convection) from the hot spot, as well as interaction with rarefaction waves; the second of these was outside of the capabilities of the two-dimensional model.

Calculated numerical results for a variety of cases were published by Mader in a series of reports[30-34], and a description of a Eulerian reactive flow model and finite difference algorithm was reported more recently[15]. This followed from the conclusion by Mader that the particle-in-cell model had insufficient accuracy for modeling of reactive flows. This improved algorithm was used to determine cases of failure to detonate[34] by hot-spot interaction, and involves the analysis of rarefaction waves passing through the reaction zone in nitromethane.

Recently, experiments were performed at BRL with hydroxylammonium nitrate liquid monopropellant[36], using a compression chamber in a blow-out gun configuration. A single 0.1 cm^3 bubble was introduced into the monopropellant under test. Pressure transducers and photo diodes were used to detect the magnitude and duration of the pressure pulses emanating from the compression charge, and to track the possible secondary ignition in the test propellant. Such evidence was indeed found, but the results tend to be admittedly inconclusive as to the exact cause and mode of secondary ignition by the occluded bubble (or other causes). Nevertheless the results indicate that further testing and analytical evaluation are required. It should be pointed out that pressure stressing of the test propellant does not occur impulsively (unlike the shocks considered by Mader[25,28,30-35] but rather gradually, as in the process of initiation of the actual propellant charge in the gun, i.e., pressure ramp durations ~O(100)μsec.

6.3 Detonation in Liquid Monopropellant: The Work by Stanford Research Institute (SRI)

The research effort by SRI was summarized in two reports[37,38] on the subject of detonation in liquid monopropellants. In essence, two separate problems were addressed in each report; first, investigation of the conditions for initiation and propagation of low velocity detonation (LVD); second, on a micro-scale, the formation of a hot spot in the liquid propellant by a collapsing bubble, in the pressurized region behind the shock front.

The two subjects mentioned were not combined within a detailed analysis of shock-bubble interaction in the manner considered by Evans, Harlow and Meixner[23] or by Mader[25,28,30-34] (neither was mention made of the latter work), although essentially the same problem was addressed. Therefore the review herein constitutes of two parts.

6.3.1 Low Velocity Detonation (LVD)

This form of detonation, compared to the common mode for explosives termed high velocity detonation (HVD), involves lower peak pressures ~O(10) kbar, lower shock front propagation velocities, ~O(2000) m/s and can be sustained by partial reaction only, in the propellant region behind the shock front.

Experiments were carried out with open steel tube holding liquid propellant, placed upright on a pad under which an explosive charge was set off. Strain gauges in the liquid recorded the progress of the shock from bottom to top. In one mode[37], the gauges were placed on the inner tube wall and measured axial and hoop-strains, presumably recording peak strains upon passage of the shock front. In the second mode[38], the gauges were placed on fiberglas partitions (perpendicular to the axis) blocking partially the tube inner bore. It would be interesting to assess the degree to which normal shock propagation and axial flow symmetry were affected by the presence of these thin bulkheas; unfortunately no such analysis was attempted.

It has been presumed in these experiments that the initiation shock strains the tube walls in such a manner as to put sufficient regions of the liquid in tension (or sub-pressure), causing vapor bubbles to form by cavitation. Since the speed of the shock in steel is higher than that in the liquid, the normal shock in the latter would then pass through cavitated regions, forming hot spots. Successful attempts to create LVD were reported[39], but it seems that the experiment was not designed to verify the interaction between the shock and the cavitation bubbles (or the number and size of these bubbles) even qualitatively.

A two-dimensional computer simulation was carried out to determine conditions for LVD in a confined liquid propellant charge, simulating the effect of hot spots by varying amounts of uniform heat release behind the shock front.[37]

A one-dimensional analysis was reported[18], to determine characteristic LVD curves on the $p - 1/\rho$ plane, again treating the reaction as an overall heat release parameter. This formulation involves a homogeneous energy equation for the region behind the shock (where heat release due to decomposition should occur), while the Rankine-Hugoniot relations (jump conditions) contain a term denoting heat of reaction. Thus, whereas the model may describe certain final states of low velocity detonation in an approximate manner, it certainly may not describe the process by which this form of detonation evolves, and these is no assurance that the final states described may indeed by achieved physically.

In addition, the degree of reaction in the model is represented by a generalized "reaction coordinate" (given as a correlation with pressure) which has no direct relationship with the chemical process at hand. Further, the question of different equations of state for the unreacted liquid propellant and for the mixture of decomposition products and unreacted liquid was not raised. A single (caloric) equation of state was considered, relating (e,p,ρ,Ψ), where e is the specific internal energy of the liquid and Ψ the reaction coordinate. Following the treatment by Mader[25] and the comments by Enig and Petrone[27], this problem seems to be of primary importance in the modeling of initiation by shock-hot spot interaction.

6.3.2 Collapse of a Vapor Bubble

The analysis of collapse of a vapor bubble was treated in an Appendix in both reports[37,38] and was carried out by Levine and Wooten of Ultrasystems. The following comments can be made, regarding the more recent report:[38]

(1) For liquid field pressures $p_0 \gtrsim 1000$ atm, (as behind the shock front), the inertial time scale associated with bubble collapse, derived by Rayleigh[1] is $R_0(\rho_L/p_0)^{1/2} \lesssim 1$ μsec for $R_0 \lesssim 1$ mm and $\rho_L \approx 1$ g/cm^3. Therefore treatment of the process of collapse is relevant within the time scales afforded by shock passage, and when interaction with a shock is sought.

However, as shown in the works of Evans et al.[23] and later by Mader[25,28,30-34] (both analytically and in experiments) two important effects prevail under these conditions. First, as an initially planar shock interacts with a spherical bubble, the shape distorts appreciably during collapse and becomes mushroomlike. Second, heat transfer due to conduction would be negligible, as the thermal diffusive time scale $R_0^2/\alpha_L \gg R_0(\rho_L/p_0)^{1/2}$ for $10^{-4} < R_0 < 0.1$ cm and hydrodynamic

convection is expected to dominate. Therefore, on the micro-scales associated with bubble collapse (R_0 and the characteristic collapse time) two-dimensional effects assume relative importance. Unfortunately, these effects were excluded. Instead, spherical symmetry was assumed, the bubble center taken stationary relative to the liquid at infinity, and the (non-reacting) heat diffusion equation in the liquid was applied.

(2) The question of liquid compressibility within this analysis was not mentioned, and the liquid was assumed incompressible as indicated by the use of the bubble-equation, in the form of Eq. 6.1 . As is well known, extremely high pressures can evolve in the liquid during bubble collapse, under which all known liquids exhibit compressibility. Thus, there seems to be no physical justification to assume incompressible liquid presently, while considering compressibility for shock propagation in the LVD analysis. As will be shown in later sections, this effect has a profound influence upon the maximal bubble pressures (and temperatures) achieved in collapse.

(3) Reaction is assumed to occur in the vapor (not in the liquid), yet the assumption of equilibrium vapor pressure is maintained, and a Clausius-Clapeyron expression (with constant heat of vaporization, Q_v) was used to determine the instantaneous vapor pressure from the bubble surface temperature. Clearly this assumption is not expected to hold when reaction is appreciable, or over a wide range of (p_B, T_B) over which Q_v is changing appreciably. A more appropriate form for the mass balance between liquid and vapor (non-equilibrium) was given by Plesset and Prosperetti.[6]

(4) The bubble properties were assumed uniform, although (regarding the temperature distribution) there might be conditions under which this assumption breaks down, and a thermal profile must be considered, as in the work by Hickling.[12] The energy equation for the uniform bubble was taken from Hsieh[16], and appears to contain a derivation error. The first law of thermodynamics, for the bubble volume,

$$\delta E = \delta Q - p\delta V$$

The variation in total internal energy is

$$\delta E = \delta(\rho V e) = \rho V \delta e + e\delta(\rho V)$$

for the case of nonvanishing mass exchange between the bubble and the liquid considered by Hsieh[16].

The second term was apparently represented by $Q_v \delta(\rho)$, but

$$e = e^0 + \int_{T^0}^{T} C_v(T')dT' \neq Q_v$$

for the temperatures considered, with e^0 being the specific internal energy at the reference state (T^0), and C_v the isochoric specific heat of the gas.

In conclusion, the simulation was intended to represent the process of bubble collapse in a shocked liquid. The various deficiencies pointed out in thepreceeding discussion seem to indicate that the actual process was inferred only in an approximate way, with may important physical aspects excluded. In this respect, the analysis of the same process by Mader[28,30-35] seems superior, although it involves a much higher level of computational effort.

The analysis was clearly not intended for modeling of secondary ignition (due to hot spot formation through bubble collapse) during the start-up transient of actual gun charge initiation, in the manner considered by Knapton et al.[36] The time scale for this process is O(0.1 - 1) msec much longer than the shock-bubble interaction times, and may not be investigated within the realm of a single bubble-collapse.

As mentioned earlier, no attempt has been made[37,38] to combine the analyses of LVD propagation and bubble collapse. Consequently, information concerning LVD evolution, failure of hot spot initiation or LVD stability cannot be obtained directly from the model.

7.0 Physical Considerations in Theory of Liquid Propellant Compression with Isolated Bubbles

7.1 Chemical Reactions and Vaporization

In the loading of liquid propellant (LP) in a gun system, bubbles might be present either as a result of unavoidable ullage in the supply system or due to cavitation somewhere in the flow passages. Such bubbles may contain, therefore, varying amounts of air and LP vapor. The presence of air under most practical rapid loading conditions must be expected. Vapor bubbles, even without air, could emanate from rapid passage of the LP over sharp edges in the loading orifice, as pointed out by Batchelor[17] in a discussion of various cavitation mechanisms in the motion of liquids at high speeds. Indeed the Flow Visualization studies of Section 2.0 for dynamic loading of the liquid monopropellant display this behavior. For these reasons, realistic modeling of hot spot initiation due to collapse of bubbles should incorporate both air as a permanent gas and the condensible vapor of the LP substance within the bubble.

Chemical reactions may occur both within the gaseous bubble and in the high temperature liquid layer surrounding the bubble. Depending on the particular type of LP, one or the other may be prominent. If the liquid consists mostly of volatile propellant material, the reaction may proceed within the bubble as well as in the liquid. On the other hand, if the liquid consists mostly of inert carrier material and its vapor phase is nonreactive, the likelihood of vapor phase reaction diminishes, and decomposition can be expected to occur mostly in the high temperature liquid layer surrounding the bubble. To present a formulation adequate for both LP types, reaction terms must be placed in both the liquid and gas phase energy conservation equations. Of course, this greatly complicates the analytical model of the process, since in addition to the "stiff" reaction terms incorporated, it becomes also necessary to follow chemical species concentrations, unavoidable in any realistic treatment involving chemical change.

The process of vaporization or condensation at the bubble surface can be expressed in terms of the Knudsen relationship,

$$m_A = \alpha[m_{out} - m_{in}] \tag{7.1}$$

where m_A is the net mass flux of the vaporizing species A, and $0 < \alpha < 1$ is the adsorption coefficient. The outward mass flux (into the gas) is given by the equilibrium expression,

$$m_{out} = f(p_A^{eq}) = \left(\frac{R_u T_s}{2\pi W_A}\right)^{\frac{1}{2}} \rho_A^{eq} \tag{7.2}$$

with $\rho_A^{eq}(T_s)$ being the equilibrium vapor density, which can be obtained from a Clausius-Clapeyron equation, and the square root term is the molecular velocity of species A perpendicular to the surface. The incoming mass flux, however, depends on the actual concentration of vapor off the surface, and hence on the physical and chemical processes in the bubble.

$$m_{in} = f(p_A) = \left(\frac{R_u T_s}{2\pi W_A}\right)^{\frac{1}{2}} \rho_A^- \tag{7.3}$$

where (-) denotes values at the gas side of the interface. Actual values of m_{in} and m_{out} are large compared with m_A due to the large molecular velocity. Therefore, at quasi-steady state, the assumption of liquid-vapor equilibrium is reasonable for calculation of $p_A^- \simeq p_A^{eq}(T_s)$, although the liquid may undergo vaporization, and $m_A \neq 0$. Under dynamic conditions, however, a relatively small change in p_A^- can result in an appreciable change in m(t), which can not be anticipated when the liquid-vapor equilibrium assumption is employed. Thus, the combination of the last three equations,

$$m_A = \alpha\left(\frac{R_u T_s}{2\pi W_A}\right)^{\frac{1}{2}} \rho^-[Y_A^{eq} - Y_A^-] \tag{7.4}$$

where $\rho_A \equiv \rho^- Y_A$ and Y_A is the mass fraction, serves as an adequate gas-liquid interface condition in the dynamic process.

In view of the large variation expected in bubble temperatures and pressures during the process of bubble compression, the Clausius-Clapeyron expression for ρ_A^{eq} should be used in its integral form to accommodate $Q_V = Q_V(T_s)$. For instance, note that $Q_V \doteq 0$ in the neighborhood of the critical point $(P_B, T_B)_{CRIT.}$

7.2 Characteristic Length and Time Scales

Heat transfer between the bubble gas and the surrounding liquid has an extremely important role in proper assessment of hot spot initiation. Therefore, detailed modeling of the bubble processes can not be avoided in the analysis, since the thermal wave and pressure field structure within the bubble determine the gas phase side of the thermal balance (the pressure field is important in the presence of gas phase reaction). The question is whether the bubble environment can be ideally considered as uniform at all times (yet time dependent) during the process, without serious loss of physical significance in the results. Further, within the time frame of start-up pressurization of the LP charge, the question is what relationships exist between the rates of bubble collapse, thermal equilibration, chemical relaxation, and the rate of pressurization itself. To obtain some preliminary insight, the following length and time scale analysis was carried out.

The length scale associated with the thermal wave within the bubble is the diffusive characteristic distance,

$$X_{TH1} = (\alpha_B \tau_{COL})^{\frac{1}{2}} = \left[\left(\frac{\lambda}{\rho_B C_p}\right) R_o \left(\rho_L/P_o\right)^{\frac{1}{2}}\right]^{\frac{1}{2}} \tag{7.5}$$

where τ_{COL} is the characteristic collapse time taken from Rayleigh's

incompressible liquid theory. A second associated characteristic thermal length is the convective-diffusive distance,

$$\chi_{TH2} - \alpha_B/\bar{U} = \left(\frac{\lambda}{\rho_B C_p}\right)(\rho_L/P_o)^{1/2} \tag{7.6}$$

where $\bar{U} \equiv R_o/\tau_{COL} = (P_o/\rho_L)^{1/2}$ is the characteristic collapse velocity. The relationship between χ_{TH1} and χ_{TH2} is

$$\chi_{TH2}/\chi_{TH1} = \chi_{TH1}/R_o \tag{7.7}$$

These scales can be calculated, depending on the driving pressure P_o, the bubble pressure ratio p_B/P_o and the reference bubble radius R_o. Utilizing the properties of water and nitrogen, the following values evolve:

P_o(atm)	p_B/P_o	R_o(cm)	χ_{TH1}(cm)	χ_{TH2}/χ_{TH1}
1	10	0.1	0.056	0.56
1000	100	10^{-2}	1.2×10^{-4}	0.012
1000	100	10^{-4}	1.2×10^{-5}	0.12

The results can be summarized as follows:

(a) At low pressures, as in the early stages of compression,
(1) relatively large bubbles, with $R_o \sim O(1$ mm, possess highly nonuniform thermal fields, since $\chi_{TH1} \sim R_o$.

(2) under these conditions, small bubbles with $R_o \sim O(1\text{-}10)\mu m$ would have uniform temperature distributions.

(b) At high driving pressures and pressure ratios,
(1) a thin, high-gradient, thermal layer near the bubble surface is inferred for relatively large bubbles, down to $R_o \sim O(100)\mu$,

(2) a nonuniform thermal field is indicated again for small bubbles, $R_o \sim O(1\text{-}10)\mu m$, with $\chi_{TH1} \sim R_o$.

The uniformity of the pressure field within the bubble can be inferred from a comparison of characteristic time scales associated with fluid dynamic equilibration, τ_{fd}, and bubble collapse, τ_{COL}:

$$\frac{\tau_{fd}}{\tau_{COL}} = \frac{R_o/c}{R_o(\rho_L/P_o)^{1/2}} = \frac{(P_o/\rho_L)^{1/2}}{(\gamma p_B/\rho_B)^{1/2}} = \left(\frac{\rho_B}{\gamma\rho_L}\right)^{1/2}\Big/\left(\frac{p_B}{P_o}\right)^{1/2} \tag{7.8}$$

where c denotes the adiabatic speed of sound in the gas. For the properties of water and nitrogen, the time scale ratio can be calculated:

P_o (atm.)	p_B/P_o	τ_{fd}/τ_{COL}
1	10	7×10^{-3}
1000	100	0.02

Evidently, at low driving pressures and low compression ratios the uniform pressure field assumption is very good, while at higher pressures it tends to be invalidated; nevertheless, the interior pressure field can be assumed uniform to a good approximation even at the high values of (P_o; p_B/P_o) shown.

Start-up of the LPG system involves an onset of pressure which applies roughly 1000 atm within a period of 0.1 to 1 msec. During this process, gas bubbles imbedded in the LP charge can collapse at a rate which may differ significantly from the rate of pressure start-up. Utilizing the Rayleigh time scale,

$$\tau_{COL} = R_o(\rho_L/P_o)^{\frac{1}{2}}$$

the calculation yields:

P_o (atm)	R_o (cm)	τ_{COL} (msec)
1	0.1	0.1
1000	10^{-2}	3×10^{-4}
1000	10^{-4}	3×10^{-6}

The calculations show that at the early stages of the process, for relatively large bubbles, the bubble collapse and the applied external pressure may interact dynamically, so that the time variation of the imposed $P_o(t)$ may not be neglected in the collapse analysis. However, for small bubbles, with $R_o \sim O(1\text{-}10)\mu m$ at practically all stages of external pressurization, the rate of bubble collapse is much faster than the rate of $P_o(t)$ variation and $P_o(t)$ can be considered as quasi-steady during any collapse-rebound cycle period In this instance, the bubble collapse process and the external pressure variation are effectively decoupled dynamically. More importantly, if the viscous dissipation in the liquid-gas system is sufficiently low, the preceeding calculations indicate that (for the relatively small-size bubbles considered), practically hundreds or thousands of collapse-rebound cycles may evolve during a single P_o-pressurization period.

The possibility of rebound of the bubble following full compression, as well as the periodicity of collapse-rebound, were mentioned already by Rayleigh[1]. To assess the implications of this process upon hot spot initiation, the characteristic collapse time should be compared with the bulk thermal relaxation time for the bubble and the liquid, defined

$$\tau_{THB} = R_o^2/\alpha_B = R_o^2/(\lambda/\rho_B C_p) \qquad (7.10)$$

and

$$\tau_{THL} = R_o^2/\alpha_L \tag{7.11}$$

respectively. For the properties of nitrogen and water,

P_o (atm)	p_B/P_o	R_o (cm)	τ_{THL} (msec)	τ_{THB} (msec)	$\frac{\tau_{THB}}{\tau_{COL}} \times 10^{-3}$	$\frac{\tau_{THL}}{\tau_{COL}} \times 10^{-3}$
1	10	0.1	7×10^3	210.	2	70
100.	10	10^{-2}	67	56.	56	70
1000.	100	10^{-4}	7×10^{-3}	0.15	47	7

The results show that

(1) Thermal relaxation within the bubble has a rate much slower than the collapse rate.
(2) Similarly, the rate of liquid thermal relaxation is also much slower than the collapse rate.

The last two observations regarding the relationship between rates of collapse, start-up pressurization and thermal relaxation may be summarized as follows:

(1) Bubble collapse and rebound occur much faster than characteristic start-up pressurization,

(2) Thermal relaxation within the bubble and in the surrounding liquid are much slower than typical bubble collapse.

7.3 The Effects of Liquid Compressibility

The relevance and importance of liquid compressibility to the present bubble compression problem cannot be over emphasized. It strongly influences two major aspects of the physical process: the dynamics of pressure waves in the liquid, and the balance of energy between the liquid and the bubble.

Neglecting for the moment the (highly localized) conductive term in the energy balance for the liquid, and considering a non-reacting liquid phase, the dynamic process can be expressed in terms of three nonlinear, coupled differential equations which form a hyperbolic set. As pointed out by Lax[39], such nonlinear hyperbolic systems can obtain weak solutions, which allow the formation and propagation of hydrodynamic shocks, observed also in practice. Previous treatments of bubble-liquid dynamics which account for liquid compressibility were concerned with the problem of shock propagation in liquids, as discussed in the book by Cole[7].

Prior to the advent of high speed computers, many of the analyses sought closed form solutions and employed suitable approximations. The most

well known approximation is due to Kirkwood and Bethe[8], based on the assumption that $\delta S \approx 0$ across the liquid shock (negligible entropy change), and leads to an expression of the total (static and kinetic) enthalpy distribution following an outgoing characteristics line, denoted by I:

$$r(h + u^2/2)_I = \text{const.}$$

This result was utilized in a first order perturbation theory by Gilmore[9], and later compared against numerical solutions of the exact equations of motion (continuity and momentum, assuming isentropicity in the liquid) by Hickling and Plesset[10], where the approximation was demonstrated to be in good agreement with the numerical results.

Regarding the influence on hot spot initiation, two effects may be considered in this instance. First, the passage of hydrodynamic shock (resulting from rebound of one bubble) over a neighboring bubble undergoing compression - or at early stages of rebound - can significantly contribute to the thermal energy accumulation in the latter, and may lead to hot spot initiation after rebound. Second, wave steepening was shown to occur[10] within a distance of $O(R_o)$ of a rebounding bubble center. Since compressed bubbles are generally much smaller than their original size, $R(t)/R_o << 1$, the effect of shock front encountering a small disturbance (e.g., another bubble) may lead to enhancement of the liquid phase reaction, a mechanism for detonation investigated by Mader[28,30-34]. On the other hand, shocks emanating from a rebounding bubble are expected to be weak, at $r/R_o >> 1$ as indicated by the results of Hickling and Plesset[10], since they are driven by a small, finite amount of energy and diminish in strength due to spherical dilation.

The second physical aspect of liquid compressibility can be invoked in terms of the energy balance in a system containing a single gaseous bubble. For simplicity, only the fully collapsed state (minimal bubble radius) is considered, but the results apply to all states of bubble surface motion. If the liquid field pressure, P_o = Const., the driving "stroke work" for the collapsing bubble is given in the incompressible liquid case, by

$$W_{STROKE} = P_o \Delta V_B = -P_o \frac{4\pi}{3} (R_{min}^3 - R_o^3) \tag{7.12}$$

However, when the liquid is compressible, the above expression is modified, as

$$W'_{STROKE} = P_o \Delta V_B - P_o \int_R^\infty \rho 4\pi r^2 dr \int_{\rho_o}^{\rho(r)} d(1/\rho) \tag{7.13}$$

where the second term corresponds to $P_o \Delta V_L$, the part of the stroke work absorbed by liquid compression. At the fully compressed state, the stroke work is converted entirely into compression work (considering viscous and other losses negligible) so that for the incompressible liquid:

$$W_{STROKE} = -\int_{V_{B_0}}^{V_{B_{min}}} p_B dV_B = -\int_{R_o}^{R_{min}} 4\pi p_B(R) R^2 dR \qquad (7.14)$$

where the functional dependence of $p_B(R)$ is determined by the nature of the bubble compression process (isothermal, adiabatic, or intermediate). On the other hand, for the compressible liquid case,

$$W'_{STROKE} = -\int_{V_{B_0}}^{V_{B_{min}}} p_B d_B - \int_R^{\infty} \rho\, 4\pi r^2 dr \int_{\rho_o}^{\rho(r)} p d(1/\rho) \qquad (7.15)$$

where the additional term arises from liquid compression work. Now since $p(r)/P_o > 1$ for $R \leq r < \infty$,

$$W_{CL} = -\int_R^{\infty} \rho r^2 dr \int_{\rho_o}^{\rho(r)} p d(1/\rho) \geq -\bar{P}_m \int_R^{\infty} \rho r^2 dr \int_{\rho_o}^{\rho(r)} d(1/\rho) \qquad (7.16)$$

$$> -P_o \int_R^{\infty} \rho r^2 dr \int_{\rho_o}^{\rho(r)} d(1/\rho) = P_o \Delta V_L$$

where $\bar{P}_m$ is a constant mean pressure in the liquid, $P_o < \bar{P}_m < p(R)$. Therefore the liquid compression work always exceeds the associated driving stroke work $P_o \Delta V_L$. This means that when the liquid is compressible (as all liquids are), less of the stroke work is available for bubble compression. In particular, this conclusion leads to the following comparisons:

COMPRESSIBLE LIQUID		INCOMPRESSIBLE LIQUID
R_{min}	>	R_{min}
$P_{B_{max}}$	<	$P_{B_{max}}$
$T_{B_{max}}$	<	$T_{B_{max}}$

Indeed, the calculated results of Appendix A for the incompressible case show enormous maximal bubble pressures (and temperatures) compared with the approximate solutions for the compressible liquid case, given in Appendix B; the above results tend to be strongly verified.

Comparison at several initial bubble pressure ratios p_B^o/P_o and

driving pressures P_o is given in the following table along with the fraction of compression work absorbed in the liquid to its compressibility. All the tabulated results are for the adiabatic bubble approximation.

TABLE 4

COMPARISON OF COMPRESSIBLE AND INCOMPRESSIBLE LIQUID SOLUTIONS AT MAXIMAL COMPRESSION STATE

$\frac{P_B^o}{P_o}$	P_o (atm)	$\frac{R_{Bmin}}{R_o}$	$\frac{P_{Bmax}}{P_o} - 1$	$\frac{T_{Bmax}}{T_B^o}$	$\frac{W_{CL}}{W_{STROKE}}$
0.002	-	0.0012	2.5×10^3	201	-
	(a) 100	.04	1.5×10^3	48	88
	(a) 500	.06	2.2×10^2	28	93
	(a) 1000	.07	1.1×10^2		
0.010	-	0.0044	4.9x10	43	-
	(a) 100	.07	7 x10	24	61
	(a) 500	.11	1.2x10	15	81
	(a) 1000	.13	60	12	95
0.100	-	0.264	27	5	-
	(a) 100	.265	25	4.7	2.4
	(a) 500	.277	21	4.67	13
	(a) 1000	.298	15	4.3	29

NOTE: (a) compressible liquid approximate solution is in Appendix B.

7.4 Summary

The following preliminary conclusions may be drawn, based on the physical considerations of the preceeding sections.

(1) Liquid compressibility has a profound effect upon the actual maximal pressures and temperatures obtained in a collapsing gaseous bubble. Compared with results for incompressible liquid, final bubble pressures are reduced by two orders of magnitude or more and temperatures by at least one order of magnitude, when the bubble is considered ideally adiabatic (fast compression). This implies that liquid compressibility must be taken into account in the analysis of hot spot initiation.

(2) The applied start-up pressurization time is typically much longer than the inertial bubble collapse time $\tau_{COL} = R_o(\rho_L P_o)^{\frac{1}{2}}$ for the range of bubble radii and pressures considered, and almost always much shorter than the bulk thermal relaxation time of the bubble-liquid system. Therefore, for sufficiently low viscous damping in the liquid, many collapse-rebound cycles can be expected during start-up pressurization, over which heat will accumulate in the bubble and in the immediately surrounding liquid. Thus, whereas a single bubble collapse may be too brief to lead directly to hot spot initiation, a series of hundreds or thousands of collapse-rebound cycles, during which the external driving pressure is continuously rising, may under favorable interaction with the chemical kinetics lead finally to runaway reaction.

8.0 Analytical Model

The analytical model concerns a single gas bubble in an infinite liquid medium. Consequently, the treatment is divided into three parts: the liquid phase, the gas-bubble interior and the interface conservation conditions at the bubble surface. Despite the indications that spherical bubble shapes are sometimes unstable, as discussed by Plesset[5] and Plesset and Prosperetti,[6] the assumption of spherical bubble shape is made, to obtain a mathematically tractable model at this stage.

8.1 The Liquid Phase

Assumptions regarding the liquid phase are as follows:

a) inviscid, homogeneous and isotropic liquid
b) body forces are negligible
c) irrotational liquid motions
d) no sources/sinks of mass, momentum and energy
e) spherical symmetry
f) compressible liquid phase
g) surface tension is negligible

In spherical polar coordinates, the equations of motion are written in Eulerian form:

$$\partial\rho/\partial t + \mathrm{div}\,(\rho \underset{\sim}{u}) = 0 \tag{8.1}$$

$$\partial(\rho \underset{\sim}{u})/\partial t + \mathrm{div}(\rho \underset{\sim}{u}\underset{\sim}{u}) = -\,\mathrm{div}\,(\bar{\bar{P}}) \tag{8.2}$$

$$\partial(\rho e_T)/\partial t + \mathrm{div}(\rho \underset{\sim}{u} e_T + \underset{\sim}{u}\bar{\bar{P}}) = \mathrm{div}(\lambda\,\mathrm{grad}\,T) + q_{R,L} \tag{8.3}$$

$\underset{\sim}{u} = u\hat{e}_r$ is the only component of velocity considered (radial); the total specific internal energy is $e_T = e(T) + u^2/2$ and the pressure tensor is $\bar{\bar{P}}$. $q_{R,L}$ is the heat release by chemical reaction in the liquid. The above formulation follows those derived by Williams[40] or Batchelor[17].

After taking the assumptions into consideration, the equations of motion for continuity, momentum and energy can be written, in simplier form:

$$\frac{\partial\rho}{\partial t} + \frac{1}{r^2}\frac{\partial}{\partial r}(r^2\rho u) = 0 \tag{8.4}$$

$$\frac{\partial u}{\partial t} + u\frac{\partial u}{\partial r} + \frac{1}{\rho}\frac{\partial p}{\partial r} = 0 \tag{8.5}$$

$$\frac{\partial e}{\partial t} + u\frac{\partial e}{\partial r} + \frac{p}{\rho}\frac{\partial u}{\partial r} = \frac{1}{\rho r^2}\frac{\partial}{\partial r}\left(r^2\lambda\frac{\partial T}{\partial r}\right) + q_{R,L}/\rho \tag{8.6}$$

for $t > 0$ and $R < r < \infty$.

The consideration of chemical reaction requires the addition of species conservation equations; for the liquid phase mass fractions Y_j, assuming all binary diffusivities to be equal to the mean ρD:

$$\frac{\partial Y_j}{\partial t} + u\frac{\partial Y_j}{\partial r} = \frac{1}{\rho r^2}\frac{\partial}{\partial r}\left(r^2\rho D\frac{\partial Y_j}{\partial r}\right) + \alpha_{L_j} W_L/\rho \tag{8.7}$$

$$j = 1, 2 \cdots N$$

where $\alpha_{L_j} \equiv W_j(\nu_j'' - \nu')_L$, ν_j' and ν_j'' being the stoichiometric coefficients of species j in the liquid reaction, and N is the total number of such species participating. For the case of a single overall reaction step, Shvab-Zeldovich coupling terms may be formed; defining

$$\beta_j \equiv Y_j/\alpha_{L_j} \qquad j=1,2,3 \cdots N \tag{8.8a}$$

such that

$$\Phi_j \equiv \beta_1 - \beta_j \ , \ J=2,3,\cdots N \tag{8.8b}$$

and the differential operator for these Φ_j terms is free of the reaction term, viz.,

$$\frac{\partial \Phi_j}{\partial t} + u\frac{\partial \Phi_j}{\partial r} = \frac{1}{\rho r^2}\frac{\partial}{\partial r}\left(r^2\rho D\frac{\partial \Phi_j}{\partial r}\right), \ j=2,3\cdots N \tag{8.9}$$

Consider an overall one-step decomposition reaction of a liquid phase species A, forming products which remain dissolved in the liquid,

$$A(\ iq) \longrightarrow B_1(g) + B_2(g) + \cdots + Q_L$$

with Q_L being the heat of reaction. If we represent approximately all the products $B_j(g)$ as a single mean species (inert), the reaction scheme simplifies to

$$A(liq) \longrightarrow B(g) + Q_L \tag{8.10}$$

If the liquid consists of reactant A and an inert diluent C, its mass fraction remains invariant at all time, $Y_c(r,t)$ = const., and only two species equations have to be solved, in the form given by Eqs. (8.7) and (8.9).

The liquid compressibility statement (i.e., equation of state) is,

$$C\rho^n = p + B \tag{8.11}$$

which has been used by Hsieh[16] as well as by Hickling and Plesset[10]. For water, the values of $n = 7$ and $B = 3000$ atm were proposed. This corresponds approximately to a bulk modulus of 300,000 psi at one atmosphere pressure. More general expressions involve polynomials including powers lower than $n = 7$. The above compressibility equation is for an isothermal process, and hence not strictly applicable to the present general formulation; a more adequate expression can be derived from basic thermodynamic principles, cf. Moelwyn-Hughes[41]. The internal energy statement is

$$e(T) = C_V T \tag{8.12}$$

and the reaction term is

$$q_{R,L} = Q_R W_L(T) \tag{8.13}$$

where $W_L(T)$ is the reaction rate, which can be fitted to an Arrhenius expression.

It should be noted that thermal transport is expected to be negligible over most of the liquid region, except within a thin, high gradient layer adjacent ot the bubble surface, where temperature is also high due to transfer from the bubble. It would be also safe to assume that the reaction term, $q_{R,L}$, is relatively important within the same layer (provided the activation energy is sufficiently high) and negligible outside. Thus, for the liquid domain outside of this thin thermal layer, the assumption of isentropic liquid may be employed, in line with the analysis of Gilmore[3] and Hickling and Plesset[10]. A suitable length scale associated with the thermal layer thickness is

$$\chi_{THL} = (\alpha_L \tau_{COL})^{1/2} \tag{8.14}$$

which arises naturally from the energy equation, and where the characteristic inertial collapse time was defined in Eq. (7.9). Explicitly,

$$\chi_{THL} = \left[\frac{\lambda_L}{C_p \rho_L} R_o \left(\frac{\rho_L}{P_o}\right)^{1/2}\right]^{1/2} \tag{8.15}$$

utilizing the properties of water,

P_o (atm)	R_o (cm)	χ_{THL} (cm)
1	0.1	4×10^{-4}
1000	10^{-2}	2×10^{-5}
1000	10^{-4}	2×10^{-6}

it is demonstrated that $\chi_{THL}/R_o \ll 1$.

The following boundedness-conditions are relevant:

$$u(\infty,t) = 0 \tag{8.16a}$$

$$p(\infty,t) = P_o(t) \tag{8.16b}$$

where $P_o(t)$ is the imposed far field pressure, which may vary with time in a specified manner (e.g., ramp function); however, the initial pressure distribution in the field is uniform:

$$p(r,o) = P_o(0) \tag{8.17}$$

Clearly, the liquid field problem, as posed by the preceeding formulation and boundary conditions is quite formidable, and considerable simplification may be achieved if $P_o(t)$ = const. is specified. This type of simplification has been used in cavitation theory.

8.2 The Gas Phase

The following assumptions are made, regarding the bubble interior:

a) the bubble environment consists of a mixture of permanent gases, as well as vapor from the liquid
b) the gas mixture may undergo chemical reaction, represented by a single overall reaction step
c) assumptions (a) through (f), made for the liquid phase, are applied to the gas phase as well.

Consequently, the gas phase system of equations has exactly the same form as the liquid phase system, employing Eulerian form.

An additional simplifying assumption can be introduced, regarding the pressure field within the bubble. During the important final stage of the process of collapse, the pressure within the bubble is expected to be much larger than the liquid pressure at infinity, while the liquid density would always be higher than that of the gas. Therefore, it can be expected that the gas-dynamic equilibration time within the bubble would be always much smaller than the characteristic process (bubble collapse) time, viz.,

$$R/c_g \ll R_o(\rho_L/P_o)^{\frac{1}{2}} \tag{8.18}$$

where $c_g = (\gamma P_g/\rho_g)^{\frac{1}{2}}$ is the adiabatic speed of sound in the gas and γ the specific heat ratio. This affords the following simplification,

$$p(r,t) = p_B(t),\ 0 \leq r < R \tag{8.19}$$

namely, the pressure is taken uniform within the bubble at all times.

The system of equations describing the process in the bubble interior is therefore,

$$\frac{\partial \rho}{\partial t} + \frac{1}{r^2}\frac{\partial}{\partial r}(r^2 \rho u) = 0 \tag{8.20}$$

$$\frac{\partial u}{\partial t} + u\frac{\partial u}{\partial r} = 0 \tag{8.21}$$

$$\frac{\partial e}{\partial t} + u\frac{\partial e}{\partial r} + \frac{P}{\rho}\frac{\partial u}{\partial r} = \frac{1}{\rho r^2}\frac{\partial}{\partial r}(r^2 \lambda \frac{\partial T}{\partial r}) + \frac{q_R}{\rho} \tag{8.22}$$

for $t > 0$ and $0 < r < R$.

To accommodate the elevated pressures expected during the period of collapse, the Noble-Abel equation of state is utilized,

$$p(\frac{1}{\rho} - \eta_B) = R_u T/\overline{W} \tag{8.23}$$

where η_B is the covolume[42], typically $1 cm^3/g$, and $\overline{W}$ the mean molecular weight of the gas.

The reaction in the gas phase may be first order or second order overall,

$$A(g) \longrightarrow B(g) + Q_g \tag{8.24a}$$

$$A_1(g) + A_2(g) \longrightarrow B(g) + Q_g \tag{8.24b}$$

where B(g) in both cases denotes the mean, inert product mixture. The presence of a diluent C(g) is also anticipated, again with invariant mass fraction. The reaction rates for the chemical mechanisms shown are, respectively:

$$\omega_g^{(1)} = \rho A_1 \exp(-\tilde{E}_1/T)(Y_A/W_A) \tag{8.25a}$$

$$\omega_g^{(2)} = \rho^2 A_2 \exp(-\tilde{E}_2/T)(Y_{A_1}/W_1)(Y_{A_2}/W_2) \tag{8.25b}$$

The species conservation equations are of the same form as those in the liquid (of course, using gas phase properties) and shall not be repeated. The mean molecular weight in the equation of state is defined

$$\overline{W} = (\sum_{j=1}^{N} Y_j/W_j)^{-1}$$

It should be emphasized that due to the presence of permanent gas in the bubble, the total interior pressure is not equal to the vapor pressure, and is not determined by the phase interface temperature.

The associated boundary conditions are given:

$$u(0,t) = 0 \tag{8.26a}$$

$$\partial T/\partial r(0,t) = 0 \tag{8.26b}$$

8.3 The Phase Interface Conservation Conditions

Following Plesset and Prosperetti [6], the pressure force balance at the bubble surface is

$$p(R^+) = p_B - \frac{2\sigma}{R} - \frac{4\mu}{R} U \tag{8.27}$$

where p_B is the interior bubble pressure (assumed uniform in the gas phase treatment), and σ and μ are the surface tension constant and the liquid viscosity respectively. For the range of pressures and bubble sizes considered, $p(R^+) \sim O(1000)$atm, $R \sim O(2)$ μm utilizing the properties of water (σ = 150 dyne/cm and $\mu \doteq 0.01$ g/cm-s) the two last terms can be shown to be negligible compared with the pressure $p(R^+)$. Hence,

$$p(R^+,t) = p_B(t) \tag{8.28}$$

In addition,

$$T(R^+,t) = T(R^-,t) = T_s(t) \tag{8.29}$$

i.e., temperature is continuous across the interface.

Heat and mass exchange across the phase interface may occur during the cavitation process through conduction and vaporization. Considering vaporization, the bubble surface velocity

$$U(t) \equiv dR/dt = U_e + v_B \tag{8.30}$$

where U_e is due to compression or expansion of the bubble gas, and $v_B(t)$ is the surface regression rate due to vaporization, defined

$$v_B = m(t)/\rho_L(R^+,t) \tag{8.31}$$

with m the vaporization mass flux. Consequently, the velocity on the gas side of the interface can be expressed as

$$u(R^-,t) = U - m/\rho_g(R^-,t) \tag{8.32}$$

During the rapid collapse process considered, the a priori assumption of equilibrium vaporization as made in the SRI report[38] is not warranted. Hence, the more general nonequilibrium expression is proposed,

$$m_A = F(T_s, W_A, \alpha)(\rho_A^{eq} - \rho_A)$$

as given by Eqs. (7.1) through (7.4).

Further, for the case of water, the latent heat of vaporization varies with temperature, and vanishes at the critical point Therefore, a general interface energy constraint would involve $Q_V = Q_V(T_s)$. Following Scala and Sutton[43] and Williams[40] the conservation conditions for enthalpy and species mass fractions are given respectively,

$$mh(R^-) - (\lambda/C_p)_g \, \partial h/\partial r(R^-) = \tag{8.33}$$

$$mh(R^+) - (\lambda/C_p)_L \, \partial h/\partial r(R^+) - mY_L Q_V(T_s)$$

where Y_L denotes the evaporating liquid mass fraction (on the liquid side, at R^+) and $Q_V(T_s)$ is the latent heat of vaporization.

$$mY_j(R^-) - (\rho D)_g \partial Y_j/\partial r(R^-) = \tag{8.34}$$

$$mY_j(R^+) - (\rho D)_L \, \partial Y_j/\partial r(R^+)$$

$$j=1,2 \cdots N$$

In conclusion, it should be emphasized that the formulation given in the last two sections is strictly for the spherically symmetric case where the field pressure at infinity, $P_o(t)$, may vary in a continuous manner, and is intended to simulate the relatively slow start-up transient. As pointed out earlier, this might involve many collapse-rebound cycles, during which heat is accumulated in a region roughly the size of the initial bubble.[30-33]

9.0 Method of Solution

9.1 The Two Time Scale Problem

Within the realm of an investigation of propellant initiation during the start-up transient by hot spots, through gas-vapor bubble compression, the foregoing physical considerations have pointed out the possible existence of two distinct time scales (at least) for the problem. Disregarding for the moment chemical kinetic time scales, the two distinct characteristic times are:

(1) The typical start-up transient time, $\tau_0 \sim O(0.1-1)$ msec characterizes the variation of the field pressure, $p_0(t)$.

(2) The characteristic bubble collapse time, $\tau_1 = \tau_{COL}$ defined earlier $O(1)$ msec.

Evidently, $\tau_0 >> \tau_1$ for the problem considered. It should be stressed that an oscillatory pressure field, with $p_0(t)$ having both monotonically, varying as well as periodic components is not excluded, but the condition on the wavelength of these oscillations is that they be much longer than R_0, the initial bubble radius, and their period be much larger than τ_{COL} [otherwise, if the opposite extreme is considered, the short wavelength, shock-bubble interaction problem addressed by Nader[28,30-34] is recovered .]

Thus, with viscous dissipation sufficiently low and with bubble-stability permitting, the overall problem concerns many collapse-rebound bubble cycles over the period of a single start-up transient. Over these periods, pressure and temperature within the bubble would oscillate with a relatively high amplitude, but their mean values are expected to vary as well, on a longer time scale. This is based on the observation that thermal dissipation in the liquid surrounding the bubble occurs on a time scale much longer than τ_{COL}, and therefore heat may accumulate in the bubble over several periods during which the driving field pressure $p_0(t)$ somewhat increases.

When chemical reactions (in the bubble and/or within the high-temperature propellant region surrounding it) are considered, the associated kinetic time scales have crucial importance regarding a process that may or may not lead to secondary ignition. Of course, these chemical time scales cannot be considered outside of the framework of the process at hand, as they are strongly temperature (and pressure) dependent.

Depending on the magnitude of the kinetic time scales, the processes of bubble collapse and chemical heat release may interact over a short time scale (within a period of collapse-rebound) or a long time scale (within many periods of collapse-rebound). Even with a given set of kinetic parameters and chemical mechanism, it would be difficult to assess a priori what type of interaction should be expected, owing to the highly nonlinear coupling between the chemical and bubble-collapse processes. Thus, analysis is proposed along two major lines, as follows.

(1) Investigation of the short time scale process. This analysis is aimed at solving the bubble-propellant interaction problem over a small number of collapse-rebound periods, during which the driving field pressure variation is small or vanishing.

(2) Investigation of the long time scale behavior, or the mean process. This part of the analysis requires re-casting of the problem in terms of two time scales (τ_0, τ_1), and involves transforming the equations given in the preceeding section. Then, following quasi-linearization, a mathematical averaging method would be applied, so that the small-scale oscillations are considered only in terms of their mean envelope, which may vary with the long time scale, τ_0.

Although put in two distinct categories, both analyses should be carried out, in the order indicated. The solutions to the micro-scale process are required to obtain a firm guidance for the linearization involved in the two-time scale analysis, over a wide enough range of initial conditions, thermophysical and kinetic parameters.

9.2 Outline of the Solution Procedure

9.2.1 Short Time Scale Analysis

The system of equations for the liquid, gas bubble and phase interface are utilized as given in Section 8.0. A single time scale and length scale are proposed, to obtain dimensionless coordinates:

$$\xi \equiv r/R_0, \quad \eta \equiv t/\tau_{COL}.$$

The sets of conservation equations for the liquid and for the gas are then solved separately by the general-implicit predictor-corrector, finite difference algorithm, applied to the system in Eulerian form. At each step during the time marching procedure, the liquid and gas solutions are matched, to satisfy the bubble interface conservation conditions. A similar procedure was successfully applied to the problem of nitramine deflagration by Ben Reuven et al.,[44,45] solving simultaneously for ten independent unknown variables; time-marching was used for obtaining a final steady state solution from a set of initial data.

9.2.2 Two Time Scale Analysis

This analysis is intended for elucidation of the long time scale behavior of the bubble-propellant system. In order to carry out the analysis, properties which oscillate (e.g., pressure and temperature in the liquid and the gas) are designated two sets of independent time coordinates, corresponding to τ_0 and τ_1, such that each variable has an amplitude and phase which are

slowly varying ($\sim\tau_0$) relative to the rapid oscillatory motion of collapse-rebound. The objective is to separate in this manner the rapid (short-time scale) behavior from the slow behavior and investigate only the latter, namely, the evolution of the aforementioned amplitude and phase in r and t/τ_0.

Problems of this nature, involving both rapid and slow time variation, arise sometimes in wave propagation (dispersive) through slowly varying media. A unique Lagrangian-approach for waves in adiabatic systems was developed by Whitham,[46-48] using an averaging method. Luke[49] investigated a similar problem utilizing a singular perturbation technique, with the small perturbation quantity being the ratio of time scales τ_1/τ_0. Kruskal[50] suggested a nonlinear WKB approach for the classical Korteweg-de Vries (shallow water wave) equation.

The scope of the proposed analytical effort is outlined as follows:

(1) Derivation of a hierarchy of partial differential equations in terms of the slowly varying properties (amplitude and phase) of the dependent variables, utilizing a perturbation method, the small perturbation quantity being the ratio $\tau_1/\tau_0 << 1$.

(2) Numerical solution by finite difference to the zeroth and first order problems.

This mode of analysis is necessary for understanding of hot spot formation during the start-up transient of LPG systems, which may lead to secondary ignition within the propellant.

Although it is possible in principle to extend the numerical short time scale analysis, proposed in the preceeding section, over many periods of bubble collapse-rebound, this is highly undesirable. It would involve a very large cost per single computer solution and the errors, accumulated over many time steps of integration, would greatly reduce the reliability of the final results.

10.0 References

1. Lord Rayleigh, "The Pressure Developed in a Liquid During the Collapse of a Spherical Cavity", Phil. Mag., 34, 1917, pp. 94-98.

2. Poritsky, H., "The Collapse or Growth of a Spherical Bubble or Cavity in a Viscous Fluid", Proc. U.S. First National Congress of Applied Mechanics, Published by ASME, June 1951, pp. 813-821.

3. Shu, SS. "Note on the Collapse of a Spherical Cavity in a Viscous Incompressible Fluid", Proc. U.S. First National Congress of Applied Mechanics, Published by ASME, June 1951, pp. 823-825.

4. Plesset, M.S., "The Dynamics of Cavitation Bubbles", Journal of Applied Mechanics, Vol. 16, Sept. 1949, pp. 277-282.

5. Plesset, M.S., "Bubble Dynamics", Cavitation in Real Fluids, Edited by M. Davis, American Elsevier, N.Y., 1964, pp. 1-18.

6. Plesset, M.S. and Prosperetti, A., "Bubble Dynamics and Cavitation", Ann.Rev. Fluid Mechanics, 9, 1977, pp. 145-185.

7. Cole, R.H., Underwater Explosions, The Detailed Evaluation of Shock Wave Propagation-(Kirkwood-Bethe Theory), Princeton Univerrity Press, Princeton, NJ, 1948, pp. 114-124.

8. Kirkwood, J.G. and Bethe, H.A., "Basic Propagation Theory", OSRD 588, 1942.

9. Gilmore, F.R., Report No 26-4 Hydrodynamics Laboratory, California Institute of Technology, Pasadena, CA, 1952.

10. Hickling, R. and Plesset, M.S., "Collapse and Rebound of a Spherical Vapor Bubble in Water", Phys. of Fluids, Vol. 7, No. 9, Jan. 1964, pp.7-14.

11. VonNeumann, J. and Richtmyer, R.D., "A Method for the Numerical Calculation of Hydrodynamic Shocks", Jour. of Applied Physics, Vol. 21, 1950, p. 232.

12. Hickling, K. "Effects of Thermal Conduction in Sonoluminescence", J. Acoust. Soc. Am., Vol. 35, No. 7, July 1963. pp. 967-974.

13. Plesset, M.S. and Zwick, S.A., Jour. of Applied Physics, Vol. 25, 1954, p. 493.

14. Skinner, L.A. and Bankoff, S.G., "Dynamics of Vapor Bubbles in Spherically Symmetric Temperature Fields of General Variation", Phys. of Fluids, Vol. 7, No. 1, Jan. 1964, pp. 1-6.

15. Skinner, L.A. and Bankoff, S.G., "Dynamics of Vapor Bubbles in Binary Liquids with Spherically Symmetric Initial Conditions", Physics of Fluids, Vol. 7, No. 5, May 1964, pp. 643-648.

16. Hsieh, D.Y., "Some Analytical Aspects of Bubble Dynamics", Jour. of Basic Engineering. Dec. 1965, pp. 991-1005.

17. Batchelor, G.K., An Introduction to Fluid Dynamics, 6.11 Large Gas Bubble In Liquid, 6.12 Cavitation in a Liquid, Cambridge at the University Press, 1970, pp. 474-493.

18. Zinn, J. and Mader, C.L., "Thermal Initiation of Explosives", Jour. of Applied Physics, Vol. 31, No. 2, Feb. 1960, pp. 323-328.

19. Walker, F.E. and Wasley, R.J., "A General Model for the Shock Initiation of Explosives", Propellants and Explosives, 1, 1976, pp. 73-80.

20. Walker, F.E. and Wasley, R.J., Explosivstoffe, Vol. 17, 1969, p. 9.

21. Zinn, J., "Initiation of Explosions by Hot Spots", J. Chem. Phys., 36, 1962, p. 1949.

22. Rosen, J.B., J. Chem. Physics, Vol. 22, 1954, pp. 733, 750.

23. Evans, M.W., Harlow, F.H., and Meixner, B.D., "Interaction of Shock or Rarefaction with a Bubble", Physics of Fluids, Vol. 5, No. 6, June 1962, pp. 651-656.

24. Harlow, F.H., "Two Dimensional Hydrodynamic Calculations", Los Alamos Scientific Laboratory Report No. LA-2301, 1959.

25. Mader, C.L., "Shock and Hot Spot Initiation of Homogeneous Explosives", Physics of Fluids, Vol. 6, No. 3, Mar. 1963, pp. 375-381.

26. Campbell, A.W., Davis, W.C., and Travis, J.R., Physics of Fluids, Vol. 4, 1961, p. 498.

27. Enig, J.W. and Petrone, F.J., "On Equations of State in Shock Initiation Problems", The Physics of Fluids (Comments), Vol. , No. 1964, pp.769-772. (including Reply by C.L. Mader)

28. Mader, C.L., "Initiation of Detonation by the Interaction of Shocks with Density Discontinuities", Physics of Fluids, Vol. 8, No. 10, Oct. 1965, pp. 1811-1816.

29. Harlow, F.H., Methods in Computational Physics, Academic Press, N.Y., Vol. 3, 1964, pp. 319-343.

30. Mader, C.L., "The Two-Dimensional Hydrodynamic Hot Spot", Los Alamos Scientific Laboratory Report LA-3077, June 1964.

31. Mader, C.L., "The Two-Dimensional Hydrodynamic Hot Spot"-Vol. II., Los Alamos Scientific Laboratory Report, LA-3235, Apr. 1965.

32. Mader, C.L., "The Two-Dimensional Hydrodynamic Hot Spot"-Vol. III, Los Alamos Scientific Laboratory Report, LA-3450, Apr. 1965.

33. Mader, C.L., "The Two-Dimensional Hydrodynamic Hot Spot"-Vol. IV, Los Alamos Scientific Laboratory Report, LA-3771, Nov. 1967.

34. Mader, C.L. and Kershner, J.D., "Two-Dimensional, Continuous, Multicomponent Eulerian Calculations of Interactions of Shocks with V-notches, Voids, and Rods in Water", Los Alamos Scientific Laboratory Report, LA-4932, May 1972.

35. Kershner, J.D. and Mader, C.L., "2DE: A Two-Dimensional Continuous Eulerian Hydrodynamic Code for Computing Multicomponent Reactive Hydrodynamic Problems", Los Alamos Scientific Laboratory Report, LA-4846, Mar. 1972.

36. Knapton, J.D., Stobie, I.C., Comer, R.H., Bensinger, B.D., and Henry, D.L., "Evidence of Secondary Ignition in a Hydroxylammonium Nitrate Based Liquid Monopropellant, BRL Interim Memorandum Report, No. 509, June 1976.

37. Wooten, D.C., Cowperthwaite, M., and Erlich, D.C., "Investigation of Low Velocity Detonation Phenomena in Liquid Propellants, Fuels, and Explosives", SRI, Ca. AFOSR Report TR-72-1716, June, 1972.

38. Cowperthwaite, M. and Erlich, D.C., "Investigation of Low-Velocity Detonation Phenomena in Liquid Monopropellants and Explosives", Stanford Research Institute (SRI), AFOSR Report, TR-74-0801, Feb. 1974.

39. Lax, P.D., "Weak Solutions of Nonlinear Hyperbolic Equations and Their Numerical Computation", Commun. Pure and Applied Math., 7, 1954, pp. 159-193.

40. Williams, F.A., Combustion Theory, Addison-Wesley Publishing Co, Mass., 1965, pp. 1-16.

41. Moelwyn-Hughes, E.A., Physical Chemistry, Chap. XVI - The Liquid State, 2nd. Edition, Pergamon Press, N.Y., 1961, pp. 688-756.

42. Corner, J., Theory of Interior Ballistics of Guns, John Wiley & Sons, 1950.

43. Scala, S.M. and Sutton, G.W., "Energy Transfer at a Chemically Reacting or Slip Interface", ARS Journal, Vol. 29, Feb. 1959, pp. 141-143.

44. Ben Reuven, M. Caveny, L.H., Vichnevetsky, R., and Summerfield, M., "Flame Zone and Subsurface Reaction Model for Deflagrating RDX", Proc. 16th. Symposium (International) on Combustion", The Combustion Institute, Pittsburgh, PA, 1976, pp. 1223-1233.

45. Ben Reuven, M. and Caveny, L.H., "Nitramine Flame Chemistry and Deflagration Interpreted in Terms of a Flame Model", AIAA/ASME 15th. Joint Propulsion Conference, Las Vegas, Nev., June 1979, paper No. 79-1133.

46. Whitham, G.B., "A General Approach to Linear and Nonlinear Dispersive Waves Using a Lagrangian", J. Fluid Mechanics, Vol. 22, Part 2, 1965, pp. 273-283.

47. Whitham, G.B., "Non-Linear Dispersive Waves", Proc. Royal Society, Sect. A, 283, 1965, pp. 238-261.

48. Whitham, G.B., Linear and Nonlinear Waves, Chapters 13,14,15,16, J. Wiley & Sons, N.Y., 1974, pp. 454-553.

49. Luke, J.C., "A Perturbation Method for Nonlinear Dispersive Wave Problems", Proc. Royal Society, Sect. A, 292, 1966, pp. 403-412.

50. Kruskal, M.D., "The Korteweg-de Vries Equation and Related Evolution Equations", Lectures in Applied Mathematics, Vol. 15, 1974, pp. 61-83.

51. Messina, N.A., Summerfield, M., Ingram, L.S., and Leyzorek, J.M., "Explosion Sensitivity Tests of Otto Fuel II in Tubes", Princeton Combustion Laboratories Report No. PCL-TR-77-001, December 1977.

52. Messina, N.A., Leyzorek, J.M., and Summerfield, M., "Compression-Ignition Sensitivity Studies of Liquid Monopropellants", Fifteenth JANNAF Combustion Meeting, CPIA Publication 297, September 1978.

53. Messina, N.A. and Summerfield, M., "Performance of Direct-Injection Liquid Propellant Gun", Princeton Combustion Laboratories Report No. PCL-TR-75-001, December 1975.

54. Bowers, J.C., O'Reilly, J.E., and Shaw, G.A., "Super-Sceptre: A Program for the Analysis of Electrical, Mechanical, Digital, and Control Systems", User's Manual, University of South Florida, May 1975.

APPENDIX A

Pressure Distributions During Bubble Collapse for Incompressible Liquid

The purpose of the present calculations is to obtain the instantaneous pressure field about a gaseous bubble, in the process of collapse in an infinite, incompressible liquid. The original spherical bubble collapse problem, as posed by Rayleigh[1] is addressed. Analytical solutions for the bubble wall velocity, $U \equiv dR/dt$, and the pressure field in the liquid, $p(r,t)$, were obtained by Rayleigh, for the case of isothermal bubble process. The bubble wall velocity is given by

$$U^2 = \frac{2P_o}{3\rho_L}\,(1/\eta^3 - 1) - \frac{2P_B^o}{\rho_L}\,(1/\eta^3)\log(1/\eta), \qquad \text{(A-1)}$$

$$P_B V_B = \text{Const.}$$

where P_o = Const. is the initial field pressure, p_B^o is the initial bubble pressure, ρ is the liquid density and

$$\eta \equiv R/R_o$$

the dimensionless instantaneous bubble radius.

For the adiabatic bubble process, a straightforward calculation yields

$$U^2 = \frac{2P_o}{3\rho_L}\,(1/\eta^3 - 1) + \frac{2p_B^o}{\rho_L}\,\frac{1/\eta^3}{3(\gamma-1)}\,[1-1/\eta^{3(\gamma-1)}] \qquad \text{(A-2)}$$

$$P_B V_B^{\gamma} = \text{Const.}$$

following the analysis by Rayleigh, where $\gamma = c_p/c_v$ for the gas. In the derivation of Eq. (A-2), the same idealizations used by Rayleigh have been employed, in particular, that no mass exchange occurs between the bubble and the liquid, and that the bubble porperties are spatially uniform.

The instantaneous liquid field pressure distribution (for incompressible liquid) corresponding to the Rayleigh problem was given by Plesset and Prosperetti[6] in the form of the general Bernoulli equation:

$$\frac{p - P_o}{P_o} = \left(\frac{P_B - P_o}{P_o}\right)/\zeta + \frac{1}{2}\rho_L U^2\left(\frac{\zeta^4 - 1}{\zeta^4}\right) \qquad \text{(A-3)}$$

where $\zeta \equiv r/R(t)$

and $p(\zeta,\eta)$ is the liquid pressure, while $p_B(\eta)$ is the bubble pressure given by

$$\text{ISOTHERMAL:} \quad \phi_B \equiv (p_B - P_o)/P_o = (p_B^o/P_o)/\eta^3 - 1 \tag{A-4}$$

$$\text{ADIABATIC:} \quad \phi_B \equiv (p_B - P_o)/P_o = (p_B^o/P_o)/\eta^{3\gamma} - 1 \tag{A-5}$$

The state at full compression is defined by $U = 0$. Thus, Eqs. (A-1) and (A-2) can be used to define η_{min} (p_B^o/P_o) for the isothermal and adiabatic cases respectively (in practice, due to the algebraic complexity of the U^2-equations, the inverse calculation is much easier to perform namely, finding p_B^o/P_o as a function of η_{min}). Then the maximal bubble pressure ratio $\phi_{B_{max}}$ can be calculated by employing the values of $(\eta_{min}, p_B^o/P_o)$ in Eqs. (A-4) and (A-5). The results of these calculations are given in Figures A-1 and A-2. Indeed it is shown that the isothermal case leads to more violent collapse, namely to significantly higher $\phi_{B_{max}}$ and lower η_{min} than the adiabatic case, as expected.

The pressure distribution in the liquid $\phi(\zeta;\eta)$ during bubble collapse can now be calculated, by substitution of the velocity U^2 from Eqs. (A-1) and (A-2) into Eq. (A-3), for specified $(\eta_{min} \leq \eta < 1;\ p_B^o/P_o)$ data. This will yield distributions due to isothermal and adiabatic bubble process respectively. Note that the actual time corresponding to the particular values of $\eta = r/R(t)$ specified is not of interest here. Four isothermal pressure distributions are plotted in Figure A-3 as functions of $\zeta = r/R(t)$, and a similar set of adiabatic pressure distributions is plotted in Figure A-4. In these diagrams, the pressure maximum discussed by Rayleigh is clearly shown, and the distribution at the instant of full collapse is given by

$$\phi(\eta_{min},\zeta) = \frac{\phi_{B_{max}}}{\zeta} \tag{A-6}$$

It should be mentioned that the ζ-coordinate is stretched with time, since $R(t)$ decreases in the process of collapse.

The pressure profiles resemble in shape those obtained by Hickling and Plesset[10] (for collapse) for compressible liquid. They demonstrate that within a distance of R_o from the bubble center, pressure in the liquid can reach values several orders of magnitude above P_o.

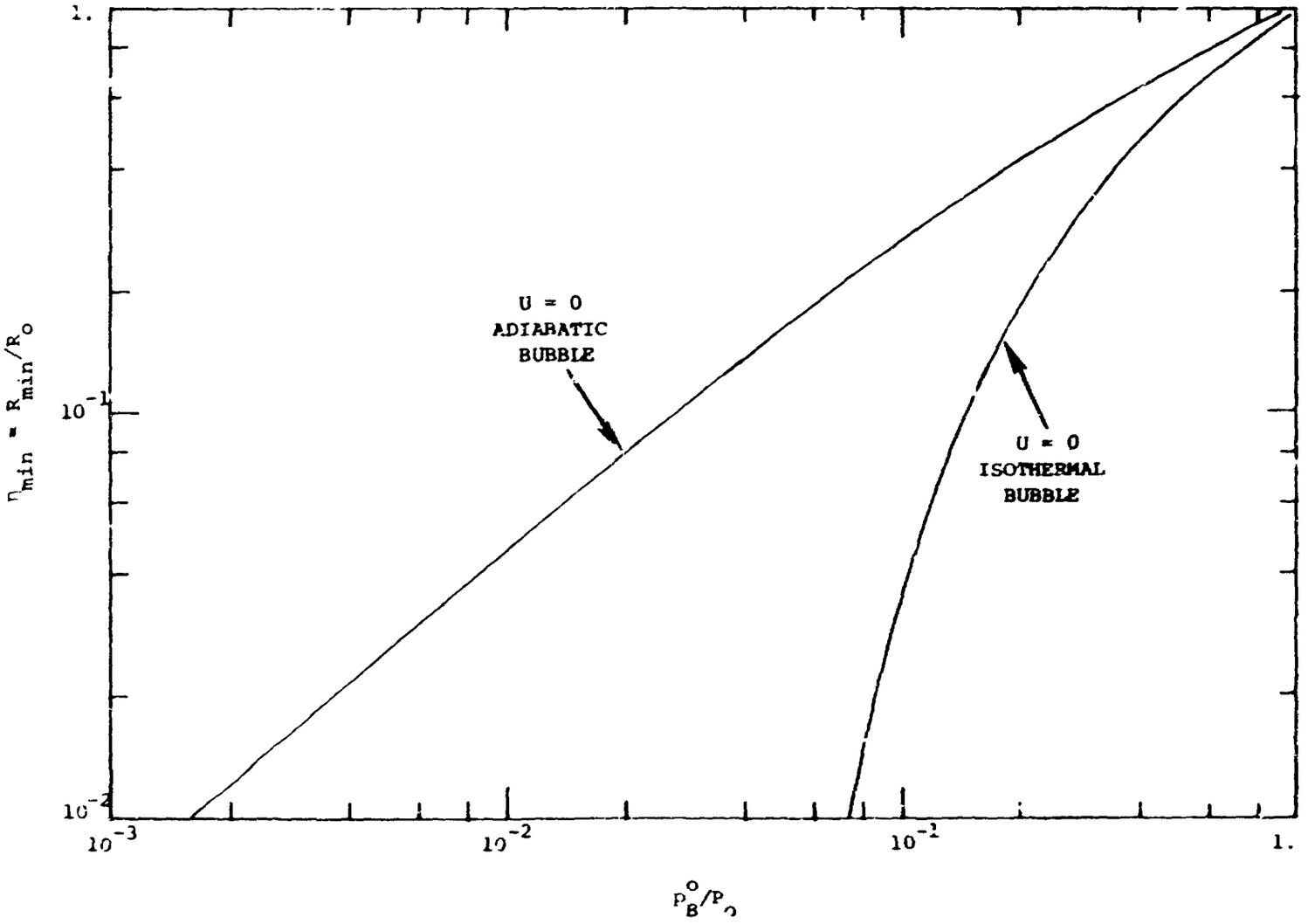

Figure A-1. Minimal values of bubble radius ratio, R_{min}/R_o, vs. the initial bubble pressure ratio, p_B^o/P_o. The isothermal case reaches lower minimal radii.

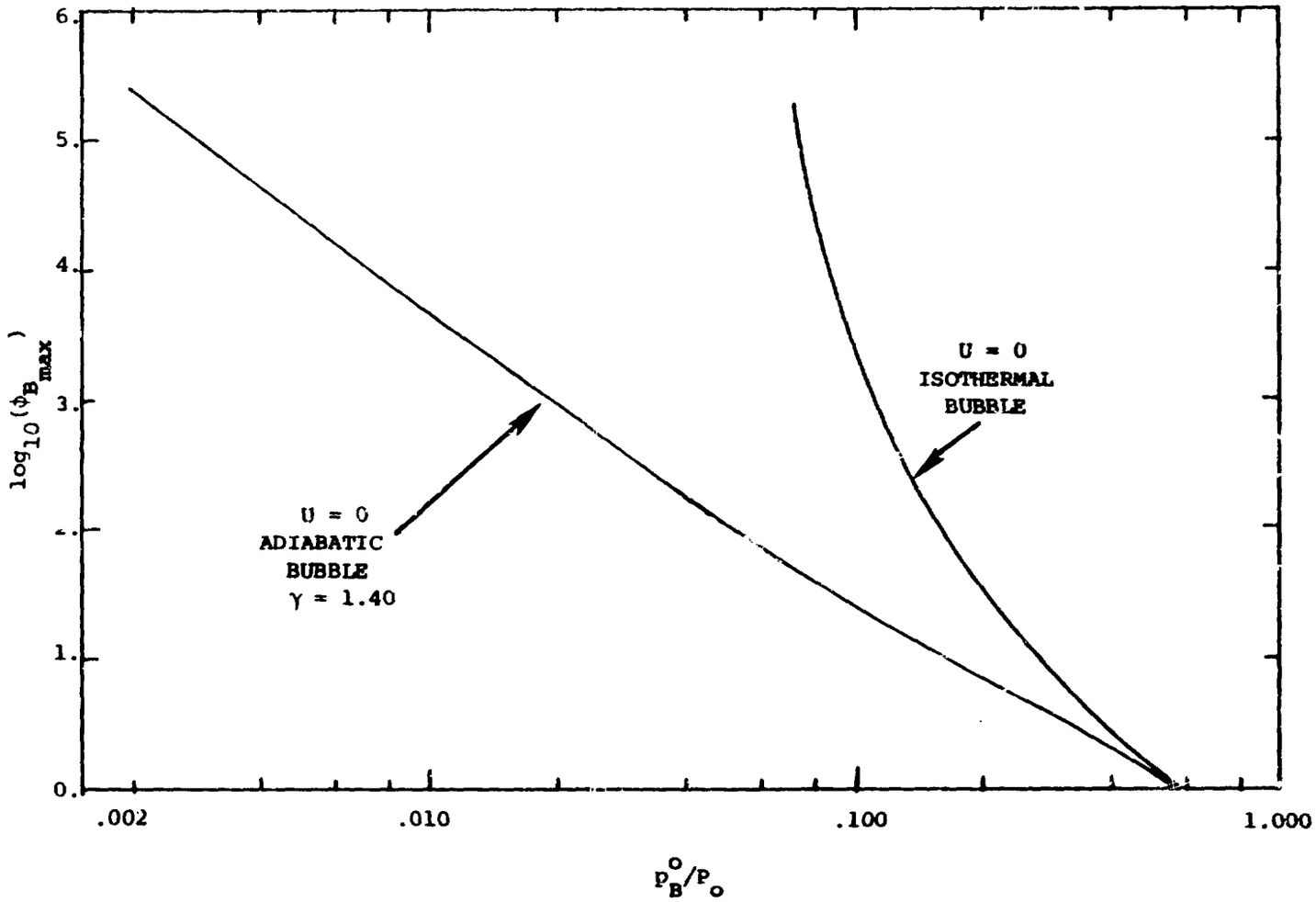

Figure A-2. Maximal bubble pressure, $\phi_{B_{max}} = p_{B_{max}}/P_o - 1$ vs. the initial bubble pressure ratio, p_B^o/P_o. The isothermal case shown significantly more violent.

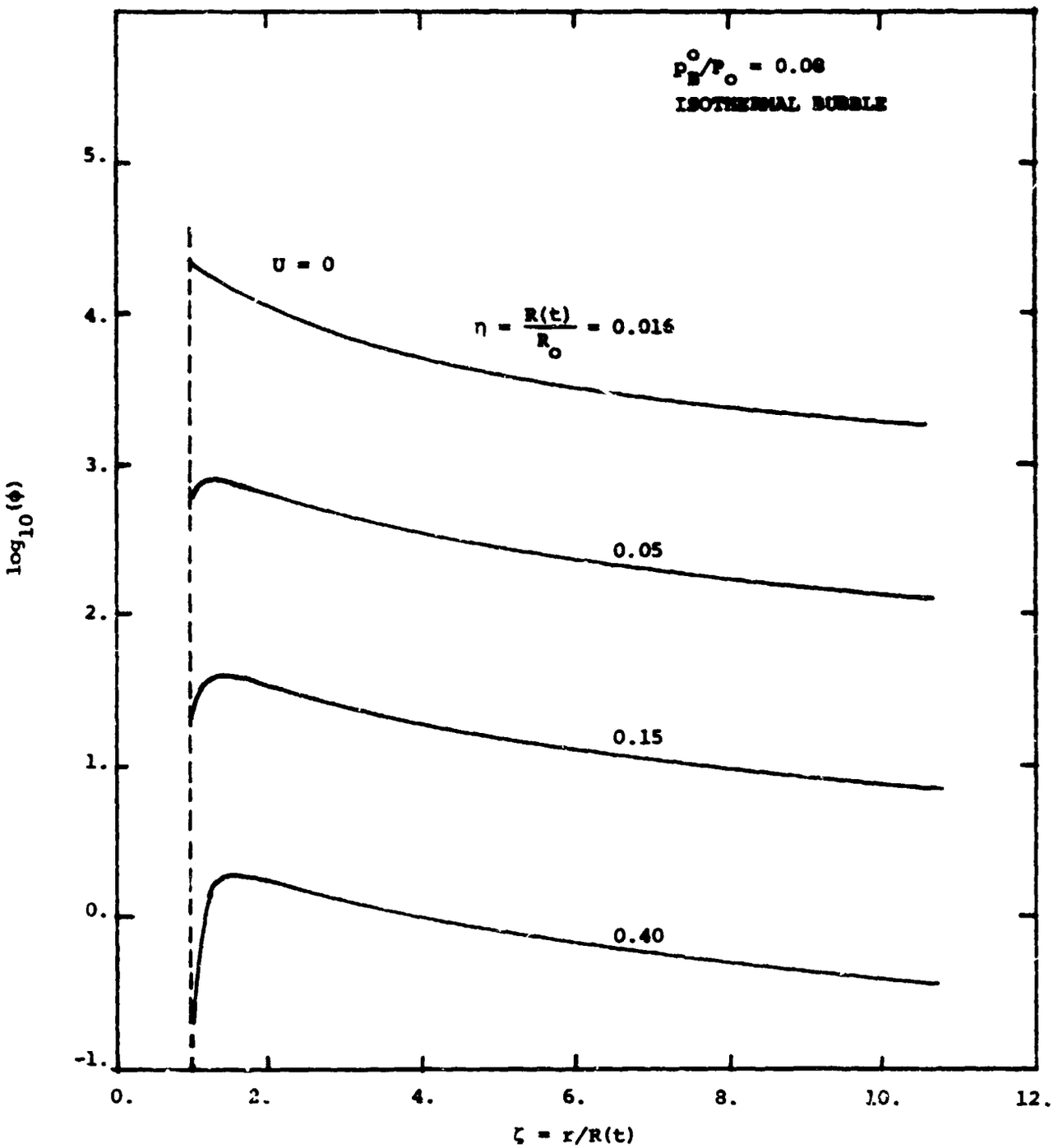

Figure A-3. Pressure distributions, $\phi = p/P_o - 1$ in the liquid phase vs. dimensionless radial distance for isothermal bubble at several stages during collapse.

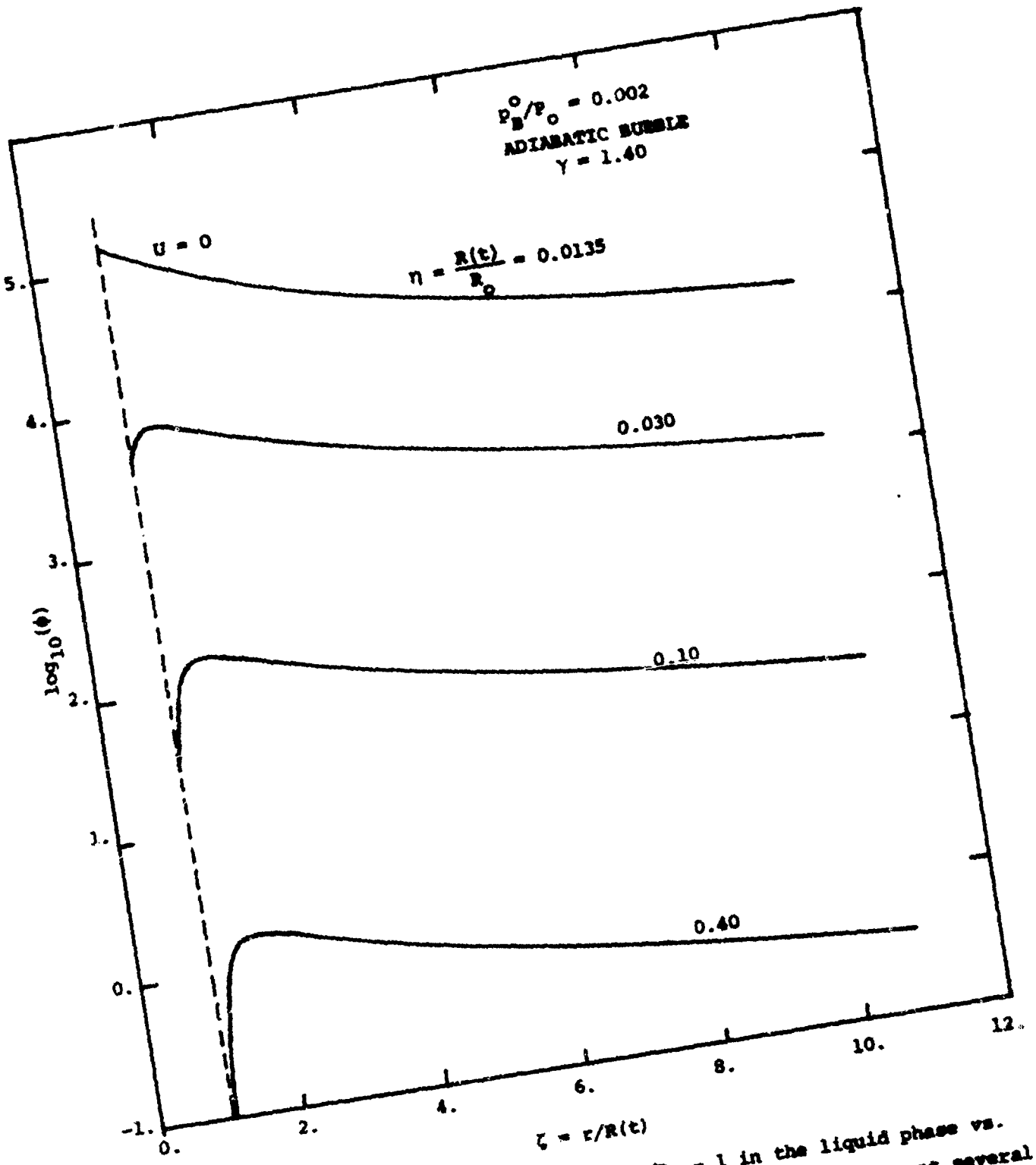

Figure A-4. Pressure distribution, $\phi = p/P_o - 1$ in the liquid phase vs. dimensionless radial distance for adiabatic bubble at several stages during collapse.

APPENDIX B

Approximate Analysis of Liquid Compressibility

The objective of the present calculation is to obtain an estimate of the effect of liquid compressibility upon the maximal pressure and temperature of a collapsing gas bubble. To carry out the calculation without solving the entire liquid-bubble dynamic problem, certain simplifications were necessary. The strongest assumption made herein was that the pressure distribution in the liquid surrounding the bubble is approximately equal to that obtained from incompressible-liquid analysis of a collapsing bubble, at the instant of full compression, i.e., when $U = dR/dt = 0$.

The ensuing calculation is based on the compression work balance mentioned in Section 7.3, viz.,

$$W_{STROKE} = W_{CL} + W_{CB} \tag{B-1}$$

where each of the terms is evaluated at the state of maximal bubble compression. The above equation will be shown to depend upon the final state $R/R_o = \eta_{min}$ of the bubble, and will have to be solved iteratively.

The results of this approximation analysis are presented in tabular form at the end of this appendix, as well as in Figures B-2 and B-3, where comparisons with the incompressible case (adiabatic bubble) are made.

B.1 The Pressure Distribution

For purposes of the present calculation, only the state of maximal bubble compression is of interest, when $U = dR/dt = 0$. The pressure distribution in the liquid is approximated by that of the incompressible liquid case (Rayleigh solution). At the instant when $U = 0$, Bernoulli's equation yields,

$$\frac{p - P_o}{P_o} = \frac{p_B - P_o}{P_o\zeta} \equiv \frac{\phi_B(\eta)}{\zeta} \tag{B-2}$$

where $p = p(\zeta,\eta)$, $\zeta = r/R(t)$ and $\eta = R(t)/R_o$. P_o is the uniform initial driving pressure in the liquid, and $p_B(\eta)$ is the (uniform) bubble pressure. When $U = 0$, $\eta = \eta_{min}$, $R = R_{min}$ and $p_B = p_{B_{max}}$

Considering the adiabatic case,

$$\frac{p_B}{P_o} = \left(\frac{p_B^o}{P_o}\right)\eta^{3\gamma} \tag{B-3}$$

where $\gamma = C_p/C_v$ for the bubble gas, and hence

$$\frac{\phi_{B_{max}}}{\zeta} = \left[\left(\frac{P_B^o}{P_o}\right)/\eta^{3\gamma} - 1\right] / \zeta \qquad \text{(B-4)}$$

with $\eta = \eta_{min}$.

B.2 The Compression Stroke Work

When liquid compressibility is considered, the net change in volume for a full compression stroke (for a single bubble) involves the sum of bubble and liquid compression, such that the stroke work is defined

$$W_{STROKE} = -P_o(\Delta V_B + \Delta V_{LC}) \qquad \text{(B-5)}$$

The bubble volume change is

$$\Delta V_B = \frac{4}{3}\pi(R^3 - R_o^3) = \frac{4}{3}\pi R_o^3 (\eta^3 - 1) \qquad \text{(B-6)}$$

where $\eta = \eta_{min}$. Determination of the liquid volume change is considerably more involved, and undertaken as follows.

The variation of volume is

$$\delta V_L = \delta(M/\rho) = \delta M/\rho + M\delta(1/\rho) \qquad \text{(B-7)}$$

where M is the mass of a liquid volume unit undergoing compression, which remains invariant. Thus, $\delta M = 0$ and the volume variation is

$$\delta V_L = M\delta(1/\rho) \qquad \text{(B-8)}$$

Considering a differential shell of radius r and thickness dr,

$$M = 4\pi\rho r^2 dr$$

and the total liquid volume change is defined

$$\Delta V_L = \int_R 4\pi r^2 d r \rho \int_{\rho_o}^{\rho(r)} d(1/\rho) = 4\pi \int_R r^2 dr(1 - \rho/\rho_o) \qquad \text{(B-9)}$$

The integrand in the last equality vanishes identically for the incompressible case, as $\rho = \rho_o$ is uniform. Further, as $r \longrightarrow \infty$ the integrand vanishes asymptotically $\rho \longrightarrow \rho_o$, but a moderate driving pressure P_o is required, such that $\rho/\rho_o \longrightarrow 1$ faster than $1/r^2 \longrightarrow 0$.

Utilizing the liquid compressibility expression,

$$C\rho^n = p + B \tag{B-10}$$

(for water, B = 3000 atm and n = 7 is proposed as good approximation[18]),

$$\rho/\rho_o = \left(\frac{p + B}{P_o + B}\right)^{1/n} = \left(\frac{\phi}{B'} + 1\right)^{1/n}$$

where

$$\phi = p/P_o - 1$$

and $\quad B' = (B/P_o + 1)$

Transforming to dimensionless coordinates, $\zeta = r/R$, and using the pressure distribution given by the incompressible solution,

$$\Delta V_L = 4\pi R_o^3 \eta^3 \int_1^{\infty} \left[1 - \left(\frac{a}{\zeta} + 1\right)^{1/n} \right] \zeta^2 d\zeta \tag{B-11}$$

where $a = \phi_B/B'$ and $\phi_B = \phi_{B_{max}}$ is defined by Eq. (B-3) ; the notation η_{min} applies as well, and will be omitted hereon. Cases of interest involve $P_o \sim 1000$ atm, and if the trend shown in Appendix A for incompressible liquid is correct, $\phi_{B_{max}}$ is expected to be large, Therefore, $a >> 1$ can be anticipated. To avoid the singularity at infinity involved in the last integral, a convenient dimensionless compressibility radius is defined by $a = \phi_B/B'$, and liquid compression is considered only within the bounds $1 < \zeta < a$. With the following change of variable,

$$x = \zeta/a$$

the problem amounts to calculating the definite integral

$$I \equiv a^3 \int_{1/a}^{1^-} \left[1 - \left(\frac{1}{x} + 1\right)^{1/n} \right] x^2 dx \tag{B-12}$$

where $a > 1$. The pressure distribution and region of integration are shown schematically in Figure B-1. Thus,

$$I \equiv a^3 \int_{1/a}^{1^-} \left[1 - \frac{(1 + x)^{1/n}}{x^{1/n}} \right] x^2 dx$$

Since $x < 1$, the term in brackets can be evaluated by use of a binomial series:

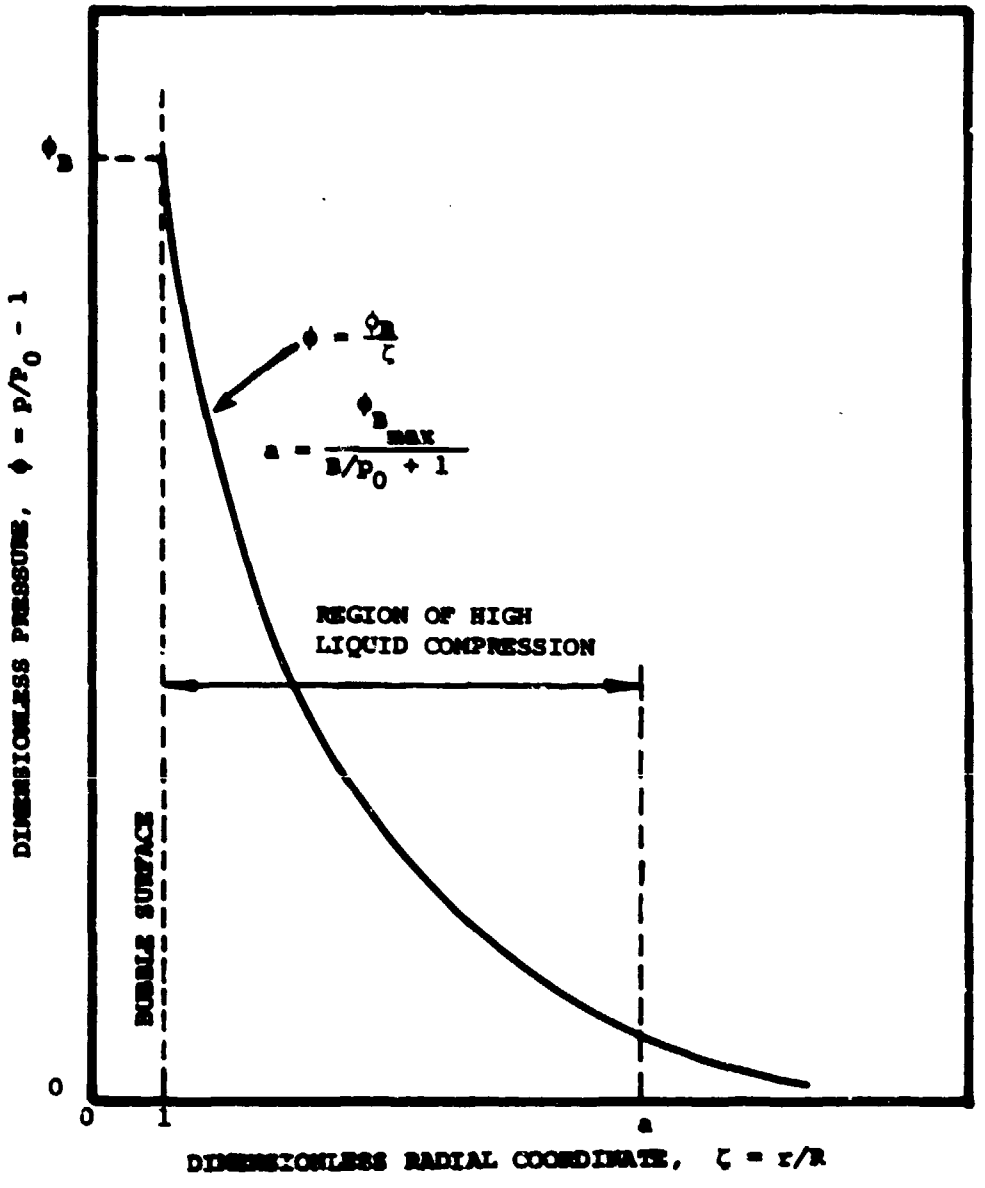

Figure B-1. Schematic Diagram of Imposed Pressure Distribution Showing Liquid Compressibility Region Considered for Evaluation of the Stroke Potential and the Liquid Compression Work.

$$(1 + x)^q = \sum_{k=0}^{\infty} \binom{q}{k} x^k = 1 + qx + \frac{q(q-1)}{2!} x^2 + O(x^3)$$

taken up to third order accuracy. Hence,

$$I \doteq a \int_{1/a}^{1^-} \left[x^2 - x^{2-1/n} - \frac{x^{3-1/n}}{n} - \frac{\frac{1}{n}(\frac{1}{n}-1)}{2!} x^{4-1/n} \right] dx$$

$$= a^3 x^3 \left[\frac{1}{3} - \frac{x^{-1/n}}{3-1/n} - \frac{x^{1-1/n}}{n(4-1/n)} - \frac{\frac{1}{n}(\frac{1}{n}-1)}{2(5-1/n)} x^{2-1/n} \right]_{1/a}^{1^-}$$

$$I \doteq -0.041a^3 \tag{B-13}$$

where values at the lower limit of integration were assumed negligible, as $1/a^3 \ll 1$ is expected. The stroke work can now be calculated, with the evaluation of the liquid compression term:

$$\Delta V_L = -4\pi R_o^3 \eta^3 \times 0.041a^3 = -\frac{4\pi}{3} R_o^3 \eta^3 \times 0.123 \left[\frac{\phi_B(\eta)}{B/P_o + 1} \right]^3$$

Hence, from Eq. (B-5),

$$W_{STROKE} = \frac{4\pi}{3} R_o^3 P_o \left\{ (1-\eta^3) + 0.123\eta^3 \left[\frac{\phi_B(\eta)}{B/P_o+1} \right]^3 \right\} \tag{B-14}$$

where $\eta = \eta_{min}$.

B.3 The Compression Work Terms

The bubble compression work is evaluated, assuming rapid process, by use of the adiabatic relationship:

$$W_{CB} = -\int_{V_o}^{V_c} P_B dV_B = -\int_{R_o}^{R} \left(\frac{P_B^o}{P_o}\right) P_o \left(\frac{1}{\eta^3 \gamma}\right) 4\pi R^2 dR =$$

$$-\frac{4\pi}{3} R_o^3 P_o \left(\frac{P_B^o}{P_o}\right) \frac{1-\eta^{-3(\gamma-1)}}{\gamma - 1} \tag{B-15}$$

where $\eta = \eta_{min}$.

The liquid compression work is given by

$$W_{CL} = -\int_R^{\infty} 4\pi r^2 dr \rho \int_{\rho_o}^{\rho(r)} p\, d(1/\rho) \tag{B-16}$$

The internal integral can be readily evaluated, using the liquid compression isotherm:

$$\int_{\rho_0}^{\rho} p\,d(1/\rho) = -\int_{\rho_0}^{\rho} \frac{C\rho^n - B}{\rho^2}\,d\rho = -\left\{ \frac{C\rho_0^{\,n}/\rho_0}{n-1}\left[\left(\frac{\rho}{\rho_0}\right)^{n-1} - 1\right] + \frac{B}{\rho}\left(1 - \frac{\rho}{\rho_0}\right)\right\} \quad \text{(B-17)}$$

Note that in the last expression,

$$C\rho_o^n \simeq P_o + B = P_oB', \text{ so that}$$

$$\rho\int_{\rho_0}^{\rho} p\,d(1/\rho) = -\frac{P_oB'}{n-1}\left[\left(\frac{\rho}{\rho_o}\right)^n - \frac{\rho}{\rho_o}\right] - B\left(1 - \frac{\rho}{\rho_o}\right) =$$

$$-\frac{P_oB'}{n-1}\left[\frac{p+B}{P_o+B} - \left(\frac{p-B}{P_o+B}\right)^{1/n}\right] - B\left[1 - \left(\frac{p+B}{P_o+B}\right)^{1/n}\right]$$

Therefore, with the same change of variable of integration as in Eq. (B-11) for ΔV_L,

$$W_{CL} = +4\pi R_o^3\eta^3 P_o\left\{\int_1^{\infty} \frac{B'}{n-1}\left[\frac{a}{\zeta} + 1 - \left(\frac{a}{\zeta} + 1\right)^{1/n}\right]\zeta^2 d\zeta\right.$$

$$\left. +(B' - 1)\int_1^{\infty}\left[1 - \left(\frac{a}{\zeta} + 1\right)^{1/n}\right]\zeta^2 d\zeta\right\} \quad \text{(B-18)}$$

Limiting the integration to the interval $1/a < \zeta < 1$ and further transform of the integration variable $x \equiv \zeta/a$:

$$W_{CL} = 4\pi R_o^3\eta^3 P_o\left\{\frac{B'}{n-1}\int_{1/a}^{1} a^3 x\,dx + \frac{B'}{n-1} I + (B'-1)I\right\}$$

$$= 4\pi R_o^3\eta^3 P_o\left\{\frac{B'a^3}{n-1}\frac{x^2}{2}\Bigg|_{1/a}^{1} - \frac{n(B'-1)+1}{n-1} \times 0.041a^3\right\}$$

where I was defined by Eq. (B-13). Assuming that $1/a^2 << 1$, the liquid compression work term can be written

$$W_{CL} = \frac{4}{3}\pi R_o^3\eta^3 P_o\left\{\frac{1.5B' - [n(B'-1)+1]\ 0.123}{n-1}\right\}a^3 \quad \text{(B-19)}$$

The Energy Balance

The energy balance at maximal bubble compression,

$$W_{STROKE} = W_{CB}(\text{ADIABATIC}) + W_{CL}$$

can be now expressed in terms of $\eta = \eta_{min}$ by use of Eqs. (B-14), (B-15), and (B-19); after substitution and dividing through by $4/3\pi R_o^3 P_o$,

$$1 - \eta^3 + 0.123\eta^3 a^3 = \frac{p_B^o/P_o}{\gamma - 1}\left[\eta^{-3(\gamma-1)} - 1\right] + k_B \eta^3 a^3 \qquad \text{(B-20)}$$

where $$a(\eta) \equiv \frac{\phi_B}{B'} = \left[\frac{p_B^o/P_o}{\eta^{3\gamma}} - 1\right]/B'$$

$$B' = B/P_o + 1$$

$$k_B(n,B') = \frac{1.5B' - 0.123[n(B'-1)+1]}{n - 1}$$

Equation (B-20) can be solved iteratively to determine $\eta = \eta_{min}$. The method chosen for this purpose is Regula Falsi (or method of false position).

For incompressible liquid, it has been demonstrated in Appendix A the the final compression ratio η_{min} for both adiabatic and isothermal cases depends only on the initial pressure p_B^o/P_o (and γ for the adiabatic bubble). The present energy balance equation for the compressible liquid shows that η_{min} depends in addition upon P_o, (as well as B and n which contain the liquid compressibility properties), since the amount of compression work done on the liquid depends on the actual value of the driving pressure.

Now that η_{min} is available, the normalized (total) bubble compression work can be calculated,

$$\bar{w}_{CB} = W_{CB}/W_{STROKE} = \frac{(p_B^o/P_o)[\eta^{3(\gamma-1)}-1]/(\gamma-1)}{(1-\eta^3+0.123\eta^3 a^3)} \qquad \text{(B-21)}$$

and the normalized overall liquid compression work is

$$\bar{w}_{CL} = W_{CL}/W_{STROKE} = 1 - \bar{w}_{CB} \qquad \text{(B-22)}$$

The maximal bubble pressure is defined by use of the calculated η_{min} in Eq. (B-3):

$$P_{B_{max}}/P_o = (p_B^o/P_o)/\eta_{min}^{3\gamma}$$

and the final bubble temperature ratio is calculated through the adiabatic relationship,

$$T_{B_{max}}/T_B^o = (P_B/p_B^o)^{\frac{\gamma-1}{\gamma}} = 1/\eta^{3(\gamma-1)} \qquad \text{(B-23)}$$

Employing values of B = 3000 atm and n = 7 (for water) and $\gamma = 1.40$ (for air bubble), the parameters η_{min}, $\phi_{B_{max}}$, $\bar{w}_{CL}$ and $T_{B_{max}}/T_B^o$ were calculated for imposed (P_o ; p_B^o/P_o) data. Three distinct values of P_o = 100, 500, and 1000 atm were employed. The results are tabulated and plots of η_{min} and $\phi_{B_{max}}$ versus p_B^o/P_o are shown in Figures B-2 and B-3 respectively, compared in each case with the incompressible liquid-adiabatic bubble solutions.

INCOMPRESSIBLE LIQUID,ADIABATIC BUBBLE (γ = 1.40)

#	PB/PO	LOG(RB/RB*#3)	PB/PO-1	MAX.TB/TB#
1	.13900E-#2	.18000E+#1	.4#16#E+#6	.35119E+#3
2	.19963E-#2	.17000E+#1	.23137E+#6	.2#137E+#3
3	.24932E-#2	.16000E+#1	.1332#E+#6	.16144E+#3
4	.31140E-#2	.12400E+#1	.76811E+#5	.12942E+#3
5	.38920E-#2	.13200E+#1	.44285E+#5	.1#375E+#3
6	.48675E-#2	.14000E+#1	.25544E+#5	.83177E+#2
7	.60899E-#2	.14800E+#1	.14743E+#5	.66681E+#2
8	.76250E-#2	.15600E+#1	.85151E+#4	.53457E+#2
9	.95560E-#2	.16400E+#1	.49226E+#4	.42855E+#2
1#	.11990E-#1	.17200E+#1	78489E+#4	.34356E+#2
11	.15#66E-#1	.18000E+#1	.4651#E+#4	.27547E+#2
12	.18967E-#1	.18800E+#1	.9584#E+#3	.22#6#E+#2
13	.23932E-#1	.19600E+#1	.55765E+#3	.177#1E+#3
14	.3#268E-#1	.2#400E+#1	.32540E+#3	.14191E+#2
15	.38461E-#1	.912#0E+#1	.19800E+#3	.11376E+#2
16	.45364E-#1	.22800E+#1	.1114#E+#3	.912#1E+#1
17	.62939E-#1	.22800E+#1	.65515E+#2	.73114E+#1
18	.81292E-#1	.23600E+#1	.38632E+#2	.58614E+#1
19	.1#500E+#0	.24400E+#1	.22813E+#2	.46989E+#1
2#	.13931E+#0	.25200E+#1	.13454E+#2	.3767#E+#1
21	.18553E+#0	.26000E+#1	.78800E+#1	.3#200E+#1
22	.25062E+#0	.26800E+#1	.45337E+#1	.2421#E+#1
23	.34412E+#0	.27600E+#1	.25652E+#1	.19409E+#1
24	.48123E+#0	.28400E+#1	.12613E+#1	.15560E+#1
25	.66640E+#0	.29200E+#1	.48609E+#0	.12474E+#1

COMPRESSIBLE LIQUID, ADIABATIC BUBBLE

B = 3000 atm, n = 7, γ = 1.40

P_o = 100 atm

N	PB0/PO	RB/R0	PB/PO-1	WCL/WSTRX	MAX.TB/TB0
1	1.00000E-03	.31815E-01	.19441E+04	.92205E+00	.62630E+02
2	.12589E-02	.34207E-01	.17075E+04	.90921E+00	.57260E+02
3	.15849E-02	.36969E-01	.16400E+04	.89411E+00	.52312E+02
4	.19953E-02	.39885E-01	.15000E+04	.87630E+00	.47756E+02
5	.25119E-02	.43063E-01	.13691E+04	.85523E+00	.43559E+02
6	.31623E-02	.46537E-01	.12443E+04	.83023E+00	.39687E+02
7	.39811E-02	.50347E-01	.11295E+04	.80044E+00	.36111E+02
8	.50119E-02	.54545E-01	.10121E+04	.76483E+00	.32802E+02
9	.63096E-02	.59190E-01	.90327E+03	.72213E+00	.29732E+02
10	.79433E-02	.64397E-01	.79841E+03	.67000E+00	.26876E+02
11	1.00000E-02	.70264E-01	.69677E+03	.60911E+00	.24206E+02
12	.12589E-01	.76980E-01	.59771E+03	.53539E+00	.21694E+02
13	.15849E-01	.84813E-01	.50072E+03	.44847E+00	.19313E+02
14	.19953E-01	.94182E-01	.40576E+03	.34966E+00	.17031E+02
15	.25119E-01	.10574E+00	.31396E+03	.24510E+00	.14823E+02
16	.31623E-01	.12041E+00	.22872E+03	.14839E+00	.12682E+02
17	.39811E-01	.13925E+00	.15604E+03	.76017E-01	.10652E+02
18	.50119E-01	.16299E+00	.10100E+03	.33970E-01	.80189E+01
19	.63096E-01	.19182E+00	.63842E+02	.14140E-01	.72532E+01
20	.79433E-01	.22579E+00	.40159E+02	.57912E-02	.59643E+01
21	.10000E+00	.26502E+00	.25439E+02	.24023E-02	.49212E+01
22	.12589E+00	.30973E+00	.16292E+02	.10196E-02	.40814E+01
23	.15849E+00	.36019E+00	.10550E+02	.44429E-03	.34054E+01
24	.19953E+00	.41662E+00	.68899E+01	.19670E-03	.28596E+01
25	.25119E+00	.47929E+00	.45144E+01	.88573E-04	.24170E+01
26	.31623E+00	.54840E+00	.29426E+01	.39697E-04	.20563E+01

P_o = 500 atm

N	PB0/PO	RB/R0	PB/PO-1	WCL/WSTRX	MAX.TB/TB0
1	1.00000E-03	.50233E-01	.28466E+03	.95703E+00	.36209E+02
2	.12589E-02	.54034E-01	.26374E+03	.95030E+00	.33174E+02
3	.15849E-02	.58162E-01	.24363E+03	.94240E+00	.30369E+02
4	.19953E-02	.62624E-01	.22479E+03	.93318E+00	.27792E+02
5	.25119E-02	.67450E-01	.20710E+03	.92243E+00	.25423E+02
6	.31623E-02	.72677E-01	.19040E+03	.90986E+00	.23245E+02
7	.39811E-02	.78347E-01	.17484E+03	.89514E+00	.21241E+02
8	.50119E-02	.84505E-01	.16010E+03	.87787E+00	.19397E+02
9	.63096E-02	.91210E-01	.14617E+03	.85755E+00	.17699E+02
10	.79433E-02	.98527E-01	.13299E+03	.83357E+00	.16134E+02
11	1.00000E-02	.10654E+00	.12040E+03	.80523E+00	.14689E+02
12	.12589E-01	.11534E+00	.10856E+03	.77162E+00	.13354E+02
13	.15849E-01	.12506E+00	.97185E+02	.73170E+00	.12118E+02
14	.19953E-01	.13587E+00	.86274E+02	.68422E+00	.10971E+02
15	.25119E-01	.14790E+00	.75772E+02	.62703E+00	.99031E+01
16	.31623E-01	.16160E+00	.65624E+02	.56120E+00	.89045E+01
17	.39811E-01	.17741E+00	.55795E+02	.48347E+00	.79658E+01
18	.50119E-01	.19577E+00	.46202E+02	.39521E+00	.70780E+01
19	.63096E-01	.21763E+00	.37155E+02	.29999E+00	.62335E+01
20	.79433E-01	.24419E+00	.28615E+02	.20606E+00	.54290E+01
21	.10000E+00	.27602E+00	.21018E+02	.12550E+00	.46705E+01
22	.12589E+00	.31659E+00	.14772E+02	.68100E-01	.39756E+01
23	.15849E+00	.36390E+00	.10063E+02	.33093E-01	.33637E+01
24	.19953E+00	.41856E+00	.67302E+01	.16059E-01	.28438E+01
25	.25119E+00	.48027E+00	.44674E+01	.74024E-02	.24111E+01
26	.31623E+00	.54880E+00	.29281E+01	.33227E-02	.20541E+01

COMPRESSIBLE LIQUID, ADIABATIC BUBBLE (con't)

P_o = 1000 atm

N	PB/PO	RB/R0	PB/PO-1	WCL/WSTRK	MAX.TB/TB0
1	1.00000E-03	.59623E-01	.13802E+03	.96564E+00	.29479E+02
2	.12589E-02	.64137E-01	.12787E+03	.96026E+00	.27007E+02
3	.15849E-02	.69005E-01	.11832E+03	.95402E+00	.24737E+02
4	.19953E-02	.74258E-01	.10938E+03	.94670E+00	.22652E+02
5	.25119E-02	.79931E-01	.10100E+03	.93836E+00	.20737E+02
6	.31623E-02	.86061E-01	.93147E+02	.92356E+00	.18977E+02
7	.39811E-02	.92693E-01	.85776E+02	.91715E+00	.17360E+02
8	.50119E-02	.99876E-01	.78847E+02	.90382E+00	.15873E+02
9	.63096E-02	.10767E+00	.72324E+02	.88825E+00	.14504E+02
10	.79433E-02	.11613E+00	.66175E+02	.87001E+00	.13245E+02
11	1.00000E-02	.12535E+00	.60365E+02	.84261E+00	.12089E+02
12	.12589E-01	.13540E+00	.54865E+02	.82344E+00	.11016E+02
13	.15849E-01	.14642E+00	.49645E+02	.79378E+00	.10030E+02
14	.19953E-01	.15852E+00	.44677E+02	.75876E+00	.91103E+01
15	.25119E-01	.17188E+00	.39935E+02	.71739E+00	.82745E+01
16	.31623E-01	.18672E+00	.35394E+02	.66851E+00	.74917E+01
17	.39811E-01	.20333E+00	.31051E+02	.61094E+00	.67634E+01
18	.50119E-01	.22210E+00	.26830E+02	.54365E+00	.60834E+01
19	.63096E-01	.24356E+00	.22781E+02	.46624E+00	.54459E+01
20	.79433E-01	.26847E+00	.18890E+02	.37904E+00	.48453E+01
21	.10000E+00	.29784E+00	.15191E+02	.28841E+00	.42778E+01
22	.12589E+00	.33295E+00	.11664E+02	.19972E+00	.37425E+01
23	.15849E+00	.37517E+00	.87330E+01	.12428E+00	.32429E+01
24	.19953E+00	.42547E+00	.62235E+01	.69445E-01	.27884E+01
25	.25119E+00	.48413E+00	.42063E+01	.35459E-01	.23881E+01
26	.31623E+00	.55089E+00	.28685E+01	.16834E-01	.20451E+01

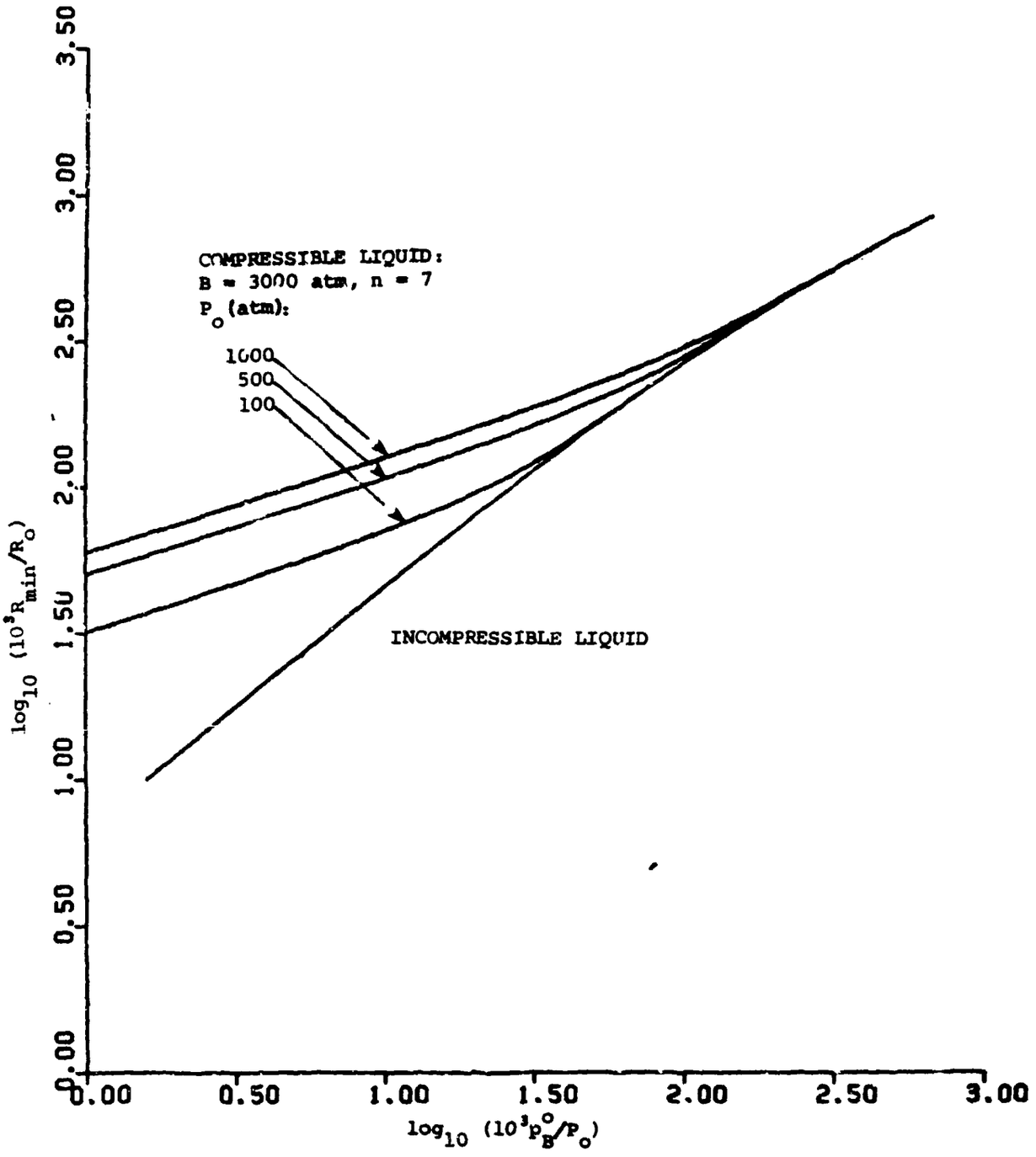

Figure B-2. Minimal radius ratio $\eta_{min} = R_{min}/R_o$ vs. initial pressure ratio p_B^o/P_o for adiabatic bubble, comparing incompressible liquid solution with compressible liquid at several driving pressures P_o.

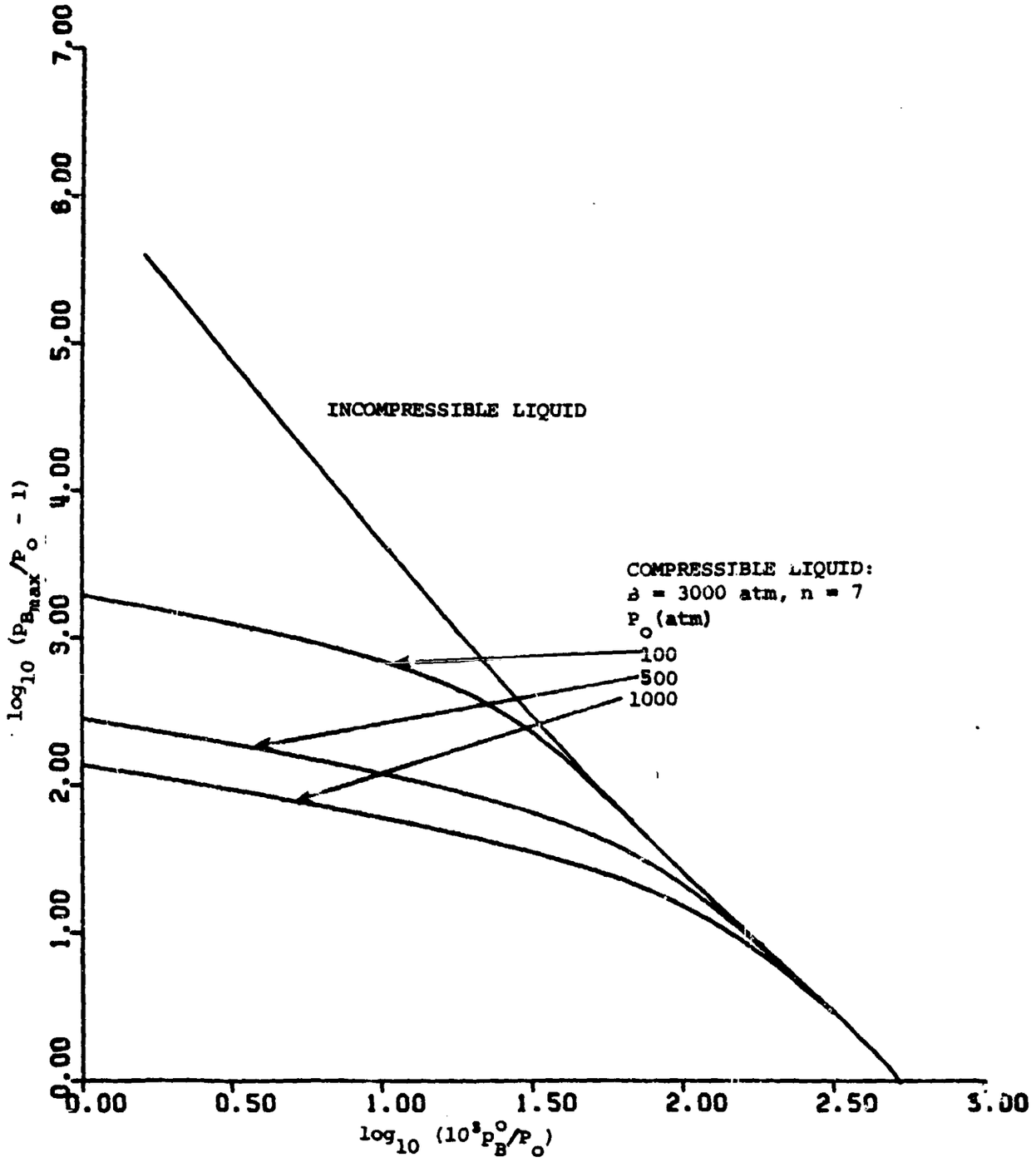

Figure B-3. Maximal bubble pressure, $\phi_{B_{max}} = p_{B_{max}}/P_o - 1$, vs. initial bubble pressure ratio p_B^o/P_o for adiabatic bubble, comparing incompressible liquid with compressible liquid solutions at several driving pressures P_o.

APPENDIX C

FLOW VISUALIZATION TESTER ASSEMBLY PROCEDURE

The following parts require "O"-rings prior to installation:

PART	"O" RING SIZE	QTY
Pneumatic Piston	#2-012-N552-70	2
Separator Piston	#2-011-N552-70	2
Projectile Piston	#2-011-N552-70	2
Septum Access Plug	#2-006-N552-70	1

Install the following items into the pneumatic loading L.P. cylinder and visualization chamber in order as shown (reference Flow Visualization Tester Assembly Drawing).

1. Pneumatic Piston with "O" rings.
2. 1/4 tube to 3/8 pipe fitting (cover pipe threads with teflon tape prior to installation).
3. 1/4 tube to 1/8 pipe fitting (cover pipe threads with teflon tape prior to installation).

Secure pneumatic load L.P. cylinder to tester stand (not shown).

4. Silicon rubber septum.
5. Septum retainer (cover with teflon tape prior to installation).
6. Septum access plug (coat "O" ring and end of plug with vacuum grease).
7. Poppet valve seat with "O" ring. Ensure "O" ring is properly seated in poppet valve seat. (Coat top sealing surface of seat with vacuum grease.)
8. Drop poppet valve thru poppet valve seat and pneumatic load L.P. cylinder.
9. Install flow guide into visualization chamber (coat top sealing surface with vacuum grease prior to installation).
10. With visualization chamber oriented as shown, place chamber on pneumatic L.P. cylinder and secure with (4) 1/2 - 13 UNC X 2" long high strength bolts and washers. Torque bolts to 15 in-lb using alternate bolt tightening method. Visually watch sealing surface of poppet valve seat to ensure correct sealing in visualization chamber.
11. Coat Parker "O" ring P/N 2-006-N552-70 with vacuum grease and push onto poppet stem. Tighten poppet packing gland into pneumatic L.P. loading cylinder.
12. Install poppet valve spring into countersink in poppet packing gland and hold in place using (2) #5-40 washers and (2) #5-40 nuts.
13. Isolation piston with "O" rings -- install piston into visualization chamber with chamfered end in first. Care should be taken during installation not to slice "O" rings while pushing past threads in chamber. (Also a requirement for installing projectile piston.)

14. Projectile piston with "O" rings.

15. Visualization chamber plug -- screw in plug until threads are flush with outside edge of visualization chamber.

16. Pressure transducer -- install transducer with adapter and copper washer until snug.

17. Bleed valve stem. (Cover thread with teflon tape prior to installation.)

18. 1/4 tube to 1/8 pipe fitting (cover pipe threads with teflon tape prior to installation).

19. L.P. drain line.

20. Install N_2 gas line and L.P. fill line.

FLOW VISUALIZATION TESTER FILLING PROCEDURE

For filling Flow Visualization Tester, the following steps must be taken (reference Flow Visualization Schematic Drawing):

1. Remove N_2 gas line from solenoid valve and ensure pneumatic piston is in proper location. Reconnect gas line.
2. Ensure all lines, valves, and fittings are properly tightened.
3. Close all valves on test fixture and remove air compressor line.
4. Open regulator valve on N_2 gas cylinder and set gas pressure as per test requirements.
5. Open bleed valve stem to L.P. drain line.
6. Using positioning rod, set projectile piston at starting location (i.e., rear edge of piston in line with edge of fill hole).
7. Set poppet spring compression (distance) as follows:
   for 300 psi tests = 21/32 total compression
   for 500 psi tests = 19/32 total compression
8. Fill L.P. reservoir
9. Connect L.P. fill hose to L.P. fill valve.
10. Open L.P. reservoir stopcock.
11. Open L.P. isolation valve.
12. Manually hold poppet valve open.
13. Slowly open L.P. fill valve until a slow flow is detected. Watch L.P. reservoir and refill when necessary. When L.P. is seen coming out the drain line and no air bubbles emerge, close L.P. fill valve.
14. Move poppet up and down to dislodge any air bubbles.
15. Close bleed valve.
16. Close stopcock on L.P. reservoir.
17. Remove L.P. fill hose from L.P. fill valve and insert hose plug.

For ullage addition (if no ullage go to step 24).

18. Open L.P. fill valve.
19. Remove septum access plug.
20. Load syringe with required amount of gas.
21. Insert syringe thru septum and inject gas into chamber.
22. Remove syringe and install septum plug.
23. Close L.P. fill valve.

---

24. Close L.P. isolation valve.
25. Check that all valves are closed.
26. Ensure contact strobe wire in chamber plug is in proper position.
27. Initiate Visualization Tests Checklist.

VISUALIZATION TESTS CHECKLIST

TEST NO.	TEST NO.	TEST NO.	TEST NO.	TEST NO.	
					PRE-FIRING:
☐	☐	☐	☐	☐	1. After filling, ensure all valves and vent plugs are closed.
☐	☐	☐	☐	☐	2. Close LP reservoir stop, disconnect fill hose, and remove LP reservoir from test area.
☐	☐	☐	☐	☐	3. Dump any leftover LP from drain bottle into used LP bottle and put drain hose back into bottle.
☐	☐	☐	☐	☐	4. Ensure strobe light is plugged in. Test fire same.
☐	☐	☐	☐	☐	5. Unlock camera film stop and advance film. Ensure lens cover is off.
☐	☐	☐	☐	☐	6. Re-check camera focus using focusing rod and re-check "f" stop.
☐	☐	☐	☐	☐	7. Close installation cover and set charge amp to "OPR" mode.
☐	☐	☐	☐	☐	8. Place Biomation in ready state. Check scale (x:1) and baseline of trace lines.
☐	☐	☐	☐	☐	9. Turn off laboratory lights.
☐	☐	☐	☐	☐	10. Open camera shutter.
☐	☐	☐	☐	☐	11. Turn on lab warning light.
☐	☐	☐	☐	☐	12. Go to control panel, insert key, arm, and fire.
					POST FIRING:
☐	☐	☐	☐	☐	13. Remove key.
☐	☐	☐	☐	☐	14. Close camera shutter.
☐	☐	☐	☐	☐	15. Set charge amp on "GND".
☐	☐	☐	☐	☐	16. Open pneumatic bleed valve, reset pneumatic piston and open chamber bleed valve.
☐	☐	☐	☐	☐	17. Disconnect strobe light.
☐	☐	☐	☐	☐	18. Turn off lab warning light.

CAMERA AND STROBE SET UP

Camera:

1. Mamiya RB67.
2. Lens: 50mm
3. Film: Kodak PXP-120 B & W, ASA 125
4. Lens at "T" time setting and "f" stop set between f11 and f16.
5. Front edge of lens placed approximately 3" from center of Visualization Chamber bore.

Strobe:

1. Vivitar Auto 252
2. "Red" flash setting
3. Face of strobe placed approximately 6" from center of Visualization Chamber bore. Strobe placed at 45 degree angle to front face of Visualization Chamber

ELECTRONICS

BIOMATION: Model 1015 wave form recorder.

INPUTS:
1. Ch 1; chamber pressure @ 5 VFS
2. Ch 2; flash discharge voltage @ 50 VFS
3. Both inputs: DC mode

Input Mode:
1. Ch. 1 and Ch. 2 (2048 words per channel)

Record Mode: Delayed

Trigger:
1. @ 300 psi = 200 words delayed
2. @ 500 psi = 370 words delayed
3. External source
4. Single sweep mode 1
5. D.C. coupling
6. Positive slope
7. trigger level at 9 o'clock

Time Base:
1. Dual
2. @ 300 psi, timebase "A" @ 0.2 ms/word
   "B" @ 0.05 ms/word
3. @ 500 psi, timebase "A" @ 0.2 ms/word
   "B" @ 0.02 ms/word

CHARGE AMPLIFIERS

INPUT:
1. chamber pressure from "Kristal" pressure transducer, type 601 A s/n 62094.
2. sensitivity = 1.075 pC/psi
3. range = 100 psi/V for 300 psi test
   500 psi/V for 500 psi test

APPENDIX D

STARTER CHARGE TESTER ASSEMBLY PROCEDURE

The following parts require "O"-rings prior to installation:

PART	"O"-RING SIZE	QTY
STARTER CHARGE CHAMBER	#2-026-N552-90	1
PRIMER GAS INTEGRATING CHAMBER	#2-020-N552-90	1

Refer to the Starter Charge Tester Assembly Drawing for the following assembly procedure. Where loading of smokeless powder and wadding is mentioned, refer to the starter charge test matrix for the type and quantity of each.

1. Install electric primer into Primer Gas Integrating Chamber. After installation, clean contact surface of primer and face of Integrating Chamber. Using a volt/ohm meter, note resistance between primer and Integrating Chamber.

2. Load powder and wadding into Integrating Chamber as required. Ensure powder does not get inside threads.

3. If, in step 2, the Integrating Chamber was fully loaded with smokeless powder (i.e., 2.60 grams), cover the four holes on the inside face of the Orifice Plug with cellophane tape (no tape is required for a partial loading). Cover threads of the Orifice Plug with grease and install into the Integrating Chamber. Tighten plug with the special spanner tool. Cover outside face of Orifice Plug with cellophane tape.

4. Coat all outside sealing surfaces of Integrating Chamber with grease and drop into end of Starter Charge Chamber as shown. Carefully push Integrating Chamber in until the "O"-ring contacts the inside bore. Using a wooden dowel, carefully tap the Integrating Chamber in until it is properly seated in the Starter Charge Chamber.

5. Clean the contact pin and end surface of the Electrical Primer Contact Assembly. Coat the threads of the Contact Assembly with grease and install into the Starter Charge Chamber. Using a volt/ohm meter, measure the resistance between center pin of electrical connector and casing. If resistance has increased by more than 25,000 ohms over the reading taken in step #1, remove the Electrical Primer Contact Assembly, re-clean it and re-clean the contact surface of the Integrating Chamber. Re-install the Contact Assembly.

6. Turn the Starter Charge Chamber over and load the chamber with smokeless powder and wadding as required. Ensure chamber does not rest on Electrical Primer Contact Assembly.

7. Install the Blast Shield into the Blind Chamber, oriented as shown, and secure with (2) #6-32 UNC x 3/4" long machine screws with lock washers.

8. Install the PCB pressure transducer with seal ring into the Blind Chamber. Torque transducer to 25 ft-lbs.

NOTE: Do not install Powder Chamber Vent Plug at this time.

9. Grease the outside sealing surfaces on the Starter Charge Chamber "neck" and "O"-ring.

10. Carefully push the Blind Chamber down onto the Starter Charge Chamber "neck" until the ends of both parts are flush against each other.

11. Grease all external threads on the Starter Charge Chamber and the Blind Chamber.

12. With Chamber Coupling Collar mounted on test stand, put tester assembly through collar in direction shown. Screw tester assembly into collar until collar is situated evenly over both parts of tester assembly.

13. Grease threads on Powder Chamber Vent Plug and install vent plug in sequence as shown.

STARTER CHARGE TESTS CHECKLIST

Test No.	Test No.	Test No.	Test No.	Test No.		
						PRE-FIRING
[ ]	[ ]	[ ]	[ ]	[ ]	1.	Make sure that the safety interlock key is removed from the remote firing panel.
[ ]	[ ]	[ ]	[ ]	[ ]	2.	Short-out the center pin of the pressure transducer lead to the connector housing.
[ ]	[ ]	[ ]	[ ]	[ ]	3.	Connect the pressure transducer lead, making certain the lead is out of the path of the vent gas.
[ ]	[ ]	[ ]	[ ]	[ ]	4.	Connect the firing lead to the Primer Electrical Contact Assembly.
[ ]	[ ]	[ ]	[ ]	[ ]	5.	Close the safety enclosure, remove the handle and insert the latch bolt.
[ ]	[ ]	[ ]	[ ]	[ ]	6.	Switch charge amp to "OPR" mode.
[ ]	[ ]	[ ]	[ ]	[ ]	7.	Make certain that channel 1 Record/Hold button on Biomation is in the out position to enable the record mode.
[ ]	[ ]	[ ]	[ ]	[ ]	8.	Switch Biomation to "Ready".
[ ]	[ ]	[ ]	[ ]	[ ]	9.	Turn on lab warning light.
[ ]	[ ]	[ ]	[ ]	[ ]	10.	Insert safety key into remote control firing panel to activate firing circuit.
[ ]	[ ]	[ ]	[ ]	[ ]	11.	Place arming switch in the "on" position.
[ ]	[ ]	[ ]	[ ]	[ ]	12.	Fire.
						POST-FIRING
[ ]	[ ]	[ ]	[ ]	[ ]	13.	Return arming switch to the "off" position.
[ ]	[ ]	[ ]	[ ]	[ ]	14.	Remove safety interlock key from the firing panel.
[ ]	[ ]	[ ]	[ ]	[ ]	15.	Push in channel 1 Record/Hold button on Biomation.
[ ]	[ ]	[ ]	[ ]	[ ]	16.	Switch charge amp to "GND".
[ ]	[ ]	[ ]	[ ]	[ ]	17.	Turn off lab warning light.

APPENDIX E

L.P. Compression-Ignition Sensitivity Tester Assembly Procedure

The following parts require "O" rings prior to installation:

Part	"O" Ring Size	QTY.
Pneumatic Piston	2-012-N674-70	2
Separator Piston	2-011-N552-90	2
Projectile Piston	2-011-N552-90	2
Septum Access Plug	2-006-N674-70	1
Bleed Valve Stem	2-013-N552-90	1
Starter Charge Chamber	2-026-N552-90	1
Primer Gas Integrating Chamber	2-020-N552-90	1

Refer to the L.P. Compression-Ignition Sensitivity Tester Assembly Drawing for the following assembly procedure. Install the following items into the Pneumatic Load L.P. Cylinder in order as shown.

1. Pneumatic Piston with "O" rings.

2. 1/4 tube to 3/8 pipe fitting (cover pipe threads with teflon tape prior to installation.

3. 1/4 tube to 1/8 pipe fitting (cover pipe threads with teflon tape prior to installation).

4. Silicon rubber septum.

5. Septum retainer (cover with teflon tape prior to installation).

6. Septum access plug (coat "O" ring and end of plug with vacuum grease).

7. Poppet valve seat with "O" ring. Ensure "O" ring is properly seated in poppet valve seat. (Coat top sealing surface of seat with vacuum grease.)

8. Drop poppet valve thru poppet valve seat and pneumatic load L.P. cylinder.

9. Coat Parker "O" ring P/N 2-006-N552-70 with vacuum grease and push onto poppet stem. Tighten poppet packing gland into pneumatic L.P. loading cylinder.

10. Install poppet valve spring into countersink in poppet packing gland and hold in place using (2) #5-40 washers and (2) #5-40 nuts.

11. Set poppet spring compression (distance) as follows:
    for 150 psi tests = 3/4 " total compression
    for 300 psi tests = 21/32" total compression
    for 500 psi tests = 19/32" total compression.

Install the following items into the L.P. Compression Chamber in order as shown.

12. Separator Piston w/"O" rings--install piston with chamfered end in first. Use a wooden dowel rod for pushing piston down chamber bore, ensuring that piston is properly seated.

13. Projectile Piston--install piston with special depth tool for proper piston alignment.

14. Install the Blast Shield, oriented as shown, and secure with (2) #6-32 unc X 3/4" long machine screws with lock washers.

Before installing any other parts, check the chamber bore, light sensor ports, and pressure transducer ports and clean out any foreign matter. Next, attach the Microswitch Mtg. Bracket to the Disc Retainer and secure with (2) #6-32 UNC X 3/16" long machine screws with flat washers. Mount the Microswitch with Push Rod onto the Mounting Bracket, oriented as shown, and secure with (2) #4-40 UNC X 5/8" long screws and nuts. Hold the Shear Disc against the end of the Disc Retainer with the Microswitch Push Rod passing thru the Shear Disc hole. Adjust the Push Rod so that 1/8" protrudes past the Shear Disc to allow for proper switch actuation.

15. Shear Disc - coat both sides of the Disc with vacuum grease and install into chamber seat.

16. Disc Retainer with Microswitch and Bracket -- grease all external threads and install into chamber. Wrench tighten.

17. Grease all external threads on the L.P. Compression Chamber.

18. With Chamber Coupling Collar mounted on test stand, screw the Compression Chamber into the collar until (1) one thread is visible on chamber.

19. Rotate the Compression Chamber until the (3) light sensor ports are on top. Install the (3) light sensors and torque to 30 ft.-lbs.

20. Cover the pipe threads on the 1/4 tube to 1/8 pipe fitting with teflon tape and install the fitting and the L.P. Drain Line as shown.

21. Rotate the Compression Chamber as necessary and install the (3) PCB pressure transducers with seal rings and the transducer port plug as shown. Torque to 25 ft.-lbs.

22. Rotate the Compression Chamber so that the L.P. Pneumatic Load Cylinder mounting holes (4) are on top.

23. Flow Guide -- coat top sealing surface with vacuum grease prior to installation.

24. With the L.P. Pneumatic Load Cylinder oriented opposite from shown, place cylinder on L.P. Compression Chamber and secure with (4) 1/2-13 UNC X 2" long high strength bolts and washers. Torque bolts to 50 ft.-lbs. using alternate bolt tightening method.

25. Rotate parts so orientation is as shown.

26. Bleed Valve Stem -- Coat threads with grease and coat "nose" with vacuum grease.

27. Install the L.P. Fill Line Valves to L.P. Reservoir and the N_2 gas line from solenoid valve to Pneumatic Cylinder.

Where loading of smokeless powder and wadding is mentioned in the following section, refer to the test matrix for type and quantity of each.

28. Install electric primer into Primer Gas Integrating Chamber. After installation, clean contact surface of primer and face of Integrating Chamber. Using a volt/ohm meter, note resistance between primer and Integrating Chamber.

29. Load powder and wadding into Integrating Chamber as required. Ensure powder does not get inside threads.

30. If, in step 2, the Integrating Chamber was fully loaded with smokeless powder (i.e., 2.60 grams), cover the four holes on the inside face of the Orifice Plug with cellophane tape (no tape is required for a partial loading). Cover threads of the Orifice Plug with grease and install into the Integrating Chamber. Tighten plug with the special spanner tool. Cover outside face of Orifice Plug with cellophane tape.

31. Coat all outside sealing surfaces of Integrating Chamber with grease and drop into end of Starter Charge Chamber as shown. Carefully push Integrating Chamber in until the "O"-ring contacts the inside bore. Using a wooden dowel, carefully tap the Integrating Chamber in until it is properly seated in the Starter Charge Chamber.

32. Clean the contact pin and end surface of the Electrical Primer Contact Assembly. Coat the threads of the Contact Assembly with grease and install into the Starter Charge Chamber. Using a volt/ohm meter, measure the resistance between center pin of electrical connector and casing. If resistance has increased by more than

25,000 ohms over the reading taken in step #1, remove the Electrical Primer Contact Assembly, re-clean it and re-clean the contact surface of the Integral Chamber. Re-install the Contact Assembly.

33. Turn the Starter Charge Chamber over and load the chamber with smokeless powder and wadding as required. Ensure chamber does not rest on Electrical Primer Contact Assembly.

34. Grease the outside sealing surfaces on the Starter Charge Chamber "neck" and "O"-ring.

35. Carefully screw the Starter Charge Chamber into the Chamber Coupling Collar until the "neck" is properly seated in the L.P. Compression Chamber.

L.P. Compression-Ignition Sensitivity Tester Filling Procedure

1. Ensure all lines, valves, and fittings are properly tightened.
2. Close all valves on test fixture and remove air compressor line.
3. Open regulator valve on N_2 gas cylinder and set gas pressure as per test requirements.
4. Open bleed valve stem to L.P. drain line.
5. Fill L.P. reservoir.
6. Connect L.P. fill hose to L.P. fill valve.
7. Open L.P. reservoir stopcock.
8. Open L.P. isolation valve.
9. Manually hold poppet valve open.
10. Slowly open L.P. fill valve until a slow flow is detected. Watch L.P. reservoir and refill when necessary. When L.P. is seen coming out the drain line and no air bubbles emerge, close L.P. fill valve.
11. Move poppet up and down to dislodge any air bubbles.
12. Close bleed valve.
13. Close stopcock on L.P. reservoir.
14. Remove L.P. fill hose from L.P. fill valve and insert hose plug.

For ullage addition (if no ullage go to step 21.)

15. Open L.P. fill valve.
16. Remove septum access plug.
17. Load syringe with required amount of gas.
18. Insert syringe thru septum and inject gas into chamber.
20. Close L.P. fill valve.

---

21. Close L.P. isolation valve.
22. Check that all valves are closed.

L.P. Compression-Ignition Sensitivity Test Checklist

TEST NO. ___	TEST NO. ___	TEST NO. ___	TEST NO. ___	TEST NO. ___	
					PRE-FIRING:
☐	☐	☐	☐	☐	1. After filling, ensure all valves and vent plugs are closed.
☐	☐	☐	☐	☐	2. Close L.P. reservoir stopcock disconnect fill hose, and remove L.P. reservoir from test area.
☐	☐	☐	☐	☐	3. Dump any leftover L.P. from drain bottle into used L.P. bottle and remove bottle.
☐	☐	☐	☐	☐	4. Connect P X-ducer and light sensor leads.
☐	☐	☐	☐	☐	5. Make sure that safety interlock keys are removed from the remote firing panel and the solenoid valve arming switch.
☐	☐	☐	☐	☐	6. Make certain that the X-ducer lead is out of the path of the vent gas and close safety enclosure. Remove handle and insert latch bolt.
☐	☐	☐	☐	☐	7. Switch charge amps to "operate".
☐	☐	☐	☐	☐	8. Make certain that all Record/Hold Buttons on Biomation are out in the "Record" Position.
☐	☐	☐	☐	☐	9. Switch Biomation to "Ready".
☐	☐	☐	☐	☐	10. Turn on Lab Warning Light.
☐	☐	☐	☐	☐	11. Insert safety key into firing panel and actuate soleroid firing circuit.
☐	☐	☐	☐	☐	12. Go to remote control firing panel, insert safety interlock key and turn to "On".
☐	☐	☐	☐	☐	13. Switch arming to "On".
☐	☐	☐	☐	☐	14. Fire.